

3-26-2018

Magnetic Gradient Drilling

Garrett Lowry Nielsen

Louisiana State University and Agricultural and Mechanical College

Follow this and additional works at: https://digitalcommons.lsu.edu/gradschool_theses



Part of the [Petroleum Engineering Commons](#)

Recommended Citation

Nielsen, Garrett Lowry, "Magnetic Gradient Drilling" (2018). *LSU Master's Theses*. 4646.
https://digitalcommons.lsu.edu/gradschool_theses/4646

This Thesis is brought to you for free and open access by the Graduate School at LSU Digital Commons. It has been accepted for inclusion in LSU Master's Theses by an authorized graduate school editor of LSU Digital Commons. For more information, please contact gradetd@lsu.edu.

MAGNETIC GRADIENT DRILLING

A Thesis

Submitted to the Graduate Faculty of the
Louisiana State University and
Agriculture and Mechanical College
in partial fulfillment of the
requirements for the degree of
Master of Science

in

The Craft and Hawkins Department of
Petroleum Engineering

by
Garrett Lowry Nielsen
B.S., Louisiana State University, 2015
May 2018

ACKNOWLEDGEMENTS

I would like to thank my advisor, Dr. Babak Akbari, for his guidance and help throughout my research. I would also like to thank my other committee members, Dr. Mileva Radonjic for her suggestions on smaller experiments, as well as Dr. Mauricio Almeida for his insights into potential field use problems. I would like to thank John Estrada-Giraldo for his help during the larger experiments.

This thesis would not have been possible without the love and support of my father Peter Nielsen, and my late mother Lynda Boydstun-Nielsen.

Lastly I would like to thank my friends for their support throughout my time here.

TABLE OF CONTENTS

ACKNOWLEDGEMENTS.....	ii
ABSTRACT	v
Chapter 1: INTRODUCTION.....	1
Chapter 2: TOOL ADVANTAGES.....	2
Chapter 3: MAGNETORHEOLOGICAL FLUID.....	5
3.1 Dimorphic Magnetorheological Fluid.....	5
3.2 Effects on Downhole Pressure.....	6
3.3 Effects of Temperature.....	7
3.4 Why Magnetorheological Instead of Electrorheological?	7
Chapter 4: MAGNETIC FIELD GENERATION.....	8
4.1 Permanent Magnet.....	8
4.2 Neodymium Magnets.....	8
4.3 Samarium Cobalt Magnets.....	9
4.4 Electromagnet	10
4.5 Magnetostrictive Material.....	12
Chapter 5: MAGNET IN FORMATION.....	14
5.1 Make Formation Magnetic.....	14
5.2 Inject Magnets into Formation.....	15
Chapter 6.:WEIGHTING MATERIAL AND NEW FLUID PROPERTIES.....	17
6.1 Shielding of MWD/LWD Tools.....	17
6.2 Erosion	17
6.3 Corrosion.....	18
6.4 Settling	19
Chapter 7: MAGNETOSTRICTIVE MATERIAL.....	20
Chapter 8: EXPERIMENT DESIGN.....	25
8.1 Basic Setup.....	25
8.2 Magnet Choice and Placement.....	26
8.3 Materials and Flow Loop Parts.....	28
8.4 Flow Loop Design.....	30
8.5 Measurements	31
8.6 Magnetorheological Drilling Mud.....	33
8.7 Safety Considerations.....	34
8.8 Experiment Setup.....	36
8.9 Mud Procedures.....	37
8.10 Experiment Procedures.....	38

Chapter 9: LAB RESULTS.....	40
9.1 Sample Creation Process.....	40
9.2 Sample Testing Procedures.....	41
9.3 Determining Bentonite Amount.....	41
9.4 Discussion of Lab Results.....	41
9.5 Rust Mixing Test.....	48
9.6 Lab Results Conclusions.....	50
Chapter 10: SEM AND EDS RESULTS.....	51
10.1 Particles	51
10.2 Lab Samples.....	52
10.3 Flow Loop Sample.....	54
Chapter 11: FLOW LOOP EXPERIMENTS.....	58
11.1 Results.....	58
11.2 Post Experiment Observations.....	64
Chapter 12: MUD WINDOW ANALYSIS (REAL WORLD SIMULATION).....	69
12.1 Explanation of Mud Characteristics.....	70
12.2 Non-Ratchet Method.....	71
12.3 Mud Window Conclusion.....	74
Chapter 13: CONCLUSION.....	75
Chapter 14: FUTURE RESEARCH.....	76
REFERENCES	77
APPENDIX A: ADDITIONAL SIMULATIONS.....	87
APPENDIX B: ADDITIONAL SIMULATION MUD WINDOW GRAPHS.....	96
APPENDIX C: ADDITIONAL FLOW LOOP GRAPHS.....	106
APPENDIX D: ADDITIONAL POST EXPERIMENT IMAGES.....	115
APPENDIX E: TABLE OF MAGNETIC FIELD STRENGTHS.....	121
APPENDIX F: ADDITIONAL SEM/EDS IMAGES, TABLES AND GRAPHS.....	124
APPENDIX G: ADDITIONAL LAB OBSERVATION IMAGES AND NOTES.....	138
VITA.....	143

ABSTRACT

The drilling industry has always had difficulties with staying within the mud weight window. The problems associated with failure to stay within the mud weight window include uncontrolled influxes and wellbore collapse on the low pressure side of the window, and fluid losses and wellbore damage on the high pressure side of the window. When the risk for getting outside of this mud window becomes too great, casing must be set in order to isolate formations from each other. If too many strings of casing are set, or if the damage from getting out of the mud weight window is too great, then the well must be plugged and abandoned. This thesis presents a method to more easily stay within the mud weight window, lessen or prevent uncontrolled fluid influxes into the well, and to extend the depths that can be reached before casing has to be set.

The current technique used is to increase the density of the drilling fluid, thereby increasing the pressure at greater depths, in order to stay within the mud weight window. This thesis proposes a new technique, one in which the drilling fluid has been changed to a magnetorheological fluid, which is a fluid whose apparent viscosity is modified through the application of a magnetic field. The experiments conducted have shown that a stable magnetorheological drilling fluid can be created. Using this magnetorheological fluid, in combination with a magnetic tool, it is possible to generate pseudo-chokes downhole. This allows for operator controlled pressure drops in the wellbore, increasing the pressure upstream of the tool location without affecting the pressure window downstream of the tool.

1. INTRODUCTION

Due to complications involved in deep water drilling, especially the very narrow mud weight windows seen at greater depths, a new method is needed in order to allow drillers to drill to their targets safely and efficiently. A new technique is proposed, which involves a new weighting material in combination with a new tool in order to accomplish these goals.

Through previous research of magnetorheological fluid, a fluid whose apparent viscosity increases in response to an applied magnetic field, it has been shown that it is possible to control the fluid's viscosity over a desired length. This allows for the creation of a pressure drop with a magnitude and length of the operator's choosing. The purpose of this research was to show that an effective tool/method, as well as a stable magnetorheological drilling fluid, could be developed in order to obtain these pressure drops.

2. TOOL ADVANTAGES

With the currently developed managed pressure drilling techniques, it is possible to drill within tighter windows by controlling the downhole pressure at a single location. A new method of drilling is proposed, one in which the viscosity of the fluid is variable, and under the operator's control. This would allow for the creation of pressure drops at locations of the operator's choosing within the well. More importantly this allows for the use of a lower density drilling mud, and create pressure drops that allow it to follow more complex casing setting lines within the drilling plan. This allows for the benefits associated with typical managed pressure drilling, such as precise control of bottom hole flowing pressure, but adds the benefit of allowing this to be performed at multiple locations within the wellbore. This will enable the operator to reach the formation with less strings of casing and cementing, and due to the time associated with casing and cementing also lower time to drill the well.

There are many challenges associated with cementing in high-temperature and/or high-pressure environments (Shadravan and Amani 2012) (Ravi et al. 2008) (Ugwu 2008) (Nelson 1990) (Bosma et al. 1999) (Hunter et al. 2007) (Stiles 2006). These challenges typically require that the cement is specially designed for each individual cementing job (Ravi et al. 2002) (Nygaard and Lavoie 2010). It is also worth noting that 13-19% of production well and 37-41% of injector wells are leaking in the Norwegian sector of the North Sea (Nygaard 2010 and references therein). These well integrity problems, up to 73% of wells in some fields, have led to an approximate 7% loss in production, which amounted to approximately \$8.4 billion in 2008 in the Norwegian North Sea alone (Randhol and Carlsen 2008). Reducing the number of casing strings that have to be set will also reduce the number of complicated cement jobs that must be completed.

Since it is possible to create the pressure drops at locations of the operator's choosing, it is also possible to follow the original casing setting plan that would be developed for a well and decrease the actual number of casing and cement settings. In theory it is possible to decrease the amount of casings to only the required surface casing by law and the final production casing, but preliminary calculations seem to suggest that it would only be safe to remove 1-2 casing strings.

As the new pressure drops are created by a tool located on the drill string, it is impossible to have it sit in one exact spot, but it is possible to have multiple tools in locations decided upon during the initial planning of the well. This allows for these pressure drops to remain in approximately the same locations as drilling is continued, by moving these pressure drops vertically by the distance kept between the tools. This would require a higher concentration of these tool on, and near the bottom-hole assembly because of the tighter windows commonly seen at greater depths.

A form of risk management is Multiple Physical Barriers. According to this increasing the number of physical barriers increases the level of safety, due to the fact that if one barrier fails the other barriers are still in place (Fraser et al. 2015). The most well-known barriers in well control currently are hydrostatic pressure and the blow-out preventers at the surface. Since each magnet assembly tool placed downhole in this proposed new well control method could be another barrier, it greatly reduces the risk factor associated with well control.

It takes longer to circulate out kicks from deeper wells, such as those encountered in the Gulf of Mexico. This takes even longer when it is taken into consideration the fact that kicks must be circulated up through the choke line due to safety concerns and regulations. The rationale behind this being that if gas fills the marine riser it could collapse due to the surrounding hydrostatic pressure of the ocean (Weems, Moore, and Leach 2016). If Magnetic Gradient Drilling reduces

kicks as proposed, then it will also greatly reduce down time, and due to the high day rates in the Gulf of Mexico potentially reduce cost as well.

Industry has pointed out that what would really help them would be the ability to drill wells that are currently undrillable (Jacobs and Donnelly 2011a). Undrillable wells are located all over the world (Gallo et al. 2016) (Hannegan 2006). Wells may be undrillable due to many reasons, such as high fluid losses or economic reasons, but this research specifically looks at wells that are undrillable due to narrow mud weight margins requiring more strings of casing than initially planned for (Hamoudi et al. 2011) (Arnon and Vieira 2009). Magnetic Gradient Drilling looks to change how the mud window is navigated and therefore reduce strings of casing. This would allow previously undrillable wells to be drilled. This is looked at further in the Mud Window Analysis section.

3. MAGNETORHEOLOGICAL FLUID

Part of this newly proposed managed pressure drilling method is the new drilling fluid that will be required for it to work. This will be, as previously mentioned, a magnetorheological fluid. A magnetorheological fluid is a fluid whose yield stress changes due to the influence of a magnetic field. The main difference between the composition of this new drilling mud and previous drilling muds is that a ferromagnetic material was used as the weighting material instead of barite. This particular project used 7.86 grams per cubic centimeter (g/cc) (65.5 pounds per gallon (PPG)), carbonyl iron particles. This is a much higher density than the 4.2 g/cc (35 PPG) of the traditional weighting material American Petroleum Institute (API) barite. The chemical composition of barite is BaSO_4 , or Barium Sulfate.

When a magnetic field is applied the iron particles align themselves with the magnetic field and create a barrier to flow. The particles are attracted to each other due to the magnetic dipoles they obtain while under the influence of the magnetic field, resembling a chain of particles (Wang and Gordaninejad 2006) (Bossis et al. 2002) (Rabinow 1948). The strength of this effect is dependent on the strength of the magnetic field, as well as the volume percent of ferromagnetic materials (Bossis et al. 2002).

3.1 DIMORPHIC MAGNETORHEOLOGICAL FLUID

Since the fluids response decreases relative to the amount of ferromagnetic particles it contains, it could be possible that at the desired fluid densities that would be applicable to field use the magnetorheological fluid does not show a strong enough yield stress response for the desired application. If this is the case then either the fluid has to be changed such that more ferromagnetic particles can be added, or the particles themselves must be changed in such a way that the magnetorheological response is increased. Research has shown that partial substitution of the iron

microspheres with iron nanowires can greatly increase the fluids response to an applied magnetic field, while also greatly decreasing the particle settling rate of the iron microspheres (Jiang et al. 2011) (Ngatu et al. 2008). This is because the nanowires attach to the microspheres in such a way that they act as reinforcement for the microsphere chains. Also, the Nano-size of the nanowires means that they are suspended due to Brownian motion instead of viscosity. Brownian motion is the random movement of particles due to their collisions with atoms or molecules. (Jiang et al. 2011) (Ngatu et al. 2008)

3.2 EFFECTS OF DOWNHOLE PRESSURE

Some research has suggested that the pressure the fluid is under also has a significant effect on the change in yield stress. According to Zhang et al. 2004, an approximately 220 psi increase in pressure, from atmospheric, can result in a 25 times increase in yield stress (Zhang et al. 2004). The method for this compression-assisted aggregation, referred to in research as the squeeze strengthening effect, is believed to be a rearrangement of the aligned ferromagnetic particles; such that the particle chains attach to each other increasing their thickness (Zhang et al. 2004) (Hegger and Maas 2016). This squeeze strengthening effect only occurs when the pressure increases while the fluid is under the influence of a magnetic field (Hegger and Maas 2016). Also this squeeze strengthening effect will diminish as higher amounts of shear on the material occur (Spaggiari and Dragoni 2012). In other words, once the material is flowing these interconnected chains break back up into single chains (Hegger and Maas 2016) (Becnel et al. 2015). The problem with this research is that it involves creating a strain on the flow path, which therefore also reduces the cross-sectional flow area and potentially gives false results for the change in apparent viscosity. It should be noted that since drilling mud will be flowing most of the time, this effect should not occur as the pressure

the magnetorheological fluid sees while passing through the magnetic field does dramatically increase before the fluid leaves the influence of the magnetic field on the downstream side.

3.3 EFFECTS OF TEMPERATURE

Another question is whether the newly proposed weighting material's magnetorheological properties will hold up to the temperatures experienced in downhole situations. The magnetorheological fluid should itself see no reduction in magnetorheological response due to the elevated temperatures. In fact, ferromagnetic iron sees no drop in its response to a magnetic field until its Curie temperature of approximately 771 degrees Celsius (1420 degrees Fahrenheit) (Arajs and Colvin 1964). A materials Curie temperature is the temperature at which a material loses its magnetic field. Other research has suggested that magnetorheological fluids are only suitable up to 150 degrees Celsius (302 degrees Fahrenheit), but note that this is due to limits of the carrying fluid being used and not the particles themselves (Carlson and Jolly 2000).

3.4 WHY MAGNETORHEOLOGICAL INSTEAD OF ELECTORRHEOLOGICAL?

An electrorheological fluid is a fluid whose rheological properties change due to the influence of an electric field. Research has consistently shown that the change in yield stress of a magnetorheological fluid is at least an order of magnitude higher than maximum change that can be created with an electrorheological fluid. More importantly a relatively constant magnetic field is created through the use of permanent magnets whereas with current technology it is not possible to have a constant electric field without constant power being sent downhole. (Bossis et al. 2002) Magnetorheological fluids are also not affected by the electrical properties of liquid being used. Therefore the weighting material can be added to either a water or an oil based mud, and there should be no significant difference in the magnetorheological response (Wang and Gordaninejad 2006).

4. MAGNETIC FIELD GENERATION

In order to obtain the desired pressure drop due to the magnetorheological properties of the newly proposed drill fluid there needs to be a magnetic field downhole. There are currently multiple methods that will be mentioned in the next few pages with ideas for a solution to this problem, such as permanent magnets and electromagnets; possibly in combination with a magnetostrictive material. A magnetostrictive material is a material that shows a strain/stress response due to the influence of a magnetic field.

4.1 PERMANENT MAGNET

The simplest, by comparison to the other methods suggested, and most reliable idea would be to have a permanent magnet on the drill string. This could be set up to only interact with the fluid through a ratchet system and multiple tools at the desired times, or through a single tool. The magnets cannot be welded to the drillstring because the increase in temperatures associated with welding would damage the magnets. Since magnets themselves cannot be welded, slots would have to be created in order to safely attach the magnets to the tool while minimizing the possibility of the magnets becoming loose and detaching into the fluid. A major barrier for acceptance and use in industry is system reliability, which would be better with a permanent magnet over an electromagnet or other magnetic field generating device (Jacobs and Donnelly 2011b).

4.2 NEODYMIUM MAGNETS

One possible choice for permanent magnets would be neodymium magnets. Strong neodymium magnets have a Curie temperature of approximately 287 degrees Celsius (549 degrees Fahrenheit) (Croat et al. 1984) (Sagawa et al. 1984). This low, for Curie temperatures, Curie temperature makes them unsuitable for field use. The magnetic flux through neodymium magnets is on the order of

1-1.23 Tesla (10000-12300 Gauss) (Sagawa et al. 1984). Magnetic flux is the density of magnetic field lines.

4.3 SAMARIUM COBALT MAGNETS

Other problems associated with putting the magnet downhole are the possibility of the magnet flux, and therefore magnetic field strength, deteriorating over time. This is because magnets gradually lose some of their magnetic flux when exposed to elevated temperatures for extended periods of time.

Magnets also lose some, up to 15% depending on how the magnets were created, magnetization when exposed to radiation doses close to 10^{10} rads. The amount of magnetic flux loss is dependent on how the magnets were created, and can be relatively low, less than 1% loss, for higher quality magnets. These losses in magnetic flux are typically reversible. (Blackmore 1985) (Mildrum et al. 1974)

It is also important to note that magnets lose their magnetic flux, not just due to long exposure times at elevated temperatures, but also relative to increases in temperature. A 200 degrees Celsius (392 degrees Fahrenheit) increase in temperature could cause a magnetic flux decrease from 5-10% in Samarium-Cobalt magnets (Abdelnour, Mildrum, and Strnat 1980). These losses are also relatively low for certain cobalt based magnets where the samarium is replaced by a less refined alloy consisting of multiple rare-earth metals (Ratnam and Wells 1974).

The addition of Boron into the atomic structure of rare earth magnets, such as neodymium and samarium cobalt, has shown to increase the magnet flux and coercivity, but also greatly increases the temperature dependence of the magnetic flux (Sagawa et al. 1984). Magnetic coercivity is a magnets ability to resist demagnetization.

The main problem with using permanent magnets is that the strength of the magnetic field decrease exponentially as the distance from the magnet increases linearly. A method to increase the strength, and area affected by the magnetic field is to connect 2 magnets together, north magnetic field end to south magnetic field end or vice versa, using their magnetic fields (Bondemark, Kurol, and Wisten 1995).

Another problem is that the magnetic field strength needs to be minimized within the drill pipe. An arrangement to solve this problem would be to connect the magnets in such a way that their magnetic fields are aligned on one side, and opposed on the other side. This would allow the magnetic fields to cancel on one side, the inner pipe side, while still existing on the other side, the annulus side (Halbach 1980) (Mallinson 1973). One of the embodiments of these arrays is to have the magnets aligned such that their north poles are all facing radially outwards and their south poles are all pointed radially inwards.

4.4 ELECTROMAGNET

One method would be to have an electromagnet downhole. The problem with this is that there would need to be a way to apply the electric current required for such a magnet to work. Currently there is no reliable method for sending power downhole through the drillpipe for drilling operations (Allen et al. 2009) (Jellison et al. 2003) (Coley and Edwards 2013) (Olberg et al. 2008). Another solution to the power problem would be to have a battery, as it this is currently done to some extent. Unfortunately batteries do not work at the high temperatures that would be expected downhole in certain narrow mud window situations and are unreliable otherwise. Current maximum battery operational temperature in the industry is about 266 degrees Fahrenheit (Fripp et al. 2008).

If there is to be a battery, then there will need to be a way to communicate with the downhole tool. Current data transmission from sub-surface equipment, such as measurement-while-drilling (MWD) or logging-while-drilling (LWD) equipment is through mud pulse telemetry. This uses a stator in the drill pipe to send pressure waves up the drill pipe that are interpreted at the surface as data. This has very slow data transmission, and if multiple tools are in the well that use this they would all have to be connected so that only one of them sends the signal to the surface. If they are not connected and there are multiple stators then the surface equipment might not be able to differentiate between which signal is coming from which tool. Currently companies are trying to get around these problems by using electromagnetic telemetry to send the data. If this ever becomes the dominate method for data transmission it might interfere with the magnetorheological fluid. According to Chen et al. 2015 the electromagnetic waves travel through the formations instead of the wellbore in this method (Chen et al. 2015).

Another method would be to have a downhole motor to generate the current needed for each tool. This would have the problem that each of these motors would require an associated pressure drop. These motor pressure drops along with the created annular pressure drops due to the magnetorheological fluid could prove to be too much for a pump to handle. Currently downhole motors are not used for power generation.

Research has been done on the creation of power downhole through piezoelectric devices. A piezoelectric material is a material where a change in the alignment of molecules, resulting from a strain on the material, causes an electric field to be created. Essentially this would mean that flow in the pipe or annulus would cause vibrations in a piezoelectric material that would then create an electric current as a response (Ahmad et al. 2015). Another method is to have a wire wrapped around a magnetostrictive material. Harmonic vibrations through this material create a magnetic

field that then induces an electric current in the wire (Zhao and Lord 2006). This method only produces a very small amount of power and would require a method to store this energy until it reaches a high enough level to power the electromagnet (Ahmad et al. 2015). This method would not be viable if the field needs to be generated for longer periods of time. More importantly it creates a small magnetic field, which would affect the magnetorheological fluid in the immediate vicinity.

Lastly, downhole power could be created through a combination of magnetostrictive and piezoelectric materials (Ryu et al. 2001). Unfortunately this method would create a magnetic field at the power generation location, which would be very undesirable if it was inside the drill pipe as the magnetorheological fluid changes viscosities based on an applied magnetic field.

4.5 MAGNETOSTRICTIVE MATERIAL

Another potential method for the creation of a downhole magnetic field would be through the use of magnetostrictive materials in combination with the previously described methods. The inverse of this is the magnetomechanical effect, which is the property that is potentially useful with regards to this project. It is possible that natural magnetization in hematite is actually a result of its magnetostrictive properties. (O'Reilly 1984) (Stacey and Banerjee 1974) This will be discussed further in a later section.

It was originally suggested that the magnetization, for steel, would increase with stress, and then remain when the stress was removed (Brown 1949). It has been shown that at higher stresses this is not the case (Craik and Wood 1970). This is important because it would have meant that the steel that is already being used downhole, such as the drillstring, could have already been magnetized slightly. Changes in stress can cause great changes in how ferromagnetic materials are

magnetized. For some materials a 98.1 mega-pascal load (14.2 thousand pounds per square inch (KSI)), can cause a 100 fold increase in magnetic permeability (Bozorth and Williams 1945).

5. MAGNET IN FORMATION

Another important variable is where to place the magnet. The least complicated method is to have the magnet attached to the drill string in some way. The following sections will look at other possible locations, such as liners, casing and possibly even downhole formations themselves.

5.1 MAKE FORMATION MAGNETIC

The following section will look at the possibility of having a downhole reaction that would allow for the formations currently, or previously drilled, to be used to create the downhole magnetic field. This section will look exclusively at silicon based formations for this purpose, i.e. sandstones and shales.

Magnets do exist that contain silicon, but only with a very small percent of silicon (0-2%) (Kaneko, et al. 1972). Therefore it might be possible to send other magnetic components downhole, and have a reaction that would allow the formation silicon to become part of the magnet and cause the other magnetic materials to adhere to the formation. In other words this would create a mud-cake-like material that would act as the magnetic field source.

These magnets are known as Fe-Cr-Co permanent magnets. The addition of silicon makes these magnets more resistant to losing their magnetic fields. This means that the silicon would actually improve magnetic properties with regards to this research's desired use for them. Some researchers suggest that this might actually be due to the oxygen that accompanies this silicon rather than the silicon itself (Szymura and Sojka 1986).

The main complication involved in this proposed reaction is that, similar to the creation of other permanent magnets, it is not a simple chemical reaction. There is a need to heat the material to high temperatures relative to downhole conditions. A maximum temperature of 1300 degrees

Fahrenheit and a sustained temperature of 932 degrees Fahrenheit are required to achieve the improved magnetic properties (Wyslocki, et al. 1990).

Another potential candidate for this would be Barium Ferrites, $\text{BaFe}_{12}\text{O}_{19}$. Barium Ferrites can be created “hydrothermally”. This involves combining different reagents at specific thermal and pressure conditions. This would have to be between water’s boiling point and its critical temperature of 374 degrees Celsius (704 degrees Fahrenheit) with pressures up to 15 mega Pascal (MPa) (2175 PSI). The creation of hydrothermal barium ferrite requires long times, approximately 10-15 hours, in order to create a sufficient amount of material at conditions that are similar to what is typically experienced downhole, with respect to pressure and temperature conditions. The drawback is that this resulting material then needs to be calcined at much higher temperatures than what is seen downhole. This calcined process is the heating of the material in order to allow for the reagents atomic structures to rearrange themselves such that a magnetic field is created. (Liu et al. 1999) (Janasi et al. 2002)

Therefore current research does not suggest that it is feasible to have a reaction downhole in order to have permanent magnets created as part of the formation. This is due to the fact that the atomic structure is what helps create the magnetic properties and the material needs to be melted at higher temperatures than typically seen downhole in order for that structure to change.

5.2 INJECT MAGNETS IN FORMATION

Another option is to inject small magnets into the formation in the immediate vicinity of the wellbore. Ceramic ferrites are a good option because they typically have particle sizes ranging from 1-1.5 micrometers and magnetic field strengths less than .36 Tesla (3600 Gauss) (Lagorce and Allen 1997). Research has shown that grinding ceramic ferrites down to these sizes will lead

them to all have the same magnetic field strength, as each particle will be a single magnetic dipole (Morrish and Haneda 1983).

It is also possible to have the previously mentioned barium ferrites at a nanoscale (less than 100nanometers) (Pillai et al. 1993). Another possible choice are Strontium Ferrites, $\text{SrFe}_{12}\text{O}_{19}$. These can be created in nano-sized particles, ranging from 52-78nm. These nano sized particles might not have enough magnetic field strength/size to cause a noticeable difference in the rheological properties of the fluid though (Fu and Lin 2005).

The next question to answer is whether or not the pore throat size of the formations would be large enough to inject these particles. Pore throat size distributions taken from the St. Peters Sandstone, also known as Ottawa sand, cores at a depth of approximately 1500 feet shows a pore throat distribution ranging from 2 micrometers up to 5000+ micrometers. The lower end, around 2 micrometers, would mean the larger possible particle sizes would not be able to enter the pore throats. The higher side, 5000+ micrometers, would mean that the pore throats are too large for the particles to bridge and become stuck in the formation. The problem with this method is that a particular particle size to pore throat size ratio near the wellbore is required, after drilling has potentially damaged it, such that the magnetic particles would become stuck very close to the open hole.

6. WEIGHTING MATERIAL AND NEW FLUID PROPERTIES

The proposed new weighting material is carbonyl iron. These are iron microspheres that are approximately the same size as API Barite, but with a density of 7.86 g/cc. This higher density of these particles results in a larger increase in mud density with a lower volume of weighting material. As there is a limit to the volume of material a fluid can hold, this increases the space for other materials, such as cuttings. A lower total solids content has a large impact on drilling rate. (Tovar et al. 1999)

6.1 SHIELDING OF MWD/LWD TOOLS

Another potential problem is that MWD/LWD tools are being used more often in the industry. There has been research that shows that current drilling fluids have a negative effect on the performance of these tools (Torkildsen et al. 2004, and references therein) (Waag et al. 2012). Thankfully other research has shown that free iron ions, such as the ones that could occur with the inclusion of the proposed weighting material, do not contribute to this shielding effect (Ding et al. 2010) (Tellefsen et al. 2012).

6.2 EROSION

It has been shown that a particle's abrasiveness is highly dependent on its shape and size (Clark 1990). The only difference between the proposed new carbonyl iron and typical API Barite is that the carbonyl iron is slightly harder. It has also been shown that iron oxides can be far more damaging when flowing through a choke than typical API Barite. This is because the iron oxides do not break down when they pass through the choke as the API Barite does (Walker 1983). Currently the proposed weighting material would not be an iron oxide though. Research has shown that the courser material has higher erosion rates for mixtures of ilmenite (an iron oxide) and barite

(Clements 1981). The current proposed iron particles are not a coarse material as they are spherical.

Papers have suggested two main methods for testing abrasiveness. One method is to use a high speed mixer and measure the differences in blade weight before and after mixing the materials for extended periods of time. The differences in blade weight between the two materials is used to suggest a difference in erosion rates (Clements 1981) (Walker 1983). Another method used was to circulate these materials through a choke, and measure the loss of choke material to determine the difference in abrasion. This second method is a more real world application (Walker 1983).

6.3 CORROSION

A substantial drawback associated with using carbonyl iron particles is that they are purified iron. The corrosion associated with carbonyl iron can limit its use to a few hours in highly acidic, PH of 1, environments to a couple of weeks with constant exposure to and mixing in air (Miao et al. 2011). One potential solution to this problem would be to have the carbonyl iron microspheres coated with a substance that will have minimal interaction with the magnetic field. This coating substance would also have to be in the nanometer thickness range in order to minimize its reduction of the magnetorheological response of the fluid (Mrlik et al. 2014) (Miao et al. 2011) (Cheng et al. 2009) (Choi et al 2006) (Cho et al. 2004) (Liu et al. 2012). A second potential solution is to have the particles submerged in an oil, which is the current embodiment envisioned for field use, in order to reduce the oxidation rate because iron rust due to iron's reaction with oxygen.

The other problem is that the oxidation of the iron will still result in carbon steel pipe having increased corrosion. The only immediate solution to this would be to coat the pipe in paint to protect it from corrosion. The problem with this is that this paint will undoubtedly be eroded away during drilling operations. Using stainless steel alone, which is more resistant to corrosion, would

not be a feasible option because the stainless steel drill pipe would not create the magnetic shielding required to prevent magnetorheological effects from taking place within the drill pipe.

6.4 SETTLING

The increased particle density of iron compared to water, 7.86g/cc compared to 1g/cc, will lead to increased particle settling in relation to barite and water mixtures. A major problem with magnetorheological fluids is that, due to remnant magnetization, it is very challenging to redistribute particles once they have settled out of suspension (Phule et al. 1999) (Lopez-Lopez et al. 2006). If the standard increases in plastic viscosity and yield stress caused by typical field viscosifying agents such as bentonite and attapulgite is not enough, then another solution must be found. One possible solution is to add nanoparticles to the microparticles (Ngatu and Wereley 2007) (Ngatu et al. 2008) (Jiang et al. 2011) (Iglesias et al. 2012) (Wereley et al. 2006). Another possible solution that research suggest would yield the best results for both reduction in sedimentation as well as increase in yield stress would be to replace all of the iron microspheres with iron microwires (Bell et al. 2008). Another possible solution is to embed the carbonyl iron particles in another medium to reduce their overall density with only a minor reduction in the change in yield stress response to the influence of a magnetic field (Fang et al. 2008) (Tan et al. 2010). It is even possible to embed the particles into the bentonite that is typically used as a viscosifying agent in drilling fluids (Galindo-Gonzalez et al. 2012). Lastly, the addition of coating materials, as described in the corrosion subsection can also reduce settling depending on the particle/fluid interactions as well as reduce the particles' density (Wu et al. 2006) (Cho et al. 2004) (Jun et al. 2005) (Ashtiani et al. 2015).

7. MAGNETOSTRICTIVE MATERIAL

The inverse of the previously mentioned magnetostriction is the magnetomechanical effect. This is a material's change in magnetic susceptibility due to a change in strain. In order for this method to work there would need to be a high enough magnetic field strength to create the desired pressure drops.

According to Le Chatelier's principle:

$$(1) \quad \left(\frac{\partial \lambda}{\partial H}\right)_{\sigma} = \left(\frac{\partial B}{\partial \sigma}\right)_H$$

Where **Lambda** is shape change of a ferromagnetic material during magnetization, a more appropriate engineering term would be ϵ as this term is axial strain. **H** is the applied magnetic field strength. **B** is flux density through the object. And **σ** is stress.

Therefore the change in a materials shape due to change in strength of magnetic field for a given stress is equal to the change of the objects magnetic flux density due to change in stress for a given magnetic field. According to this formula if Magnetostriction is change in shape due to magnetization, with the change in shape being the effects of strain due to unrestrained stress, the change in stress, under a constant magnetic field strength, should change the strength of the magnetic flux. In other words, how much the magnetostrictive material becomes magnetized due to the influence of a magnet is based on the amount of stress the material sees (Ekreem et al. 2007). As an example, it has been shown with manganese-zinc-ferrites that applying a compressive force while under the influence of a constant magnetic field will reduce the magnetic flux through the ferrites (Bieńkowski 2000) (Szewczyk and Bieńkowski 2003).

The magnetomechanical effect has been seen in large structures, which when stressed in the presence of Earth's magnetic field, become magnetized (Jiles 1995). Steel has shown a maximum magnetostriction in the vicinity of 25ppm without other applied stresses (Wun-Fogle et al. 2009).

Terfenol-D is a possible magnetostrictive material that shows a very high strain response, with respect to magnetostrictive materials, in relation to the applied magnetic field strength. The maximum strain is on the order of magnitude of 1000-2000 parts per million (ppm). One limiting factor is that it has a very low tensile strength with respect to petroleum field applications. This tensile strength is on the order of 28-40 MPA (4.061 – 5.801 KSI). Terfenol-D shows a high compressive strength on the order of 300-880MPA (43.51 – 127.63 KSI). It begins to lose its magnetostriction at 200 degrees Celsius (392 degrees Fahrenheit). The material has a relatively high density of 9.2-9.3 g/cc. The lack of tensile strength, in combination with the material's low Curie temperature makes it unsuitable as the sole material for the magnetic field requirements.

Iron Gallium alloys (Galfenol) are a more promising magnetostrictive material that shows a lower strain, 200-250ppm, in relation to the applied magnetic field. It also shows a much higher tensile strength than Terfenol-D of 350MPA (50.7KSI). This puts Galfenol's tensile strength below that of aluminum drill pipe, which has 564MPA (81KSI) of tensile strength (Mehrabi, et al. 2014). Aluminum drill pipe is being used for comparison because it is already being used in the industry (Lehner and Garcia 2015). Galfenol is more promising because it also has a higher Curie temperature of 670 degrees Celsius (1238 degrees Fahrenheit).

Galfenol with a combination of approximately $\text{Fe}_{0.81} \text{Ga}_{0.19}$ would yield the highest magnetostriction for Galfenol. Iron has magnetostriction as previously discussed, but it is very low. For comparison the magnetostriction of iron is around 30ppm whereas the magnetostriction of $\text{Fe}_{0.81} \text{Ga}_{0.19}$ Galfenol is around 390ppm near room temperature. Also, Galfenol's density of 7.8g/cm^3 is very close to that of iron's 7.874g/cm^3 . (Clark et al., 2002) Adding Gallium to iron only increases the magnetostriction along the λ_{100} crystallographic axis direction. This means that

the λ_{100} crystallographic axis would have to be oriented in the radial direction so that the resulting change in magnetization will be perpendicular to the fluid's flow direction (Kellogg et al., 2002). Other potential benefits to using Galfenol are that it's machineable, ductile and can be welded, which are required properties for drill pipe construction material. "Thus they can be easily threaded, attached to existing structures and used as load bearing members" (Atulasimha and Flatau 2011). They are also corrosion-resistant (Jayaraman et al., 2007). Another benefit to this combination of Galfenol is that it has almost acceptable tensile strength of ~500MPa (~72.5KSI), and is relatively temperature independent with regards to its magnetostrictive properties (Kellogg 2003). The tensile strength of Galfenol is highly dependent on the amount of each component. For comparison Aluminum drill pipe has ~564MPa (81.8KSI) tensile strength; and Steel pipe grade E has ~689MPa (~100KSI) tensile strength.

Galfenol shows softening from 450-800 degrees Celsius (842-1472 degrees Fahrenheit) (Cheng et al. 2007). This is outside the range of temperatures that would typically be seen downhole so it should not be a problem for field implementation. Different percent mixtures of iron and gallium yield different magnetostrictive responses. There are multiple spikes in magnetostrictive response for mixtures of iron and gallium, but the strongest of these magnetostrictive responses is when the mixture is 81% iron and 19% gallium. This combination is most typically associated with the name Galfenol, but the term Galfenol does not exclusively refer to this specific mixture of iron and gallium. (Clark et al. 2002) (Wu 2002) (Kellogg 2003) (Atulasimha and Flatau 2011)

Another magnetostrictive material is iron. The direction of the iron crystal axis for a material greatly affects its magnetostrictive response. As shown with iron crystals, certain directions can expand with respect to any increases in magnetic field strength up to magnetic saturation. Another crystal axis direction could decrease with any increase in magnetic field strength up to magnetic

saturation. Most importantly the material could initially expand with low magnetic field strengths and then contract as the material nears its magnetic saturation. This last crystal direction, listed as (1, 1, 0), has been shown in iron rods to show this last response of expanding and the contracting. The magnetomechanical effect, could therefore be used in combination with different crystallographic axis directions to have a relatively null change in the magnetic susceptibility at lower strain levels, and a large decrease in susceptibility at higher strain levels. (Webster 1925)

By having different crystal alignments within the magnetostrictive material it might be possible to have them cancel out at certain strains, and increase at later ones. For instance, if it is engineered so that there are crystal directions that first increase, then decrease due to strain with the ones that only decrease due to strain to create the magnetostrictive material this would create a material that at first does nothing when a magnetic field is applied, due to the strains being in opposite directions, and lastly the strains will both be in the same direction. To clarify how this would work with the inverse effect in the magnet assembly: At low strain levels, which would occur near the neutral point of buckling, the magnetic field determined at the surface will remain unchanged. At higher strain levels, which would occur above and below the neutral point of buckling, the magnetic susceptibility, and therefore magnetic shielding would be decreased. This would allow for the magnetic field generated by the tool to be larger, and extend farther into the open hole. The neutral point of buckling's location would be controlled through initial design and slacking off or picking up on the drill pipe.

In order for this to be used there would be a prerequisite of knowing how the crystallographic axis change under strain. Currently there does not appear to be software that can model this (Quey et al. 2011).

From the above information it is clear that it will not be feasible to have a solid cross section comprised solely of magnetostrictive material. Therefore the rest of the tool would need to be made out of a stronger material that could withstand the loads expected downhole, with a precise portion of these loads being transmitted through the magnetostrictive material. Also, there would still need to be a magnetic field source as the magnetostrictive material would act mainly as a controllable shielding between the magnetic field and the annulus.

Since the magnetostrictive property of the material is created by the grains re-orienting themselves due to strain, using a magnetostrictive material to create a magnetic field downhole could possibly compromise the tool's integrity resulting in failure.

8. EXPERIMENT DESIGN

8.1 BASIC SETUP

Based on the above literature review it has been determined that the best design to test these ideas would be a flow loop. This flow loop will be described in more detail in the Flow Loop Design subsection. These experiments were designed with flow down an inner pipe and up an annulus in order to simulate annular flow as seen in the drilling industry.

Due to the before mentioned problems associated with magnetostrictive materials, as well as the different methods for possibly having the formation magnetized, it has been determined that a magnetic field generator attached to the outside of the inner pipe would be the best method for these experiments. Due to the previously mentioned complexity and challenges involved in having an electromagnet down hole, especially with regards to its possible reliability, it has also been decided that a permanent magnet would be the best option for these experiments as well as for the real world application.

Even though an electromagnet would allow for an improved study of how the magnetorheological drilling mud changes due to the influence of a magnetic field, it would be very arduous to design a setup such that the electromagnet is attached to the inner pipe. Other researchers have gotten around this complication by applying a magnetic field from outside of the outer pipe, but this would not be very realistic with regards to the current embodiment of the tool because this would involve the magnetic field originating from the formation (Spaggiari and Dragoni 2012) (Zhang et al. 2004) (Wang and Gordaninejad 2006) (Becnel et al. 2015) (Ngatu and Wereley 2007) (Lopez-Lopez et al. 2006).

A vertical setup would be more realistic given that this technology would be most likely not be used in horizontal wells, where changes in the pressure/window are relatively small. Due to the

lack of suitable locations for a vertical setup, a horizontal setup was used. A horizontal pipe will also make cleaning and adjustments between experiments, which will be discussed in more detail later, much easier.

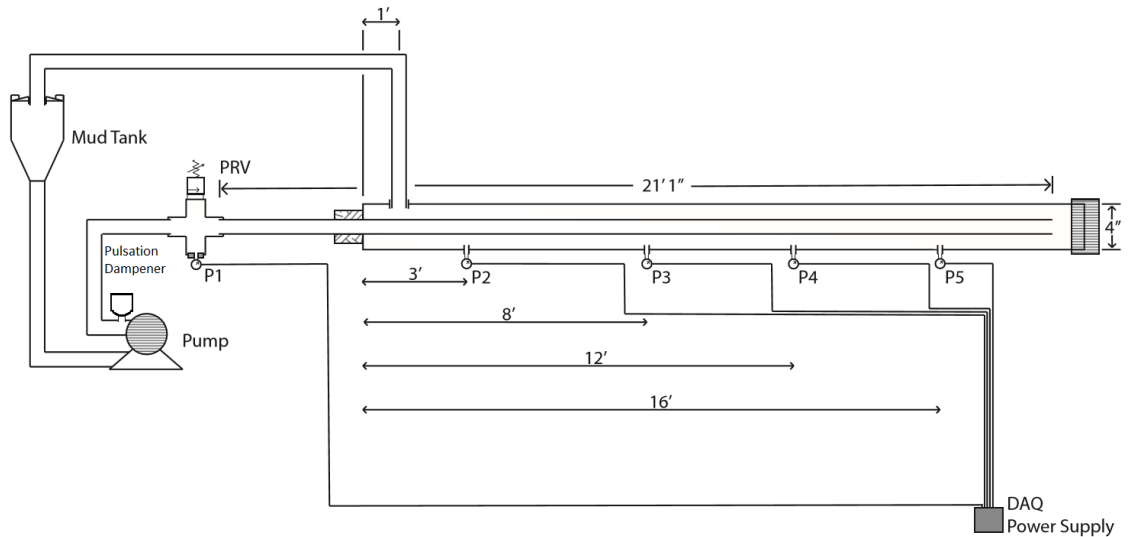


Diagram of flow loop.

In summation this experiment involved the magnetorheological drilling mud being pumped down an inner pipe, and then returning back through the annulus. The magnets were securely attached to the outside of the inner pipe.

8.2 MAGNET CHOICE AND PLACEMENT

As previously mentioned the magnets were attached to the outside of the inner pipe. Research indicated that the best permanent magnets for field use would be samarium-cobalt magnets. The main issue preventing these specific magnets from being used in the experiments that were conducted is that samarium-cobalt magnets are relatively expensive and do not already come in the sizes and shapes that were required based on the experiment design. Neodymium motor magnets come in segmented rings with inner diameters slightly above, and slightly below the

experiment's inner pipe's outer diameter. The magnetic flux of these magnets is very similar, though potentially slightly higher, than the samarium cobalt magnets that research suggested would be better suited for field use. Both magnets are around 1 tesla (10000 Gauss) of magnetic flux on their surfaces.

The magnet segments being used are neodymium motor magnet segments purchased from Apex Magnets. The smaller of the magnet segment rings is 43mm (1.69") outside diameter, by 39mm (1.54") inside diameter, by 5mm (0.2") axial length. The larger of the magnet segments rings is 54mm (2.13") outside diameter, by 46mm (1.81") inside diameter, by 20mm (0.79") axial length. The ring segments are grade N45H neodymium magnets with a nickel coating with the magnetic dipoles pointing radially outwards.

The magnet segments were placed such that they form a nearly complete ring around a section of the inner pipe. This allowed for a more uniform magnet placement and field with regards to circumferential location. The magnets were arranged such that the magnetic dipoles of the individual segments are identical for all magnet segments comprising each individual ring. The rings were arranged such that the first two rings were composed of smaller magnet segments and the next two rings were made up of the larger ring segments. The first and last rings in this arrangement had their south magnetic dipole facing outwards into the annulus. The inner two rings had their north magnetic dipole facing outwards into the annulus. The locations of the first smaller magnet ring was 9 feet and 3 inches from the outlet of the inner pipe. The next rings were 1 inch, 1.5 inches and 1.5 inches downstream from this first ring, respectively. Therefore these magnets occupied 6 inches of axial length.



Image showing magnet rings and middle centralizer on inner pipe

An Extech Model MF100 Hall Effect sensor was used to determine the magnetic field strength of the rings at various circumferential phases and radially distance from the pipe. It was to confirm that the magnetic fields produced by the magnet segments was not detectable within the inner pipe. This data is shown in Appendix E.

8.3 MATERIALS AND FLOW LOOP PARTS

The purpose of these experiments is to upscale previous work and get closer to a real world test of the theories involved. In a real world application, it is theoretically possible to have the magnets attached to the inside of a casing string instead of on the pipe. This would eliminate the problems associated with the tool moving downhole with the drill pipe, but would neglect its benefits and purpose since the casing strings would already be protecting less competent formations. Therefore, at least in theory, this tool would be operating in open hole, i.e. no casing on the outside. As casing is typically made of steel, which would interact with a magnetic field; it was decided that a stainless steel, specifically 304 stainless steel, was to be used for the outer pipe for the purpose of these

experiments. This will prevent interactions, such as changes in the magnetic field and additional pull forces on the magnets, between the magnets and the open hole formation substitute.

The inner pipe was made of iron/carbon steel, specifically Society of Automotive Engineers (SAE) grade A106 carbon steel. The purpose of using carbon steel as the inner pipe is that it would interact with the magnetic field and magnets. This means that the magnets were attracted to the inner pipe. It also means that the inner pipe acted as shielding to prevent, or at least greatly reduce, the magnetic field from influencing the magnetorheological drilling mud while it is inside the inner pipe. This last part was important because, as explained previously, it would be very undesirable to have the magnetorheological fluid affected within the drill pipe for this researches intended purpose.

Four separate $\frac{1}{4}$ " threaded outlets (thread-o-lets), made of 304 stainless steel, were welded to the outer pipe at pre-determined locations. The threaded outlets were the same stainless steel as the outer pipe to prevent galvanic corrosion. The locations of these threaded outlets will be discussed in the measurements subsection. A larger, $1\frac{1}{2}$ " threaded outlet was welded on to act as the outlet for the flow loop.

The end cap on the 4" outer pipe, $1\frac{1}{2}$ " cross, 4" to 2" reduction bushing, $1\frac{1}{2}$ " to $1\frac{1}{4}$ " reduction bushing, $1\frac{1}{2}$ " to $\frac{1}{4}$ " reduction bushings are all 304 stainless steel as well. These parts are rated for higher pressures than the pressure relief valve, to reduce the chance that they are damaged during the experiments.

There is an annular sealing gland that the inner pipe passes through. This forces the fluid to exit through the larger $1\frac{1}{2}$ " threaded outlet to allow for the collection and reuse of the drilling fluids. A PG9-125P-A-T annular sealing gland from Conax Technologies was used for this purpose. This sealing gland consist of a main body that has a male 2" NPT connection and an inner hole for a

pipe to pass through. The inner hole is specifically designed for a 1.66" O.D. pipe (a standard 1.25" schedule 40 pipe) to pass through it. There is a thick Teflon element that lines this inner hole. When a flange on top of the sealing gland is tightened down using its 6 bolts, it pushes down on a metal ring on top of the Teflon sealing element. This in turn pushes the Teflon sealing element down on a bevel in the main body of the sealing gland, compressing it around the inner pipe.

8.4 FLOW LOOP DESIGN

The outer pipe is 20 feet and 2.6 inches long. The additional 2.6 inches are so that each end can be threaded with 1.3 inches of 4" NPT. The inner pipe is approximately 21 feet of 106A carbon steel. A 4" end cap was threaded onto the end of the 4" stainless steel outer pipe farthest from the 1 1/2" welded outlet. The other end of the outer pipe had a reduction bushing from 4" NPT to 2" NPT. The 2" NPT end was attached to the male 2" NPT of the annular sealing gland.

The inner 106A carbon steel pipe passed through this annular sealing gland and terminated approximately 6 inches from the other end of the outer pipe. The upstream end of the inner pipe screwed into a 1 1/2" to 1 1/4" reduction bushing that was itself threaded into the 1 1/2" cross. One of the cross ends perpendicular to the pipe contained a 1 1/2" to 1/4" reduction bushing. This reduction bushings had one of the pressure transducers threaded into it. The other end perpendicular to the primary flow direction had a pressure relief valve (PRV) threaded into it. The end of the cross directly across from where the inner pipe was threaded in contained the hose coming from the pump. The pump was a Watson Marlow Bredel 40-57 peristaltic pump. In order to reduce the pulsation associated with peristaltic pumps, also known as hose pumps, a Blacoh 905ND pulsation dampener was attached between the pump outlet and hose.

The hoses were standard tank truck hoses with steel 1 1/2" NPT ends. A 4' hose went from the outlet of the pump to the inlet of the pipe. This 4' hose was threaded into union type connections

to allow for quicker and easier connection and disconnection while allowing it to maintain a higher pressure rating. The bottom of the mud tank was connected to the inlet for the pump through a 7' hose. The 7' hose used cam and groove type connections to allow for quick disconnects. Union connections were used instead of cam and groove type connections on the upstream hoses due to the higher pressures seen there. The outlet of the pipe was connected back to the inlet for the mud tank through a 12' hose.

The inner pipe has an inner diameter of 1.38" and an outer diameter of 1.66". This gives it a capacity factor of 0.00185001 barrels per foot, or 0.077700408 gallons per foot. The outer pipe has an inner diameter of approximately 4" and an outer diameter of 4.5". This gives it a capacity factor, with the inner 1.66" outside diameter pipe, of 0.012866136 barrels per foot, or 0.540377696 gallons per foot. This also gives it a capacity factor, without the inner pipe inserted, of 0.015543035 barrels per foot, or 0.652807461 gallons per foot. When a 253 inch inner pipe inside of the 20 foot long outer pipe is taken into account, with 6 inches of open outer pipe, the result is approximately 0.259 barrels of volume, or 12.5 gallons. Due to hoses and other flow loop parts the actual flow loop needed approximately 15 gallons of fluid to fill it. The total amount of fluid used for experiments was 55 gallons to ensure that there was always enough fluid to prevent the pumps from running dry.

8.5 MEASUREMENTS

If it is to be shown that the setup does indeed create a pressure drop in the desired location, then there also needed to be a measuring system in place in order to obtain evidence to either support or disprove these claims. The first of these pressure measurement points, going from upstream to downstream, was at the inlet to the inner pipe, specifically in the previously mentioned cross. The next pressure measurement was taken 4 feet up the annulus from the 4" end cap. This was

approximately 3 feet and 6 inches downstream from the inner pipe outlet. The difference between these measurements gave an approximate value for the pressure losses in the inner pipe. This is important because it had to be shown what influence, if any, the magnets would have had on flow through the inner pipe.

The next pressure measurement occurred four feet farther up the annulus. This measurement would also be approximately 1 foot and 9 inches upstream from the magnet assembly. The difference between these measurements gave a pressure loss in the annulus without the influence of the magnetic field.

The next pressure measurement occurred an additional 4 feet up the annulus. This was also approximately 1 foot and 9 inches downstream from the magnet assembly. This differences in pressure measurements between the different fluid types gave an estimate of the pressure drop being caused by magnetorheological effect.

The last pressure measurement occurred an additional 5 feet downstream of the preceding one. This was 2 feet upstream of the outlet, which was open to the atmosphere. The difference between this pressure measurement and the one immediately downstream of the magnetic fields location showed the pressure drop occurring after the fluid had left the magnetic field. The purpose of this last pressure measurement differential was to provide evidence for the magnetorheological fluid having its rheological properties return to what they were before the influence of the magnetic field.

In order for the pressure measurements to be taken and read accurately, in real-time, it was decided to use pressure transducers that would allow for the eventual output of the data as an easy to analyze computer file. This allowed for the easy comparison of the pressures from different locations in the pipe while the experiments are being conducted, as well as after. The pressure

transducers being used were Honeywell FP2000 model transducers with a 0-750psi range, with 0.25% accuracy and with a 1/4" NPT male connector. These are silicon based piezoelectric pressure transducers.

These pressure transducers, which contain an internal amplifier, output the readings as a single current based analog signal. This signal traveled to a National Instruments (NI) 9203 electrical current based analog signal module inside a compact data acquisition (cDAQ) 9174 chassis. The data was transmitted via a universal serial bus (USB) to a computer containing Laboratory Virtual Instrument Engineering Workbench (LabVIEW) software. This accommodated easy acquisition and reading of the data.

The power supply was a SolaHD model 1-24-100T. This converted the 120 volt alternating current municipality power to 24 volts of direct current that the pressure transducers require. The power supply was connected to a fuse block containing a 1/2amp fuse to protect the pressure transducers. These smaller electrical parts, as well as the cDAQ chassis were located within a NEMA 4 rated enclosure to protect them from the elements.

8.6 MAGNETORHEOLOGICAL DRILLING MUD

The drilling mud's design was based on previous experiments and desired final characteristics. Previous work had shown that the carbonyl iron weighting material had negligible effects on the rheological properties of the drilling mud when not under the influence of a magnetic field. The batch size was based off of the standard 350 milliliter (mL) samples created for lab experiments. Under this scenario 41 grams of carbonyl iron particles with 23 grams of bentonite were added to 350 milliliters of water. A barite weighted mud of the same density would consist of 48 grams of barite with 30 grams of bentonite being added for the same lab experiments.

The carbonyl iron particles have a density of 7.86 g/cc. Bentonite has a density of approximately 2.6 g/cc and it is also assumed that the water was approximately 1 g/cc. This means that there was 5.216 cubic centimeters (cc) of iron particles, 7.69 cc of bentonite and 350 mL of water. The total mass of 411 grams divided by the 362.91 cc per batch comes to a density of approximately 1.13 g/cc, or 9.43 PPG.

These smaller sized batches were created in a lab setup first in order to determine the base rheological properties of the fluid as well as confirm that the desired density was correct. An API filter press experiment was conducted as well to confirm that the new weighting material did not significantly alter the fluid's ability to create a mud cake and to prevent excessive fluid loss when it was not desired.

It can be shown through simple calculations that the previously mentioned 55 gallons of drilling mud required 23.44kg (51.75lbs.) of carbonyl iron microspheres in order to maintain the desired 10% by weight iron particles. It has also been determined that this experiment required 13.15 kilograms of bentonite. These materials were added to 52.87 gallons of water.

The iron particles were added in batches of 0.5kg/batch. This number was chosen to simplify the process and to allow for multiple experiments to be conducted as more weighting material is added. These particles were added slowly, over a 6 day period, with test being conducted after every 1-3 batches were added. How many batches to be added between tests was determined based on the results of the previous test, and quick comparison between the last two tests conducted. These comparisons were done in the field in real time.

8.7 SAFETY CONSIDERATIONS

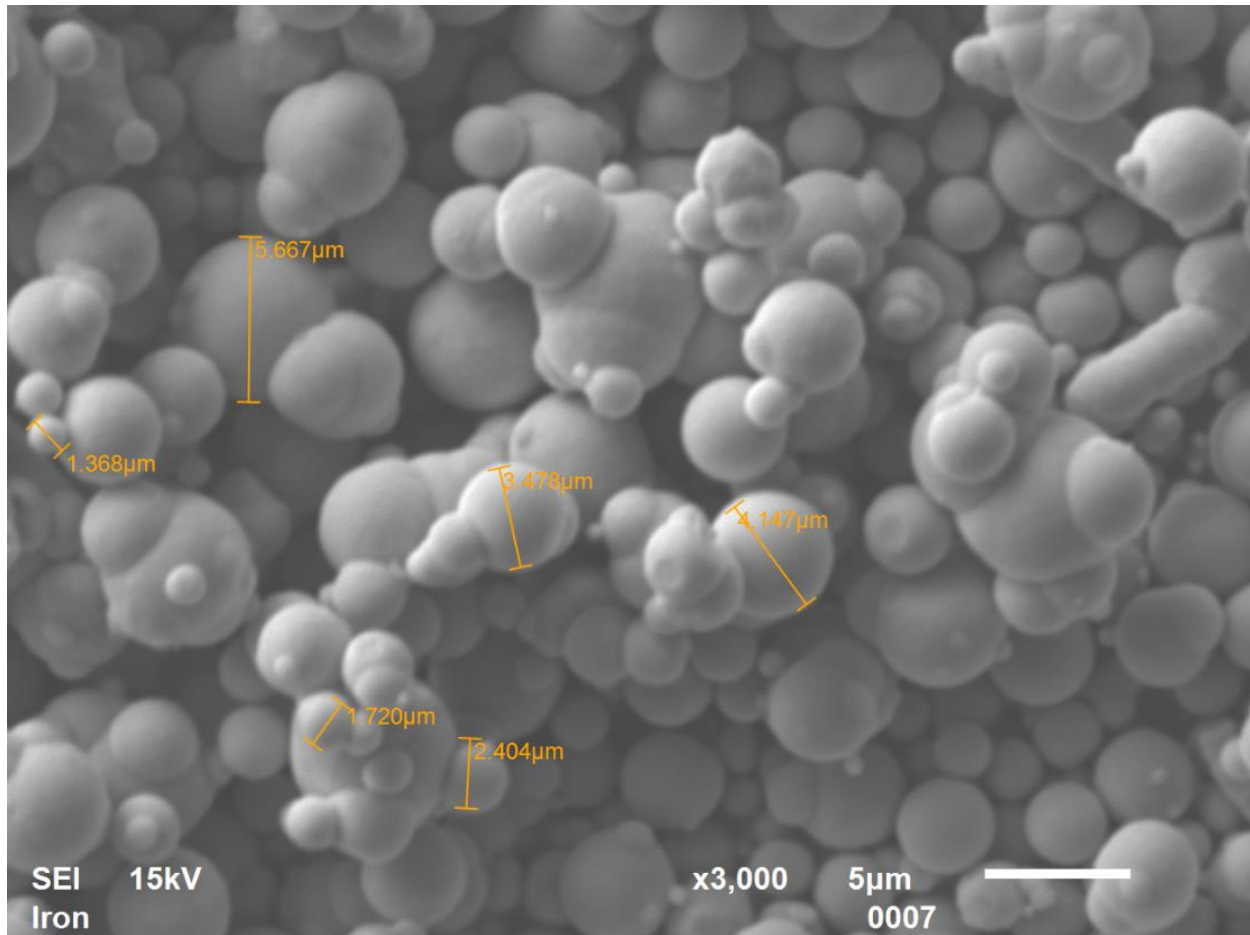
A major consideration before the start of any experiment is the health and safety of those involved, and potential impact to the immediate surrounding environment. Work was done with the suppliers

of the materials as well as with Environmental Health and Safety (EHS) at Louisiana State University in order to ensure that those involved in the experiments, as well as those in the immediate vicinity, were protected at all times.

The carbonyl iron microspheres have a diameter in the 1-10 micrometer range. This, in combination with their high density of 7.8 g/cc means that the particles are not a major inhalation or explosion risk. Even so, the mixing process has the potential to force the carbonyl iron particles to become airborne. EHS at LSU suggested anyone working near the mud tank during mixing wears an N100 mask to prevent the possible inhalation of particles. EHS also suggested glasses or goggles be worn to prevent the particles from entering the eyes and lab coats be worn to prevent the particles from coating workers clothes. Lastly EHS suggest that, depending on the wind velocity, anyone without the proper protective gear stay at least 5 feet away from the mixing.

As the carbonyl iron particles are a flammable solid, they were stored in such a way as to prevent them from coming in direct contact with flames or sparks. EHS has suggested that the particles be stored in their original containers where possible, and in plastic, air tight containers when their original containers have been compromised (opened). They also suggested that the containers be stored in a fume hood to further reduce the risk.

A geomembrane produced by Plastatech was used for spill containment. This geomembrane was 30' by 4' by 1'. This allowed for the entire system, excluding the electronics enclosure, to be within the spill containment area. This spill containment area was also able to hold approximately 897 gallons of material, minus the volume occupied by experiment equipment contained within the geomembrane.



Scanning Electron Microscope image of iron microspheres at 3000x zoom.

8.8 EXPERIMENT SETUP

First the inner pipe had its rust removed with an angle grinder with an attached grinder wire wheel. Then the centralizers were welded on. The centralizers were located near the outlet of the inner pipe, as well as approximately 9 inches downstream of the magnet assembly.

The individual centralizer blades were phased 90 degrees from each other and beveled to reduce upsetting the flow. The inner pipe was also rotated such that the centralizer located after the magnet assembly were phased 45 degrees from the pressure transducers. The magnets were then placed on the inner pipe as described in the magnet choice and placement subsection. Loctite heavy duty two part epoxy was used to coat these magnets, and help keep them protected and assure that they remain attached to the inner pipe during experiments.

The annular sealing gland was then threaded into the 4" to 2" reduction bushing. The inner pipe was then inserted, upstream side first, into the annular sealing gland. The reason for inserting the upstream side of the inner pipe through the annular sealing gland is due to the fact that the magnets and centralizers cannot pass through the sealing gland as well as reducing the amount of pipe that must be fed through the sealing gland. Once this had been done the annular sealing gland was tightened down. The 4" to 2" reduction bushing was then threaded onto the outer pipe, on the end closes to the 1 ½" threaded outlet.

8.9 MUD PROCEDURES

The first fluid tested was water. This allowed for a proper calibration and test of the pressure transducers. It also gave a good indication as to whether or not the connections were liquid tight. After the system had been tested with water, a bentonite and barite based mud, using the same mass of bentonite as the planned magnetorheological drilling fluid, was created. The previously mentioned 48 grams of barite per lab sample batch leads to adding 27kg (59.8lbs.) of barite to 52.2 gallons of water and approximately 13 (28.7lbs) of bentonite for a 55 gallon batch.

First the correct amount of water was added and attached mixer started. The mixer was a Grovhac Inc. 1/2hp variable speed drum mixer with 0-1725rpm output. Next the bentonite was added and allowed to mix for approximately 24 hours. After the bentonite had been properly mixed and hydrated the barite was added. The barite was added in batches of 0.575 kilograms each. This was done to have measurements at different mud weights. The 0.575 kg/batch was chosen based on having the same total number of batches as the magnetorheological drilling fluid.

The magnetorheological drilling fluid was created next. The procedure was the same as was used for the barite based drilling fluid, except the proper safety equipment was used as described in the

safety considerations subsection. Iron particles were added, in amounts specified in the magnetorheological drilling mud subsection, instead of barite.

8.10 EXPERIMENT PROCEDURES

Once all the individual parts had been properly connected the outer pipe was rotated such that the 1 ½” threaded outlet was facing up. This allowed the air inside the pipe to escape. Once the fluid has started flowing out of the outlet, the end closest to the 1 ½” threaded outlet was slightly elevated to allow for the gas to accumulate and escape through the outlet. The other end was then slightly elevated relative to the rest of the pipe before the threaded outlet end was elevated again. This allowed for any gas trapped near the previously elevated 4” to 2” reduction bushing to escape. The experiment setup was then set back down on its pipe stands and rotated such that the 1 ½” threaded outlet is facing down.

The fluid was run through the system and pressure measurements recorded. The system started flow at the 60 Hz rating (57 rpm, 0.62ft/s in the annulus) setting on the pump. After 5 minutes of pressure measurements the pump speed was reduced by 10 Hz. This process was repeated until the readings at 10 Hz were taken, at which point the measurements were stopped so that new batches could be added. Once the experiments had finished the pump was turned off.

The outlet hose was then removed from the mud tank and placed into 55 gallon waste disposal drums, and the pump was turned on. Once the fluid level in the mud tank was significantly reduced water was added to the mud tank. This was then sent through the flow loop until the fluid leaving the other end of the flow loop was clear water. The waste disposal drums then had their bungs closed before being taken to Hazardous Materials Management at LSU for disposal. This cleanup and disposal was only done after all experiments had been conducted.

It should be noted that lab experiment results have shown that the particles will not significantly settle over the course of a week, and therefore can be left to gel in the flow loop between experiments.

9. LAB RESULTS

In this section the results of standard petroleum bench top experiments will be discussed. This will include the experiments that were used to determine how much bentonite should be used for the larger flow loop setup, as well as observations of these mixtures over time. These test were done using the API 13B-1 standards.

9.1 SAMPLE CREATION PROCEDURES

It was determined, through poor early test results, that in order for the bentonite to be effective it had to be hydrated first. An effective bentonite in these experiments is one that either greatly reduces, or prevents the iron microspheres from settling over the course of a few days. It is not uncommon that additional time must be taken for bentonite to hydrate in field scale operations. All materials were mixed in a Hamilton Beach model 936-1 mixer. The speed ratings on this mixer were 10,000 rpm at low speed, 14,000 rpm at medium speed, and 17,000 rpm at high speed. It should be noted that as the viscosity of the fluid increases the rotational speed of the mixer decreases, which is why the mixing speed is being listed as the machine setting instead of that settings associated rpm rating.

For all lab mixtures, first the bentonite was mixed with approximately 350 mL of water for 10 minutes at the high mixing speed. These mixtures were then allowed to sit in their respective storage cups for approximately 24 hours to allow the bentonite to hydrate. The hydrated bentonite mixes were then added back to the mixing container. The weighting material, whether barite or iron microspheres, was finally added and mixed at the high speed setting for 10 minutes. The mixer was therefore not on during the addition of the weighting materials, but turned on immediately after the particles were added. The mixer was off for the initial seconds that the weighting material was added to prevent the particles from becoming airborne.

9.2 SAMPLE TESTING PROCEDURES

After the weighting material was mixed in the sample was immediately taken to a Fann 35A rotating bob viscometer in order to test the fluids rheological properties. Initially the rotating viscometer was set to 600rpm for the first reading. After waiting 10-15 seconds for the reading dial to stop changing the value was recorded. Next the 200 rpm and 6 rpm readings were taken using the same procedure as the 600 rpm reading. The Fann 35A was then switched over to its lower speed settings and the 300 rpm, 100 rpm, and 3 rpm readings were taken. The fluid was then allowed to sit for 10 seconds before the viscometer was turned on again at 3 rpm to take the 10 second fluid gel strength reading. Finally the viscometer was rotated at 600 rpm again for 1 minutes and then stopped. The fluid was then allowed to sit for 10 minutes before turning the viscometer on again to take the 10 minute gel strength reading. Combined, all of these readings make up standard API viscometer readings for petroleum drilling fluids.

9.3 DETERMINING BENTONITE AMOUNT

The amount of bentonite used was determined based on multiple lab experiments. These experiments focused on obtaining viscoelastic properties for the magnetorheological fluid that would allow for the proper suspension of the weighting materials, without also having a prohibitively high apparent viscosity. The higher the viscosity of the fluid being used in the field the higher the frictional pressure losses and associated work required by the pump.

9.4 DISCUSSION OF LAB RESULTS

The samples listed as 0.1 and 0.2 were the first samples made that did not suffer from high settling of particles and low viscosity due to lack of bentonite hydration. This was determined based on the observation that there was not significant settling of particles after letting the samples sit

undisturbed for approximately 24 hours. Putting the samples back into the mixer at high speed for 10 minutes brought most of, if not all, of the observed settled particles back into suspension.

Sample Names and Compositions

Sample Name	Date Created	Bentonite (grams)	Barite (grams)	Iron (grams)
Sample 0.1	7-11-17	25	48	0
Sample 0.2	7-11-17	30	48	0
Sample 1	7-26-17	30	0	41.53
Sample 2	7-27-17	25	0	41.6
Sample 3	7-27-17	20	0	41.51
Sample 4	8-1-17	20	0	82.16
Sample 5	8-1-17	0	0	41.38
Sample 6	8-4-17	23	0	41.08
Sample 7	8-13-17	23	0	41.03
Sample 8	8-13-17	23	0	41.14
Sample 9	9-27-17	23	0	41
Sample 10	9-27-17	23	0	41
Flow Loop	1-24 to 1-30	23lbs./bbl.	0	41lbs./bbl.

When Sample 1 was created the effect of the magnetic field on the fluid was briefly tested. Observations of this sample clearly showed the iron particles being removed from suspension when a stack of the larger magnets was placed on the outside of the low magnetic permeability mixing cup. A material with a lower magnetic permeability will only slightly influence a magnetic field. It is possible that this is due to the particle size being in the 4 micron range. This assumption was based on previous experiments that have been conducted with particles in the 40 micron range

not showing this same phenomenon. It should also be noted that the 40 micron samples previously worked with were also at a higher weight percent; 40% by weight as opposed to 10% by weight. The radius of effect of this phenomenon was between 1 and 2 inches.

Sample Rheological Testing Results

Readings (rpm)		3	6	100	200	300	600	10s.	10 min.	Density
Sample Name	Date									
Sample 0.1	7-11-17	3.5	4	10.5	13.5	18	36	3	7	9.1
Sample 0.2	7-11-17	4	6	14	19	23	32.5	4	11	9.35
Sample 1	7-26-17	12	13	29.5	38.5	47.5	62	8	21	9.35
Sample 2	7-27-17	11	12	26	33.5	40	53	8	19	9.4
Sample 3	7-27-17	4	4.75	9	12	15	21	4	6	
Sample 4	8-1-17	6	6	14	18.5	22.5	31.5	4	9	10.15
Sample 6	8-4-17	5	6	16	21	25	34	5	9	9.35
Sample 2	8-7-17	8	10	27	37.5	47	66	7	16	
Sample 7	8-13-17	5	5	14	19	23	32	4	9	
Sample 8	8-13-17	6	6	16.5	21	26	35	4	9	
Sample 9	9-27-17	5.5	6	15	19.5	24	32	4		
Sample 10	9-27-17	6	6	16	21	25.5	35	4.5		
Field	1-31-18	4	5	17	24	29	42	4	9	9.3

A top was put on the Sample 1 container, creating an airtight seal. The sample was then allowed to sit for approximately 24 hours in its container. Based on these results, specifically the particles not significantly settling, it was determined that lower amounts of bentonite should be tested.

Filter Press Test Results

Sample Name	Time	.25	1	2	3	4	5	6	7.5	pH
Sample 2		3 drops	.9	2	2.5	3	3.5	4	4.5	N/A
Sample 9		1	1.5	3	3.5	4.25	5	5.5	6.5	8
Sample 10		0.5	1	2.5	3.5	4	5	5.75	6.5	9
Field		1	1.5	2.5	3.5	4.5	5	5.5	6.5	8

There was not significant settling of Sample 3 after 21.5 hours of sitting in its container with the airtight top on, and no agitation. It was not possible to see the bottom of the container due to the opacity of the fluid. Therefore the lack of particle settling was determined by physically disturbing the bottom of the container. Another method for determining particle settling was to turn the container on its side and see if there was a layer of particles on the bottom.

Samples 1, 2 and 3 were reexamined for settling at 4, 5, and 5 days respectively after mixing. Minor agitation (turning the container on its side) returned any settled particles into suspension in Sample 2. The other samples, samples 1 and 3, were too opaque to visually determine amount of settled particles. From these observations it was decided that a sample should be created with the lower amount of bentonite, 20g, and double the amount of iron particles, 82g, in order to increase the amount of settling.

Sample 2 was put back into the mixer for another 10 minutes and then its properties were re-tested at 11 days after its initial creation to test for time dependent rheological effects. It was also at this time that Sample 2 was used for an API filter press test.

A small amount of rust developed on the filter cake particles after they had dried, but most of the particles remained visually rust free. It is also possible that there is some sort of chemical reaction

between the bentonite and the iron particles that prevents the rust, but this research was not able to confirm this with equipment.

The particles in Sample 4 did not settle out immediately (within the first hour of observation). Also the viscosity and yield strength values were lower than expected considering the much higher amount of suspended particles in the fluid.

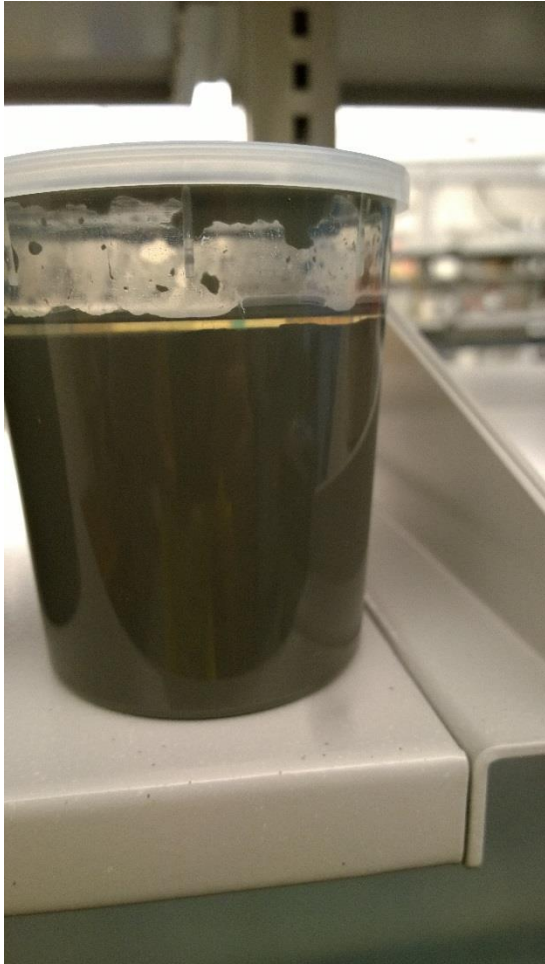


Image of sample 4 taken 15 days after mixing.

An interesting phenomenon was first noticed in sample 4, and then all closed container samples, where an upper water layer develops. It is unknown if this is due to particles settling out of the top layers, or some sort of evaporation and precipitation of the water over time. The evidence for the

evaporation and precipitation hypothesis is the amount of liquid that appears on the upper container walls and top even though no agitation has occurred.

Another interesting observation is that the upper layer of the particle containing fluid matches the top of the upper water layer. This happens regardless of how the fluid layer is, such as the fluid still containing particles following the water layer up the edges of the container. This means that the upper water layer has a uniform thickness, regardless of shape, when not in agitation.

Sample 5 was then created, with the purpose of determining the amount of rust and settling that would occur on the iron microspheres in water open to the air and in the absence of bentonite.

24 hours after mixing Sample 5 there were still some iron particles floating on the surface of the water. One side of the settled particles had a slightly brownish tone to them after 24 hours as well. It is possible that these slightly brownish particles were particles originally floating on the surface that rusted and then sank down.



Image of Sample 5 approximately 1 week after mixing

Sample 6 was created to have rheological properties between Sample 2 and 3. The container for Sample 6 was left open to the atmosphere, similar to Sample 5, in order to determine if any

significant phenomenon such as rust would occur over the course of a few days. This was an important test because the flow loop sample would be left outside, in the open air for at least 7 days during experiments.



Sample 6 at 71 hours after mixing

After approximately 72 hours Sample 6 showed a highly gelled surface. It is believed that this was due to water evaporating near the surface of the container, leaving a much higher concentration of particles at/near the surface. The fluid was inspected by hand to confirm that there was not a significant amount of settled particles on the bottom of the container.

As sample 6 continued to dehydrate a ring of particles on the container wall began to form and follow the top of fluid layer down due to gravity. As these particles dried, some of them began to rust as well. Only some of the particles rusted, and even then only the dried particles on the container walls. It is possible that the reasons for some of these particles not rusting was due to them being physically embedded in the bentonite, and therefore unable to chemically interact with oxygen. As Sample 6 continued to dehydrate, and the level of the fluid decreased, the thickness of the particles against the container walls increased.

Samples 7 and 8 were created to confirm that the rheological properties seen in Sample 6 were consistent and not a product of chance. Sample 7 was put in an airtight container and Sample 8 was left open to the atmosphere. Sample 8 was left open to the atmosphere to test whether or not the same phenomenon seen in Sample 6 were observed again.

Samples 9 and 10 were created in order to increase the amount of data points to support the decision to use 23g of bentonite and 41g of iron particles for the flow loop experiments. These samples were also put through a filter press test for more data points, as well as to create the mud cakes that were examined with SEM and EDS. Results of these test were consistent with the results seen from sample 2. The SEM and EDS results will be discussed in their respective section later.

9.5 RUST MIXING TEST

Before the flow loop sample was created a final test was attempted based on previous results. Previous experiments had all been conducted with static fluid, and the flow loop test would involve constant agitation in the mud tank, and static fluid in the rest of the flow loop when experiments were not being conducted. The test was to keep the fluid in constant agitation in the lab mixer for 24 hours and observe the results.



Image of Sample 8 at 31 days after mixing

The main problem with this little experiment was the amount of agitation that the Hamilton Beach mixer created regardless of its speed setting. After only 3 hours of constant mixing it was found that approximately 50mL of fluid had been ejected from the container due to agitation. It was then decided that the test would not be possible with the lab equipment at hand and was abandoned. Particles coated onto the mixing cups walls showed significant signs of rust after 24 hours. This

amount of rust was not seen in any other experiments and is likely to be attributed to the particles being caked onto the wall of a tin cup instead of a plastic container.

9.6 LAB CONCLUSIONS

The lab observations suggest that the combination of water and bentonite helps to prevent, or at least retard rusting. The particles began to rust in the lab experiments only after drying, and even then only when the dried particles were in a thin layer instead of a large chunk. The only exception to this being Sample 5 that consisted only of water and iron particles. Even in these thin layers, rusting only occurs when the particle layers had shrunk due to dehydration. This can clearly be seen in images of Sample 8 in Appendix G, but these phenomenon were consistent across all samples.

10. SEM AND EDS RESULTS

The base particles used to create samples, as well as some of the samples themselves, were examined using Scanning Electron Microscopy (SEM) and Energy Dispersive Spectrometer (EDS). This was done to confirm that the different materials being used were what they were claimed to be, as well as to test for things such as interactions involving the iron particles. The SEM used was a JOEL JSM-6610LV SEM, with EDAX EDS.

Before being put into the SEM, particles were coated for 3 minutes in an EMS550X Sputter Coater set at 0.1mbar vacuum and 25mA current with platinum. This was done to prevent the electrons from charging up the areas being examined. Insufficient coating, and therefore excessive charges piling up, would be seen as bright white areas on the images, or horizontal lines shifting the image sideways in places.

10.1 PARTICLES

The API Barite used conformed to API standards for barite sizes. It also was almost entirely Barium Sulfate, with small readings in the EDS for Aluminum, silicon and calcium that appeared with full area EDS, but were smaller than their own error bands.

The bentonite used was sifted through both 10 and 20 mesh sifters. This was done to remove larger, harder particles that were in the older, already opened bentonite bags. There were no unexpected observations from the SEM/EDS imaging of the bentonite. This sifting was not done for the bentonite used in the magnetorheological experiments, as that bentonite came from a new, unopened bag and hand sifting showed none of these harder particles.

The iron microspheres were 99.5% purity, 1-10 micrometer carbonyl iron powder, listed as CBL-FE-025M-P.10UM from American Elements. The actual analysis, furnished by American Elements, states that the powder sent to us was specifically 98.6% iron, 0.68% carbon, 0.18%

oxygen, and 0.1% nitrogen. American Elements did not specify how they analyzed the particles though.

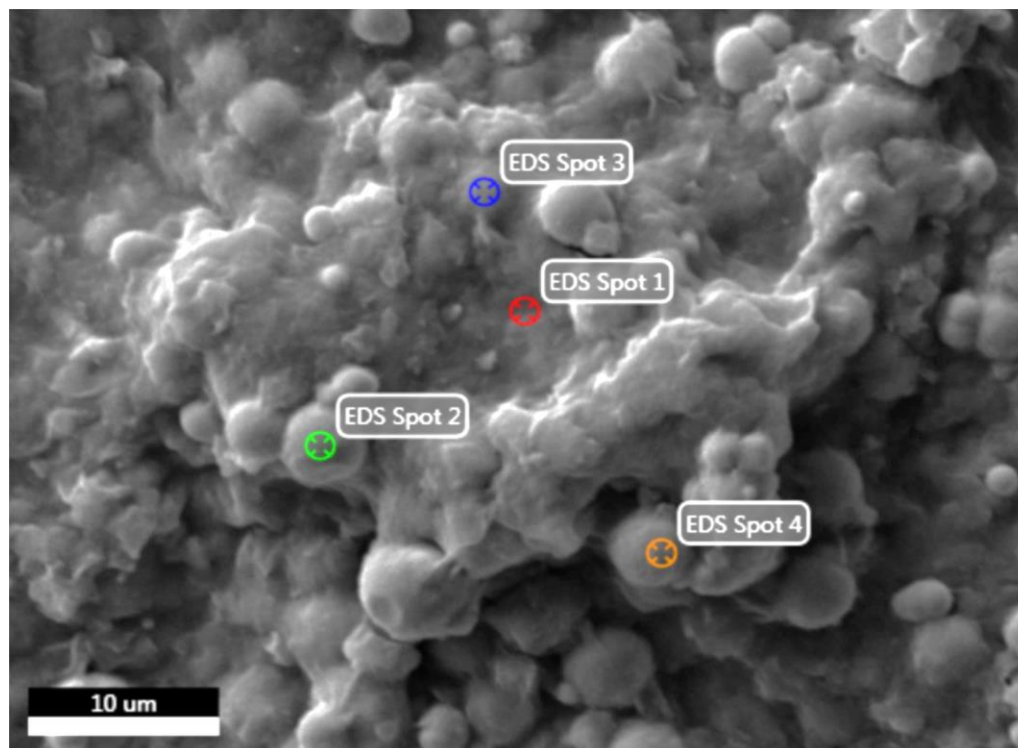
The particles were confirmed to be almost completely iron. The platinum coating was not necessarily needed to prevent the iron particles from gaining charge, but was used anyways to keep the particles consistent with particles that would be examined in the mixed samples. The cobalt listed was within its own range of error, and is also listed very close to the iron particles. It is highly likely that the cobalt shown is purely an error and is only shown because of its similarity to iron within EDS. It is possible that the carbon, oxygen, and nitrogen particles exist within these samples, as stated by American Elements, and are just too scarce to be properly detected.

The pile that this iron sample was originally taken from was left in a petri dish with its lid sitting on it for 107 days. Whereas there was a lid on this dish, it was in no way air tight. This was confirmed by the lab samples that were in similar petri dishes oxidizing (rusting) when stored under the same conditions over the same period of time. After these 107 days these particles were taken to be coated and tested in the same manner as previous samples. The results of the EDS test surprisingly showed similar results to the previous iron microspheres test. This would suggest that no rusting had occurred on the particles and would indicate that these particles do not rust in open air in the atmospheric conditions present in the lab.

10.2 LAB SAMPLE

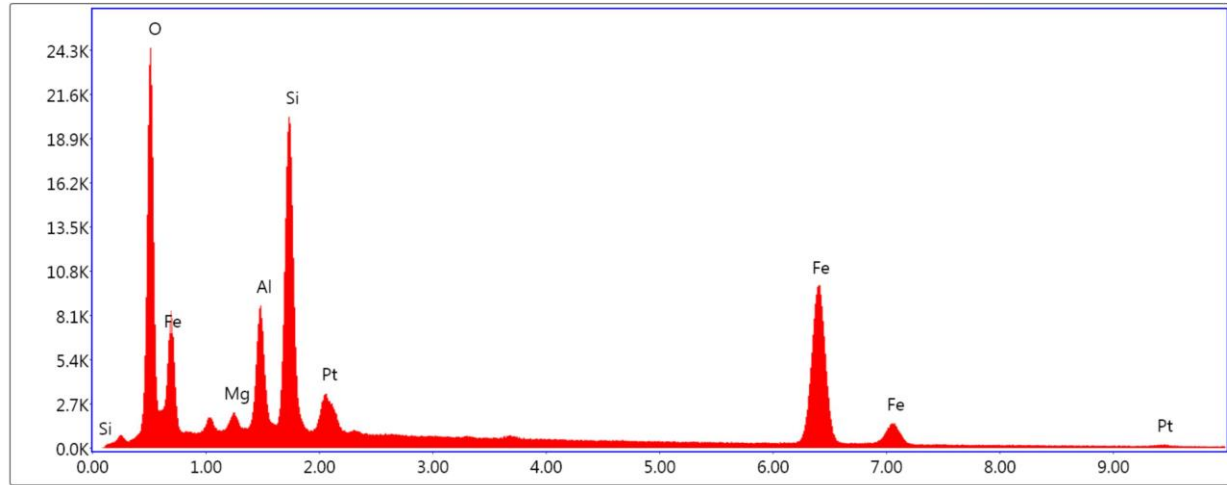
The lab mixed Sample 10 was also examined in SEM/EDS. Since the lab and flow loop samples primarily consisted of liquid, and the SEM/EDS examines a thin layer, it was decided to remove the particles so that they could be more easily examined in the SEM/EDS. This was done by taking the mud cake remnants from the API filter press test and using them for the SEM/EDS.

The first observation was that the iron particles had embedded themselves in the bentonite. This most likely occurred during mixing. This is important because it would explain why a large portion of the dried particles had not immediately rusted in previous samples. The bentonite platelets could be acting as a physical barrier to prevent the iron particles interaction with oxygen. After drying, these bentonite platelets could have shrunk, allowing for the iron particles to finally rust. Another observation was that the iron particles had not been dented by the mixing blade during mixing. The EDS data confirms that the iron is indeed embedded in the bentonite platelets. By comparing the data from EDS Spots 3 and 4 it was seen that the amounts of aluminum, silicon and oxygen are tied to each other. The relative percent of these elements to each other does not significantly change between these two spots, even though the percent of iron is greatly increased. This suggest that there are not additional oxygen atoms attached to the iron particles, which would be the case if significant oxidation (rusting) had occurred.



SEM image of sample 10 showing EDS locations

Sample 10 EDS Spot 3 graph and table



Lsec: 100.0 0 Cnts 0.000 keV Det: Octane Plus Det

Element	Weight %	Atomic %	Net Int.	Error %	Kratio	Z	R	A	F
O K	26.09	49.83	1660.62	6.30	0.1599	1.1777	0.9135	0.5205	1.0000
MgK	1.20	1.50	112.67	9.06	0.0059	1.0864	0.9521	0.4548	1.0032
AlK	5.45	6.17	624.84	6.04	0.0335	1.0459	0.9604	0.5848	1.0048
SiK	13.32	14.50	1693.44	4.89	0.0966	1.0685	0.9682	0.6757	1.0040
PtM	3.88	0.61	193.67	5.80	0.0321	0.6729	1.3214	1.0610	1.1612
FeK	50.07	27.40	1393.40	2.65	0.4591	0.8943	1.0301	0.9993	1.0260

10.3 FLOW LOOP SAMPLE

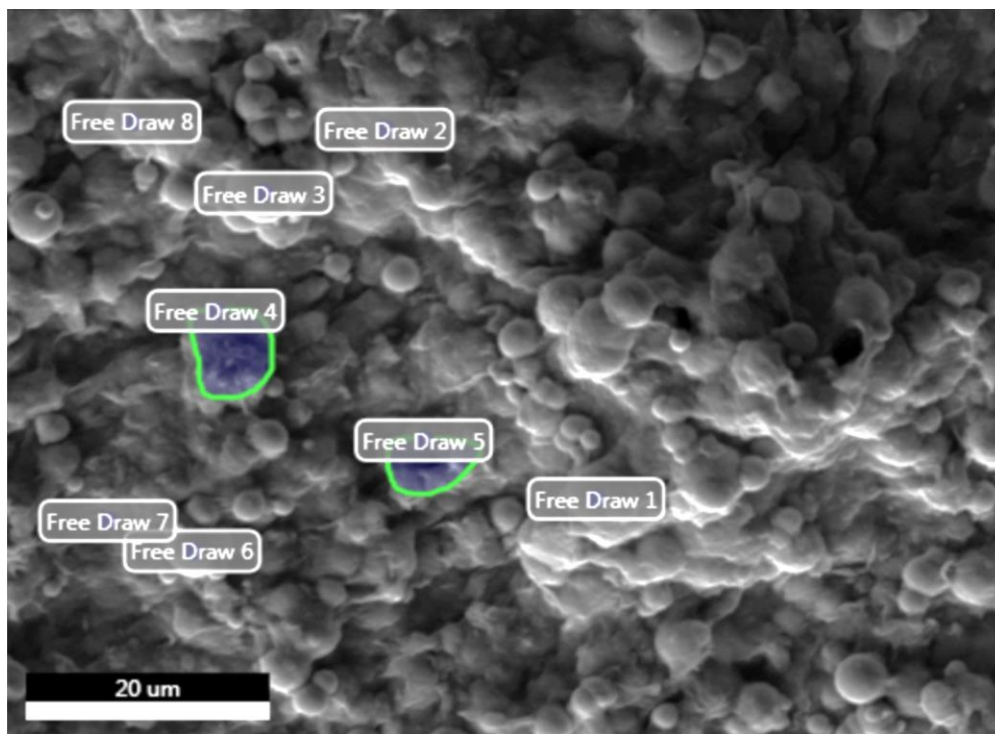
In order to not reduce the amount of particles in the flow loop during testing, fluid was not removed from the flow loop for lab testing until after the final experiment. Due to this, the particles themselves had been left mixing, flowing and sitting, for 7 days before the fluid sample was collected. For comparison, the previously created lab samples 9 and 10 were prepared, tested and examined in the SEM/EDS within a few hours.

Even though the flow loop was cleaned between the bentonite/barite experiments and the magnetorheological fluid experiments, some settled particles still remained in the flow loop. It

should be noted that only 3 or 4 barite particles were seen in the flow loop sample examined in the SEM. This would suggest that the amount of particles from the previous experiment that settled, and then were subsequently picked up in the new flow experiments was minimal.

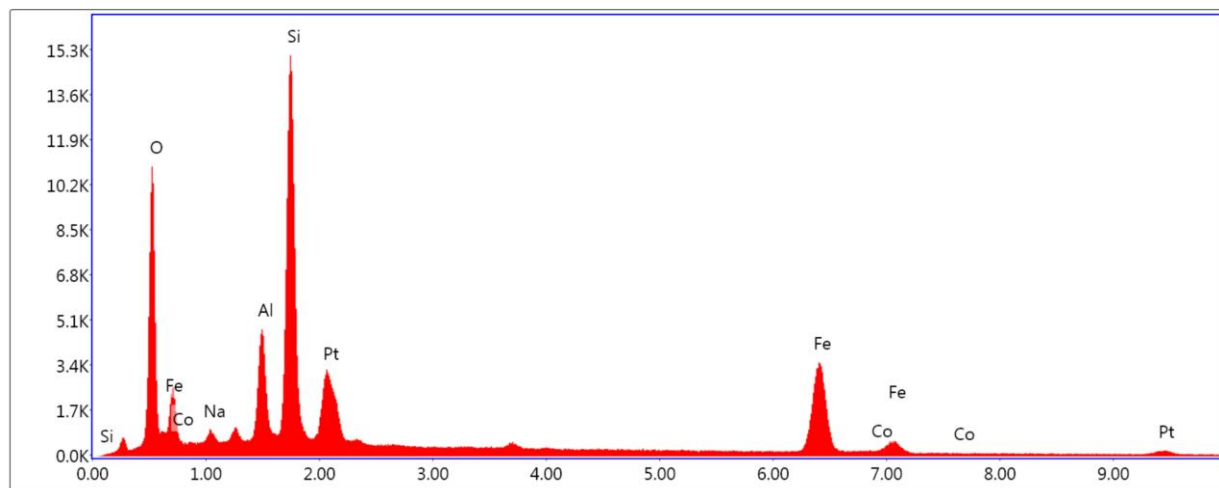
It should also be noted that the change in the ratios of oxygen, silicon and aluminum seen in the EDS data for free draw spots 1 and 3 in location 1 are most likely due to an increase in oxygen associated with the barite (BaSO_4), and not associated with oxidation of the iron. This lack of oxidation is supported by the EDS results of free draw 4 of location 1, which lacks barite and has oxygen, silicon and aluminum ratios similar to the lab samples. There is a large increase in the amount of platinum seen in the flow loop samples due to problems when coating the materials before their SEM/EDS analysis, which lead to the particles being coated multiple times.

Another area was examined in the EDS that was completely devoid of barite particles and showed similar oxygen, silicon and aluminum ratios to the lab samples. This again suggest that oxidation of the iron particles was minimal to non-existent at the time this sample was examined, 8 days after the iron was first added.



SEM image of flow loop sample showing EDS locations

Flow Loop Sample location 2 Free Draw 1 graph and table



Lsec: 30.0 0 Cnts 0.000 keV Det: Octane Plus Det

Element	Weight %	Atomic %	Net Int.	Error %	Kratio	Z	R	A	F
O K	21.80	43.61	2188.10	7.23	0.1143	1.1975	0.9032	0.4380	1.0000
NaK	1.48	2.06	126.92	11.25	0.0054	1.0869	0.9334	0.3345	1.0016
AlK	5.79	6.87	1043.09	6.22	0.0374	1.0643	0.9509	0.6039	1.0045
SiK	19.79	22.56	3917.40	4.77	0.1483	1.0876	0.9589	0.6869	1.0031
PtM	10.64	1.75	730.60	3.27	0.0806	0.6851	1.3093	1.0313	1.0723
FeK	38.60	22.12	1601.43	3.06	0.3576	0.9126	1.0244	0.9930	1.0224
CoK	1.90	1.03	62.62	14.27	0.0173	0.8904	1.0261	0.9928	1.0281

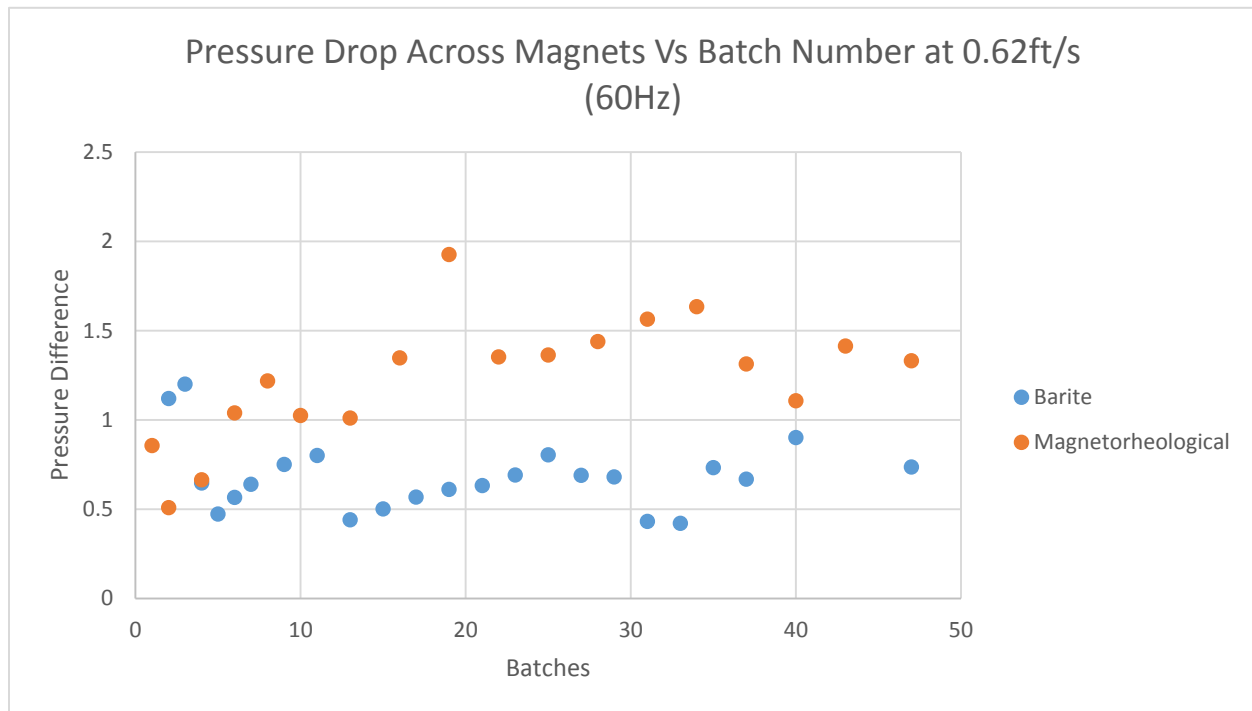
11. FLOW LOOP EXPERIMENTS

In order to test real world application viability, previous hypothesis had to be tested in the flow loop. This flow loop tested not only the shielding effect of the inner pipe, but also the effect of the magnets on the fluid as well as allowing for more time dependent variables to be tested, such as the rusting of the iron. The results of these experiments showed that there was an observable pressure drop across the magnets with the presence of the magnetorheological fluid when compared to the barite fluid. The inner pipe provided sufficient magnetic shielding, and that there was sufficient time between fluid creation and oxidation to allow for testing. Due to the large amount of noise in the raw data, the data presented here has been averaged using rectangular averaging with 9 half-widths.

11.1 RESULTS

The pressure drop across the magnets was plotted vs the number of batches of weighting material that had been added, for each flowrate tested. The 60Hz (0.62ft/s in the annulus and 5.23ft/s in the inner pipe), 50Hz (0.51ft/s in the annulus and 4.36ft/s in the inner pipe) and 10Hz (0.10ft/s in the annulus and 0.87ft/s in the inner pipe) graphs are shown for comparisons. The other graphs are included in Appendix C. The graphs shown in this section were chosen due to their clarity in relation to the phenomenon being examined and discussed.

It can be seen from the 60Hz graph that the pressure drop across the magnets is clearly different for the magnetorheological fluid versus the barite fluid. This difference is not seen in the lower batch numbers, which suggest that there are either not enough ferromagnetic particles for the effect to exist, or not enough for it to be measured in this setup.



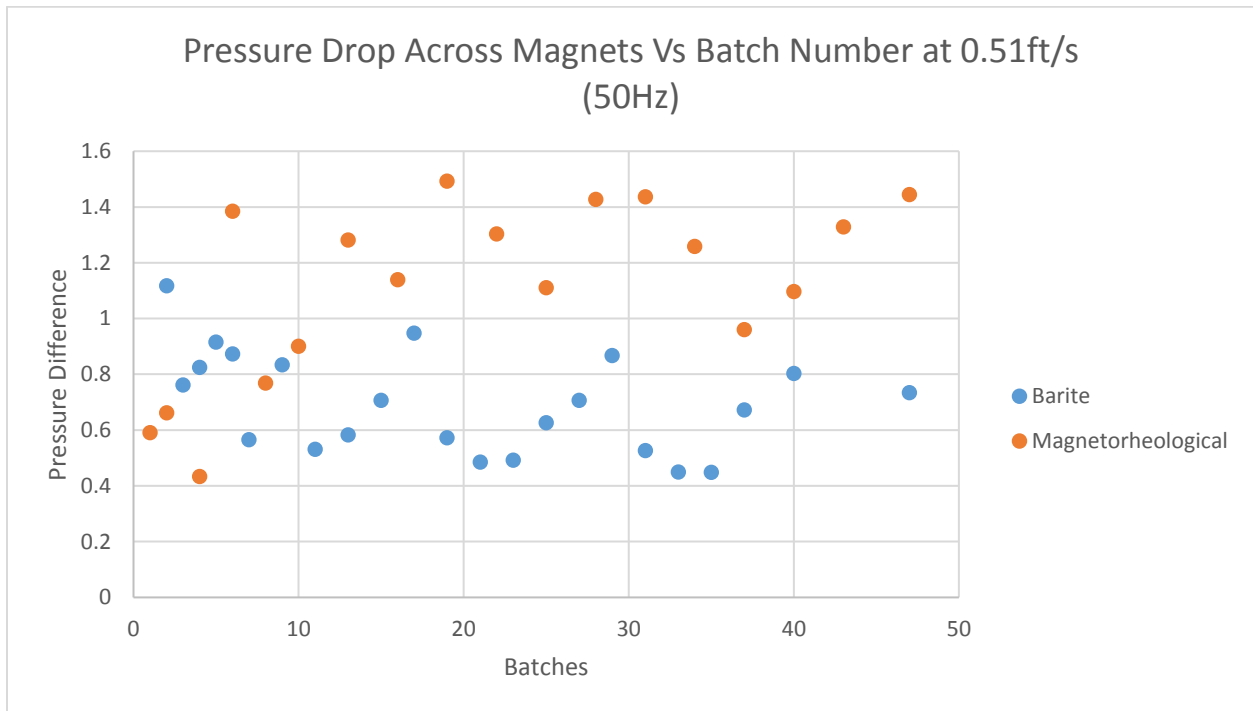
Pressure differential across the magnets in the annulus at 60Hz.

There is also the question of whether or not the iron microspheres were being pulled out of suspension in the early batches, potentially preventing the desired effects from occurring. It should be noted that the size of the built up particles on the magnets, as can be seen in the post experiment observations subsection, was larger than the number of particles being added in the early batches. This means that if the particles had been removed from suspension in these early experiments, then the fluid would have changed from its darker magnetorheological color to the lighter bentonite color. Observations of the fluid flowing back into the tank during these first few batches did not show any noticeable change in fluid color

As the number of batches increased the difference in pressure drop increased until somewhere between 16 and 22 batches. At this point it is believed that the minimum saturation of particles has been reached for the particles to begin bridging the annulus. This bridging would cause a plugging effect leading to a reduction, and then a temporary stop in flow before enough pressure was built

up to break the plug. This leads to a dynamic pressure, where the pressure increases until it breaks the plug, at which point the pressure is lower. At this point the pressure difference across the magnets no longer shows an increasing trend with batch number due to a different phenomenon becoming the dominant reason for the difference in pressure differential.

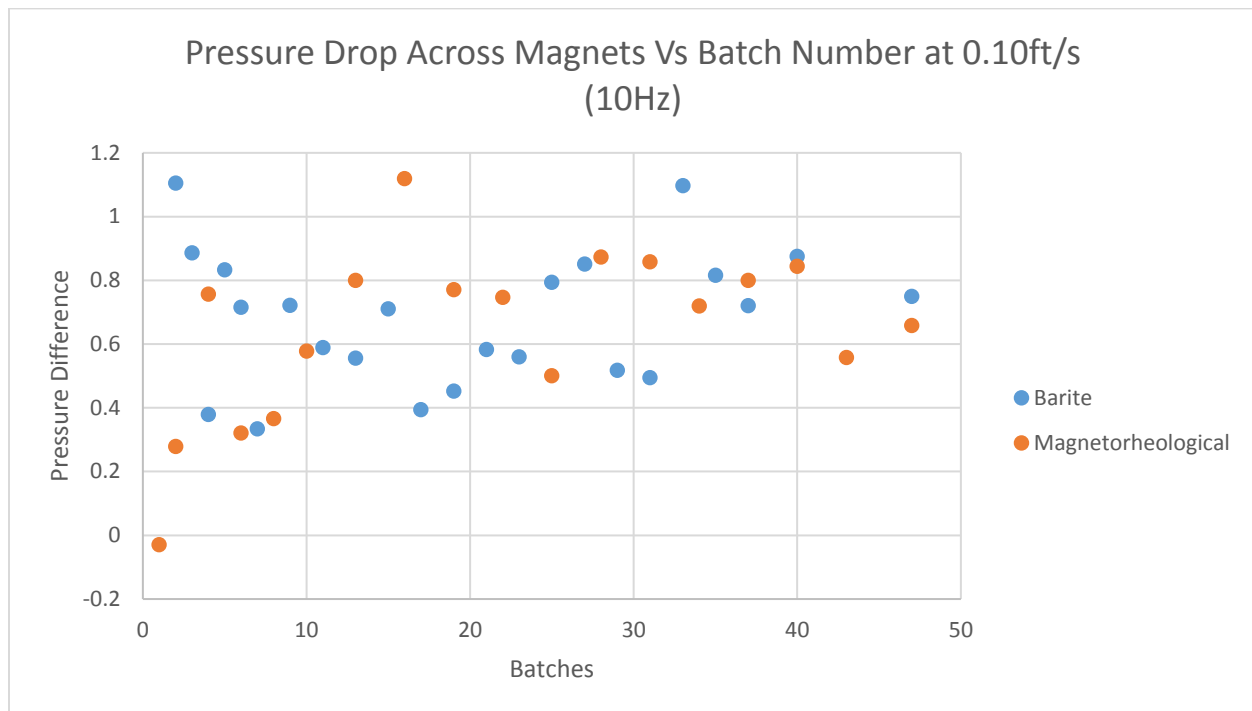
If the 16 to 22 batch range is indeed the point at which annular plugging began for the 60Hz pump rate, then this bridging should be occurring at lower batch numbers when less energy, and therefore force, is being sent through the annulus at lower pump speeds. It can be seen in the 50Hz graph that the increase in pressure with batch number does appear to stop at a lower number of batches.



Pressure differential across the magnets in the annulus at 50Hz.

As previously stated, the magnetorheological effect is an increase in the yield stress of a fluid, and should therefore not be a function of the flowrate, as long as there is sufficient flow rate to prevent plugging. Therefore all of the graphs should show constant yield stress pressure change for all flowrates for each batch, with only the plastic viscosity changing. This is assuming that plugging isn't occurring. Since lab results showed that the magnetorheological fluid had a higher plastic

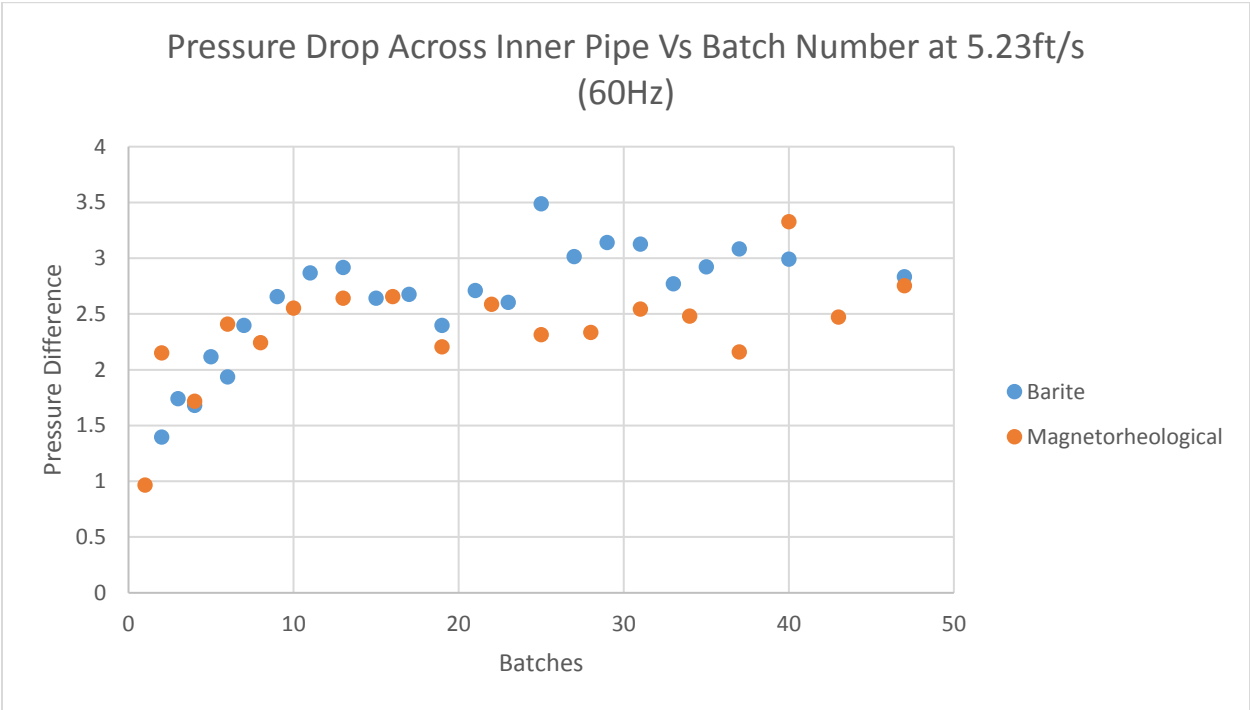
viscosity, it should therefore always have a high pressure differential across the magnets unless the dynamic pressure effect somehow prevented this from being seen. This higher pressure differential is not seen in either the 10Hz graph below, or the 20Hz (0.21 ft/s and 1.74 ft/s) graph in Appendix C.



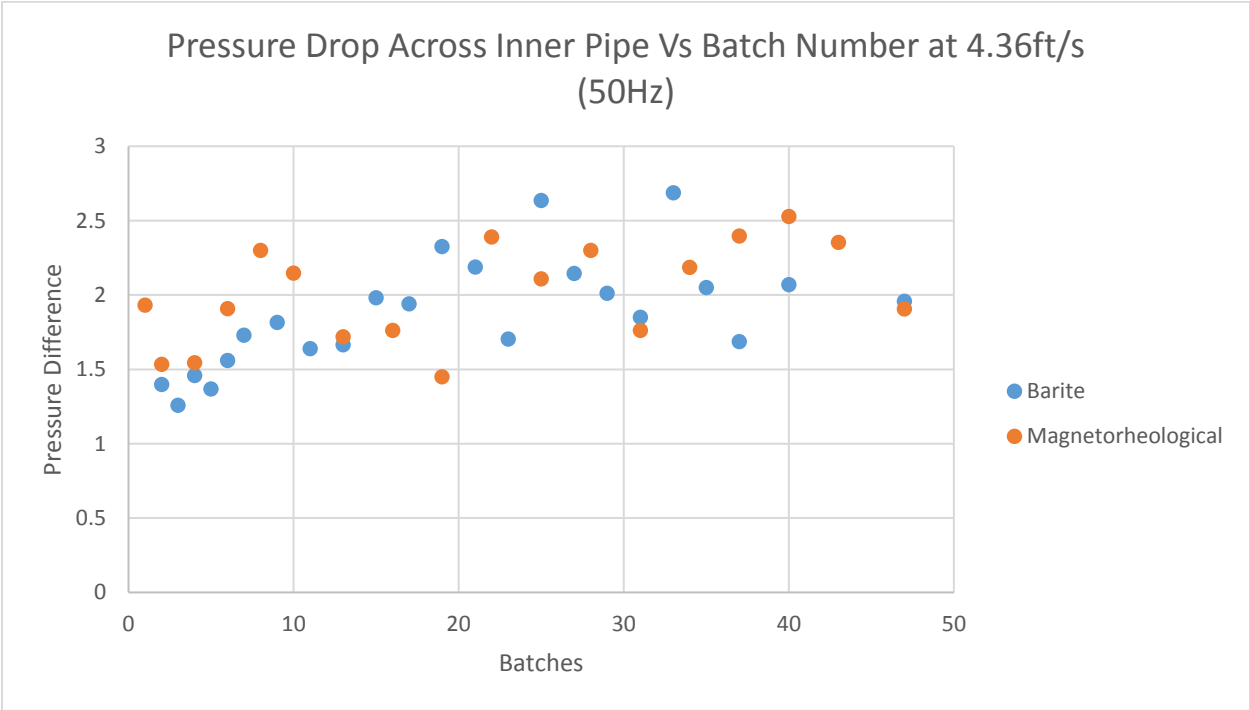
Pressure differential across the magnets in the annulus at 10Hz.

By comparing the inner pressure graphs it can be seen that the inner pipe pressure differential is approximately the same for barite and magnetorheological fluids at higher flow rates. This supports the earlier Hall Effect sensor results showing that the inner pipe could sufficiently shield the inside of the inner pipe from the magnets. It does show a difference at the 20Hz and 10Hz speeds though. There is a similar phenomenon in the before the magnets pressure differential graphs, where the difference between the barite and the magnetorheological fluid is more erratic compared to the downstream of the magnet pressure differential. These results suggest that plugging and therefore the dynamic pressure effect is present at these lower flowrates in the annulus. This can also be seen at higher batch numbers for higher flow rates, where the difference

between the barite and magnetorheological fluid becomes more erratic both in the upstream of the magnets, and the inner pipe pressure differentials.

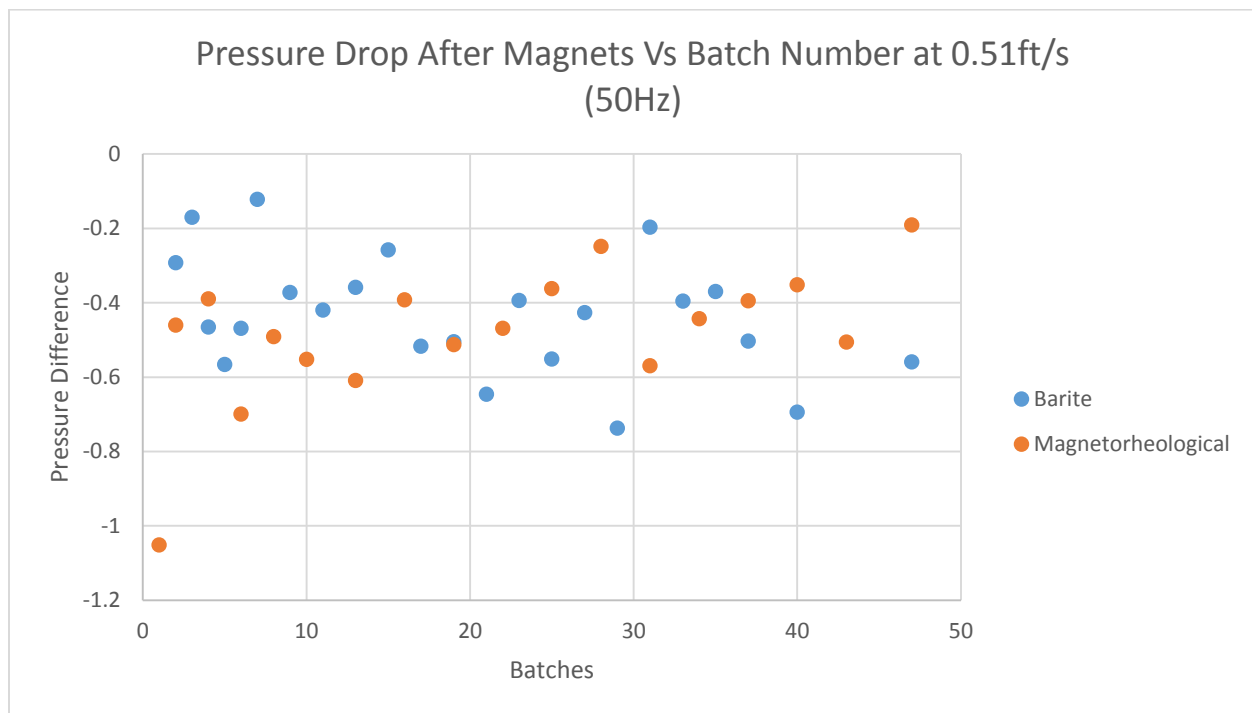


Pressure differential through the inner pipe at 60Hz.



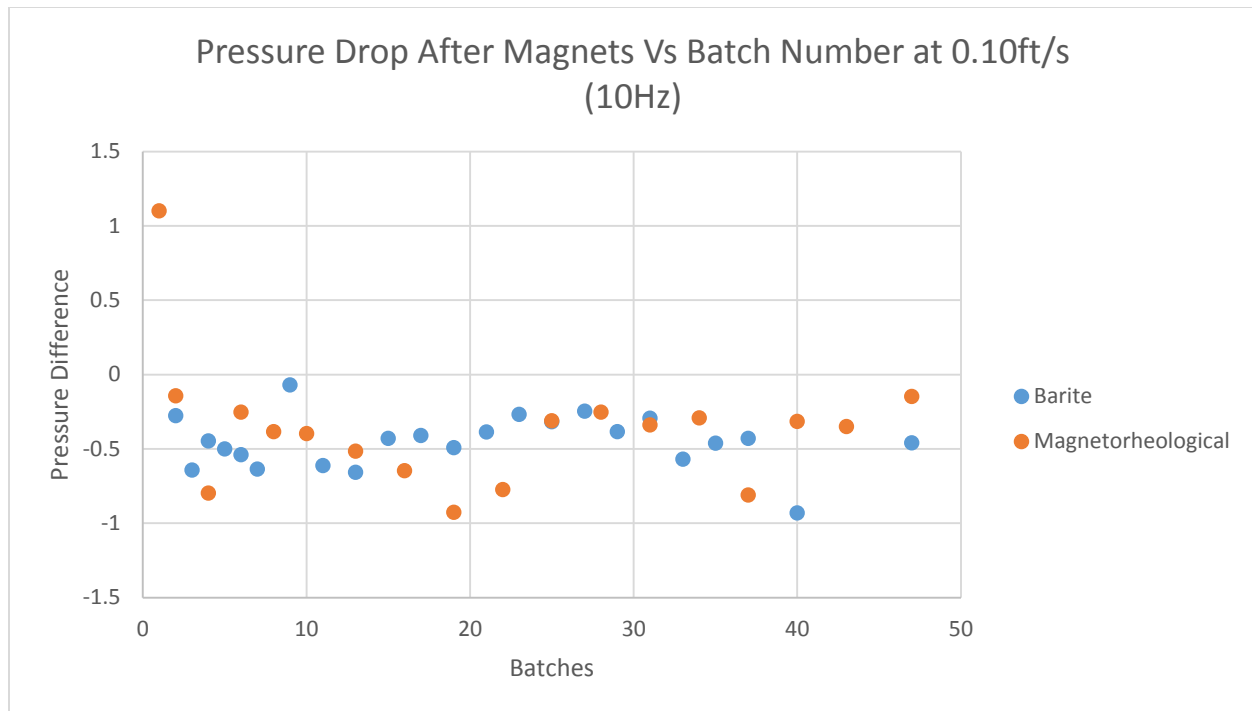
Pressure differential through the inner pipe at 50Hz.

As pointed out earlier in this paper, the magnetorheological fluid should return to approximately its pre-magnetized state once it leaves the influence of the magnetic field. This is confirmed by comparing the before the magnets graphs to the after the magnets graphs. It can be seen that the difference between the barite and magnetorheological pressure differentials are not a clear gap such as the ones that can be seen during the magnet pressure differentials.



Pressure differential downstream of the magnets in the annulus at 50Hz.

Not all of the pressure differentials are positive. This is strange considering that this is the pressure differential from upstream to downstream for a viscous fluid. This could be due to multiple reasons, such as the noise at the testing facility, the large range of the pressure transducers, or possibly them not being calibrated correctly before testing.



Pressure differential downstream of the magnets in the annulus at 10Hz.

11.2 POST EXPERIMENT OBSERVATIONS

The fluid did not show signs of significant oxidation at the conclusion of the experiments. Based on this observation it was decided to keep the fluid in the flow loop and mud tank for possible future experiments. At 12 days after mixing had started the fluid finally began to show signs of oxidation. This was seen as the fluid changing from its previous low viscosity state to a highly gelled one accompanied with a change in color to a slightly greenish tint characteristic of the early stages of oxidation.

The inner pipe was removed from the flow loop and examined. It can be seen from the following images that particles had built up around the magnets. In the barite based fluid these particles are most likely rust that had broken off of the inner pipe and became attracted to the magnets. In the magnetorheological based fluid this is clearly the highly gelled magnetorheological fluid.



Image of particles built up around magnet rings after barite experiments.

As can be seen from the magnetorheological experiment images below, a considerable amount of fluid has gelled around the magnet rings, as well as the outside of the inner pipe in general. The gelled particles on the pipe and around the centralizer can be attributed to the amount of gelation the fluid experienced before the pipe was removed. To support this is the fact that it took approximately 40 psi of pump pressure to get the gelled fluid to flow after 12 day of sitting, whereas during the experiments the pump never saw 10 psi sustained pump pressure even while

flowing at higher flow rates. Even taking this into account, it can clearly be seen that the magnetorheological fluid is attracted to the magnets, and has created a plug.



Image of particles built up around magnet rings after magnetorheological experiments.

It can be seen in the images below that the magnetorheological fluid aligns itself with the magnetic field lines produced by the magnet rings. The force required to move the particles increased with decreasing distance between the fluid and the magnet rings. This evidence, along with the sight of less fluid gelled around the smaller magnet rings confirms that the effect is dependent upon magnetic field strength.



Images showing magnetorheological fluid aligning with magnetic field lines.



Images of fluid during (left) and 2 days after (right) cleaning.

As previously mentioned the fluid had a greenish tint to it when it was removed from the flow loop at 21 days after mixing started. Once the fluid was left sitting outside of the flow loop this quickly changed to the orange color that is characteristic of significant rust. This suggest that the rusting

that occurred in the flow loop was sudden, and likely used all of, or almost all of the materials required for the reaction to occur. The rusting then stopped until more of the deficient material was added when the fluid was removed from the flow loop.

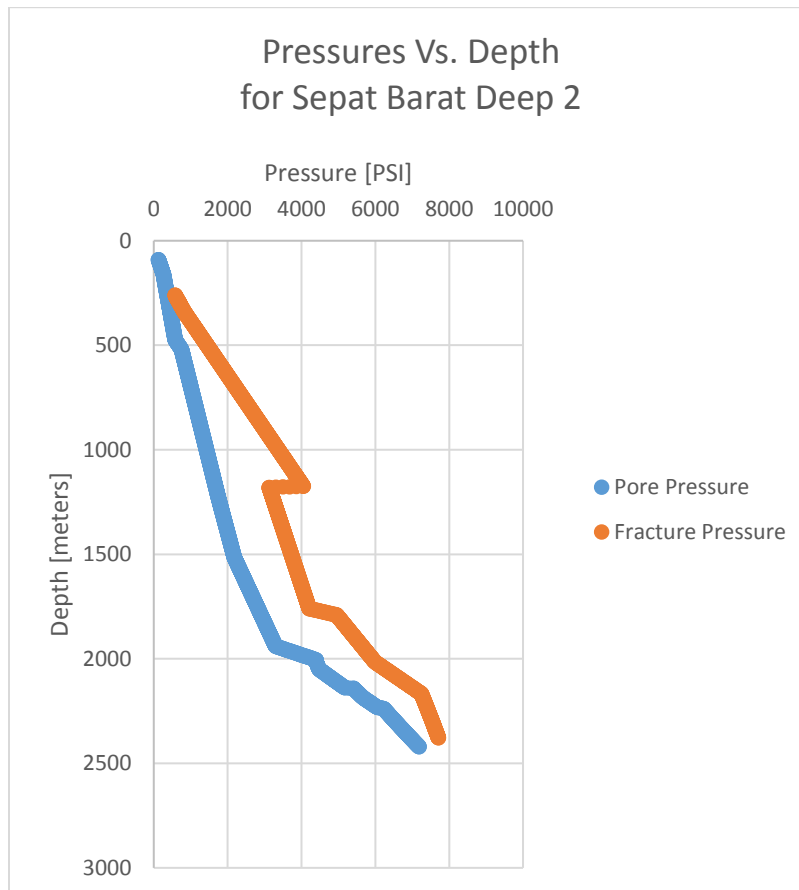
12. MUD WINDOW ANALYSIS (REAL WORLD SIMULATION)

If it is to be said this new technology will be able to achieve its supposed benefits then it must also be shown that a real world scenario exist where this technology would be advantageous to more conventional methods. Current managed pressure drilling candidates include the Gulf of Mexico, where downhole pressures might not be known beforehand, as well as other places that could potentially lead to failure to reach the target, such as Malaysia (Hannegan 2006). Feedback from industry, as well as published papers, have pointed out that a major benefit from using managed pressure drilling is the ability to drill formations that were not previously drillable (Jacobs and Donnelly 2011a). Though this is not the only use for managed pressure drilling. Managed pressure drilling is also used extensively to increase drilling efficiency and safety (Grayson 2009).

One of the desired abilities of this new technology is to drill previously undrillable wells. The problem in finding one of these wells is that companies tend to not publish all of their failed wells. Therefore the Sepat Barat Deep well number 2 from the Sepat Barat field in the PM block of the Malay Basin in Malaysia will be analyzed (Ismail et al. 2012) (Nordin et al. 2012). Information from the failed well was used to reach a depth of X240 meters in the second well; where the actual depth is assumed to be 2240 meters (7349 feet) based on the mud window (Ismail et al. 2012). This section will look at a single magnetic gradient drilling embodiment combining the last string of casing with the liner above it. Appendix A looks at another embodiment that would combine the liner and the casing above it.

The first Sepat Barat Deep well was drilled approximately 50 meters (164 feet) away from the second Sepat Barat Deep well. The first Sepat Barat Deep well had to be plugged and abandoned after significant hole problems related to well control. The close vicinity of these two wells would suggest that the mud windows would have similar profiles. More importantly the mud window for

the second well is published, and therefore available. Both wells were drilled using managed pressure drilling. (Ismail et al. 2012) (Nordin et al. 2012)



Pressure Window for Sepat Barat Deep 2 well based on information from Ismail et al. 2012, Nordin et al. 2012 and interpretation.

12.1 EXPLANATION OF MUD CHARACTERISTICS

Previous research suggest that at shear rates seen in drilling situations magnetorheological fluids follow a Bingham Plastic rheological model. Using the Bingham Plastic rheological model it can be seen that at such a high yield stress the plastic viscosity of the fluid is negligible in the apparent viscosity calculations. A concern with using the Bingham Plastic model is that the Herschel Buckley model is more applicable to drilling fluids. More importantly the Bingham Plastic model might not be effective for a yield stress several orders of magnitude above what the model was developed for. Unfortunately there is little experimental data on high yield stress fluids being used

at flow rates near field values because a lower viscosity fluid is typically desired in these scenarios to reduce pumping requirements. The yield stress used for this simulation was 2400 lbs. / 100 ft². This was chosen so that the simulation had the same 3 psi / ft. pressure difference between magnetorheological and barite fluids as seen in the experimental data.

Bingham Plastic Model with Slot Approximation for laminar flow:

$$(2) \quad \frac{dP}{dL} = \frac{\mu_p v}{1000(D_o - D_i)^2} + \frac{\mu_y}{200(D_o - D_i)}$$

μ_p is the plastic viscosity given in centipoise. D_o is the inner diameter of the outer pipe given in inches. D_i is the outer diameter of the inner pipe given in inches. μ_y is the yield stress given in pounds per 100 square feet. dP/dL is the frictional pressure loss per unit length traveled, given in units of PSI per foot. V is the average velocity of the fluid given in feet per second.

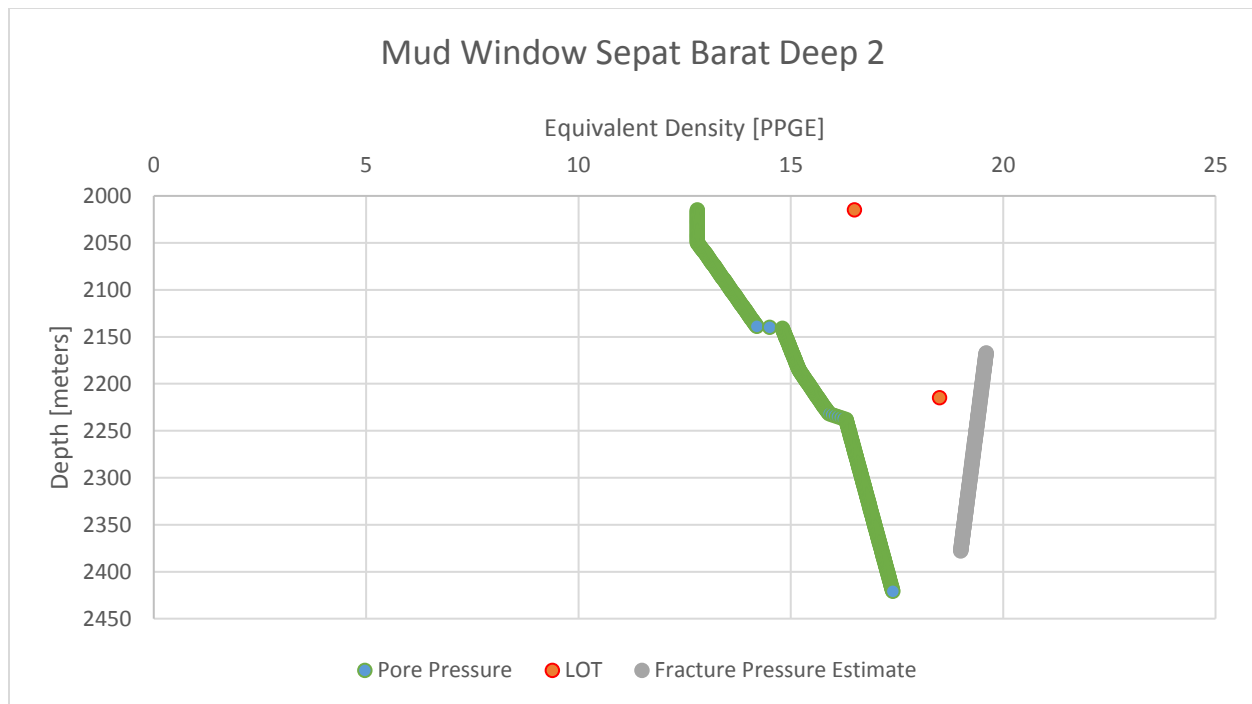
12.2 NON RATCHET METHOD

As mentioned before, having lots of ratchets downhole will create a very serious reliability problem; especially if all the ratchets have to be operated at different times. A solution to this would be to only use a single tool to be activated at a single point and used continuously. This was not possible for the 2017 to 2213 meter section due to lower fracture equivalent circulating density of 14 pounds per gallon at 1760 meters, but would be possible for the 2213 to 2426 meter casing. This would allow for the combination of the 2017 to 2213 liner section with the 2213 to 2426 casing section. As this is specifically looking at these lower sections, anything above the 2017 meter casing setting depth will not be looked at in this section.

If this analysis is started at the 2017 meter casing depth then it would be best to use the 16.5 PPGE leak off test results instead of the interpolated fracture pressure at this depth. It is also not known what the leak off pressure below this point is and whether there is an immediate formation change that would allow for a much higher leak off pressure. It is assumed that there is a formation change

that would allow for the activation of a single tool slightly below this depth, though this is not the only possible solution.

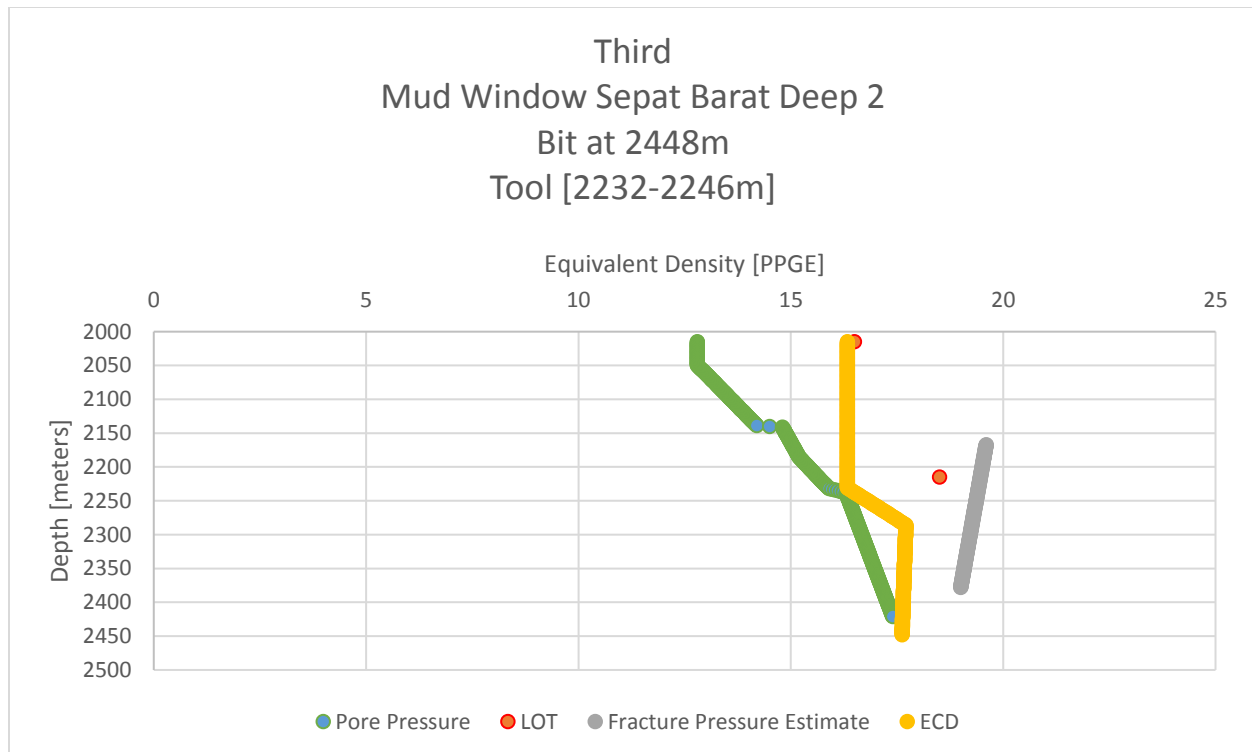
First it is assumed that the well is drillable to the liner setting depth of 2213 meters, 7260 feet, as was the case in the actual well, without the need for magnetic gradient drilling. Unlike the actual well though, it is undesirable to set the liner at this depth because the object is to remove it. Therefore the tool will already be located approximately 156 meters, 512 feet, behind the drill bit. The drilling fluid used in the actual Sepat Barat Deep well 2 was 16 pounds per gallon static and had 16.2 PPGE circulating density due to frictional pressure losses (Ismail et al. 2012) (Nordin et al. 2012). An assumption that the change in weighting material will not significantly change the frictional pressure losses outside the influence of a magnetic field has been made for simplicity.



Mud Density Window for only the lower sections of Sepat Barat Deep 2

Any changes to the rheological properties that would affect the equivalent circulating density could be corrected by changes in the mud density, such that a combination of the mud density and frictional pressure losses equals the 16.2 PPGE circulating density seen in the field.

After reaching 2232 the drilling fluid is switched to a magnetorheological drilling fluid. The tool is already located between 2016 and 2076 meters depth. This gives a tool length of 61 meters (~200 feet). This would be the length of 6 and 2/3rds standard 30 foot sections of drill pipe. With this tool activated the well will be below the leak off test pressure at 2017 meters and far below the linearly interpolated formation fracture pressure seen in this section.



Bit at 2448 meters with tool applying magnetic field. This is using the pressure differentials obtained from the flow experiments.

Now that the drilling fluid has been switched over it is safe to continue drilling until the next casing setting point 2426 meters (7959 feet). Not only is it safe to drill to the casing setting depth, but due to the location of the magnet assembly tool it is possible continue drilling until the drill bit reaches 2448 meters (8031 feet). As seen in the previous figure, the drill bit remains far below the calculated fracture pressure as well as the leak of test pressure performed at 2215 meters, which converts to an equivalent circulating density of 18.5 PPG.

Now that the drill bit is at 2448 meters it is time to set the next string of casing. To reiterate, through the use of a single magnet assembly tool in combination with magnetorheological fluid it was possible to combine the liner and the string of casing that would have been set after it into a single casing string in this simulation.

The non-ratchet method was simulated again, as well as a ratchet method. These simulations used a higher weight percent (30%) of iron particles. Increases in yield stress were determined through logarithmic regression since magnetorheological response data was not available for this weight percent of iron particles. The results and discussion for these additional simulations can be seen in Appendix A.

12.3 MUD WINDOW CONCLUSION

Using the differences in pressure drop between the magnetorheological fluid and barite fluids seen in the experimental data, a simulation was done to demonstrate that magnetic gradient drilling could be advantageous in a real well. Other embodiments, as well as different weight percent, were also simulated, with similar final results.

13. CONCLUSION

The desired outcome of this research was to show that a magnetorheological fluid, in combination with a magnetic tool, could modify the pressure in the annulus in such a way as to allow for the continuation of drilling for a longer interval before having to set casing. The magnetic field was generated by a permanent magnet, and could possibly be combined with some form of controllable magnetic shielding. The magnet showed a significant influence on the fluid in the annulus with no verifiable effect on the fluid within the inner pipe.

The magnetorheological fluid was created through a complete change in weighting material, though a partial change in weighting material would also be effective. This fluid had stable properties over the course of the experiments. This could potentially extend formation setting points, or reduce the chances or sizes of influxes.

14. FUTURE RESEARCH

Future experiments along this same line of research would preferably be done at higher flow rates in the flow loop. This would allow for the system to be tested with the higher velocities typically required in the annulus to have proper cuttings removal. Another possible experiment that could be conducted would be to only produce a small amount (a few barrels) of magnetorheological fluid and to include very small magnets within this fluid. This fluid could then be pumped as a slug, as a replacement for the high density slugs that are currently pumped. These magnets could possibly be added in such a way as to prevent them from being present inside the pump, or only be present once the fluid has been pumped out of the drill bit. Another idea, currently being researched by others at LSU, would look into whether or not the fluid could be completely jelled within the annulus in a pseudo-packer scenario. This could potentially allow for an increase in the sealing between the pseudo-packer and non-uniform wellbore formations, and could potentially be removable/repairable as well.

If these experiments are to be continued in the same fashion, then there are some improvements that should be made:

1. Use iron microspheres that are coated to prevent corrosion.
2. Use only the smaller magnet rings for flow experiments, or use an electromagnet.
3. Have more magnet rings, with the same spacing, in order to increase the effective length
4. Use pressure transducers that cover a much shorter range, such as 0-25psi.
5. Use a pump more typically seen in the field, such as a triplex pump
6. Conduct benchtop experiments using a magnetic rheometer.

REFERENCES:

- Ashtiani, M., Hashemabadi, S. H., Ghaffari, A. (2015) A Review on the Magnetorheological Fluid Preparation and Stabilization. *Journal of Magnetism and Magnetic Materials*. Volume 374. doi:10.1016/j.jmmm.2014.09.020
- Abdelnour, Z. A., Mildrum, H. F., Strnat, K. J. (1980) Properties of Various Sintered Rare Earth-Cobalt Permanent Magnets Between -60 and +200 Degrees Celcius. *Institute of Electrical and Electronics Engineers Transactions on Magnetics*. Volume MAG-16. doi:10.1109/TMAG.1980.1060663
- Ahmad, T. J., Arsalan, M., Black, M. J., & Noui-Mehidi, M. N. (2015, September 15). Piezoelectric Based Flow Power Harvesting for Downhole Environment. *Society of Petroleum Engineers*. doi:10.2118/176777-MS
- Allen, S., McCartney, C., Hernandez, M., Reeves, M., Baksh, A., MacFarlane, D. (2009) Step-Change Improvements with Wired-Pipe Telemetry. *Society of Petroleum Engineers*. doi:10.2118/119570
- Arajs, S., and Colvin, R. V. (1964) Ferromagnetic-Paramagnetic Transition in Iron. *Journal of Applied Physics*. Volume 35. doi:10.1063/1.1702873
- Arnone, M. A., Vieira, P. (2009) Drilling Wells With Narrow Operating Windows Applying the MPD Constant Bottom Hole Pressure Technology-How Much the Temperature and Pressure Affects the Operation's Design. *Society of Petroleum Engineers*. doi:10.2118/119882-MS
- Atulasimha, J., Flatau, A. B., (2011) A Review of Magnetostrictive Iron-Gallium Alloys. *Smart Materials and Structures*. Volume 20. doi:10.1088/0964-1726/20/4/043001
- Becnel, A. C., Sherman, S. G., Hu, W., Wereley, N. M. (2015) Squeeze Strengthening of Magnetorheological Fluids Using Mixed Mode Operation. *Journal of Applied Physics*. Volume 117. doi:10.1063/1.4907603
- Bell, R. C., Karli, J. O., Vavreck, A. N., Zimmerman, D. T., Ngatu, G. T., Wereley, N. M. (2008) Magnetorheology of Submicron Diameter Iron Microwires Dispersed in Silicone Oil. *Smart Materials and Structures*. Volume 17. doi:10.1088/0964-1726/17/01/015028
- Bieńkowski, A., (2000) Magnetoelastic Villari effect in Mn-Zn ferrites. *Journal of Magnetism and Magnetic Materials*. Volume 215-216. doi:10.1016/S0304-8853(00)00124-4
- Blackmore, E. W. (1985) Radiation Effects of Protons on Samarium-Cobalt Permanent Magnets. *Institute of Electrical and Electronics Engineers Transactions on Nuclear Science*. Volume NS-32. doi:10.1109/TNS.1985.4334463

- Bondemark, L., Kurol, J., and Wisten, A. (1995) Extent and Flux Density of Static Magnetic Fields Generated by Orthodontic Samarium-Cobalt Magnets. *American Journal of Orthodontics and Dentofacial Orthopedics*. Volume 107. doi: 10.1016/S0889-5406(95)70116-8
- Bosma, M., Ravi, K., van Driel, W., Jan Schreppers, G. (1999) Design Approach to Sealant Selection for the Life of the Well. *Society of Petroleum Engineers*. doi:10.2118/56536-MS
- Bossis, G., Lacis, S., Meunier, A., Volkova, O. (2002) Magnetorheological Fluids. *Journal of Magnetism and Magnetic Materials*. Volume 252. doi:10.1016/S0304-8853(02)00680-7
- Bozorth, R. M., Williams, H. J. (1945) Effect of Small Stresses on Magnetic Properties. *Reviews of Modern Physics*. Volume 17. doi:10.1103/RevModPhys.17.72
- Brown, W. F. (1949) Irreversible Magnetic Effects of Stress. *Physical Review*. Volume 75. doi:10.1103/PhysRev.75.147
- Carlson, J. D., Jolly, M. R. (2000) MR Fluid, Foam and Elastomer Devices. *Mechatronics*. Colume 10. doi:10.1016/S0957-4158(99)00064-1
- Chen, J., Li, S., MacMillan, C., Cortes, G., & Wood, D. (2015, September 28). Long Range Electromagnetic Telemetry Using An Innovative Casing Antenna System. *Society of Petroleum Engineers*. doi:10.2118/174821-MS
- Cheng, H. B., Wang, J. M., Zhang, Q. J., Wereley, N. M. (2009) Preparation of Composite Magnetic Particles and Aqueous Magnetorheological Fluids. *Smart Materials and Structures*. Volume 18. doi:10.1088/0964-1726/18/8/085009
- Cheng, L. M., Nolting, A. E., Voyzelle, B., Galvani, C. (2007) Deformation Behavior of Polycrystalline Galfenol at Elevated Temperatures. *Behavior and Mechanics of Multifunctional and Composite Materials*. Conference Volume 6526. doi:10.1117/12.720664
- Cho, M. S., Lim, S. T., Jang, I. B., Choi, H. J., Jhon, M. S. (2004) Encapsulation of Spherical Iron-Particle with PMMA and its Magnetorheological Particles. *Institute of Electrical and Electronics Engineers Transactions on Magnetics*. Volume 40. doi:10.1109/TMAG.2004.830413
- Choi, J. S., Park, B. J., Cho, M. S., Choi, H. J. (2006) Preparation and Magnetorheological Characteristics of Polymer Coated Carbonyl Iron Suspensions. *Journal of Magnetism and Magnetic Materials*. Volume 304. Doi:10.1016/j.jmmm.2006.02.055
- Clark, A. E., Wun-Fogle, M., Restorff, J. B., Lograsso, T. A., (2002) Magnetostrictive Properties of Galfenol Alloys Under Compressive Stress. *Materials Transactions*. Volume 43. doi:10.2320/matertrans.43.881

- Clark, H. M. (1990, January 1). A Comparison of the Erosion Rate of Casing Steels by Sand/Oil Suspensions. Offshore Technology Conference. doi:10.4043/6279-MS
- Clements, W. R. (1981, June) Ilmenite and Barite Abrasion Tests on Rig-Size Equipment. NL Baroid. Unpublished.
- Coley, C. J., Edwards, S. T. (2013) The Use of Along String Annular Pressure Measurements to Monitor Solids Transport and Hole Cleaning. Society of Petroleum Engineers. doi:10.2118/163567-MS
- Craik, D. J., Wood, M. J. (1970) Magnetization Changes Induced by Stress in a Constant Applied Field. Journal of Physics D: Applied Physics. Volume 3. doi:10.1088/0022-3727/3/7/303
- Croat, J. J., Herbst, J. F., Lee, R. W., Pinkerton, F. E. (1984) Pr-Fe and Nd-Fe-Based Materials: A New Class of High-Performance Permanent Magnets. Journal of Applied Physics. Volume 55. Doi:10.1063/1.333571
- Ding, S., Datta B. K., Saasen A., Amundsen P. A. (2010). Experimental Investigation of the Magnetic Shielding Effect of Mineral Powders in a Drilling Fluid. Particulate Science and Technology. Vol.28, Iss. 1
- Ekreem, N. B., Olabi, A. G., Prescott, T., Rafferty, A., Hashmi, M. S. J., (2007) An overview of magnetostriction, its use and methods to measure these properties. Journal of Materials Processing Technology. Volume 191. doi:10.1016/j.jmatprotec.2007.03.064
- Fang, F. F., Yang, M. S., Choi, H. J. (2008) Novel Magnetic Composite Particles of Carbonyl Iron Embedded in Polystyrene and their Magnetorheological Characteristics. Institute of Electrical and Electronics Engineers Transactions on Magnetics. Volume 44. doi:10.1109/TMAG.2008.2001665
- Fraser, D., Braun, J., Cunningham, M., Marple, B., Moore, D. D., Sas-Jaworsky, A., & Wilson, J. (2015, September 28). Operational Risk: Stepping Beyond Bow-Ties. Society of Petroleum Engineers. doi:10.2118/174995-MS
- Fripp, M. L., Hamid, S., Moore, D. W., Kyle, D., Caja, J., & Dunstan, T. D. (2008, January 1). Development of a High-Temperature Rechargeable Battery for Downhole Use in Petroleum Industry. Offshore Technology Conference. doi:10.4043/19621-MS
- Fu, Y. P., Lin, C. H. (2005) Fe/Sr Ratio Effect on Magnetic Properties of Strontium Ferrite Powders Synthesized by Microwave-Induced Combustion Process. Journal of Alloys and Compounds. Volume 386. Doi:10.1016/j.jallcom.2004.04.148
- Galindo-Gonzalez, C., Lopez-Lopez, M. T., Duran, J. D. G. (2012) Magnetorheological Behavior of Magnetite Covered Clay Particles in Aqueous Suspensions. Journal of Applied Physics. Volume 112. doi:10.1063/1.4748878

- Gallo, F., Rubianto, I., Rojas, F., Subroto, B., Prasetya, A. E., Torres, J. T. (2016) MPD and MPC Successfully Applied to Deliver a Defying Exploratory Ultra-HPHT Well in Offshore Malaysia. Society of Petroleum Engineers. doi:10.2118/173812-MS
- Grayson, M. B. (2009) Increased Operational Safety and Efficiency with Managed Pressure Drilling. Society of Petroleum Engineers. doi:10.2118/120982-MS
- Halbach, K. (1980) Design of Permanent Multipole Magnets with Oriented Rare Earth Cobalt Material. Nuclear Instruments and Methods. Volume 169. doi:10.1016/0029-554X(80)90094-4
- Hamoudi, I., Kartobi, K., Vieira, P., Saad, M. A., Torres, F., Qutob, H. (2011) Drilling Hazard Mitigation Technologies Enables Drilling a Conventionally Undrillable Prospect. Society of Petroleum Engineers. doi:10.2118/148515-MS
- Hannegan, D. (2006) Case Studies-Offshore Managed Pressure Drilling. Society of Petroleum Engineers. doi:10.2118/101855-MS
- Hegger, C., Maas, J. (2016) Investigation of the Squeeze Strengthening Effect in Shear Mode. Journal of Intelligent Material Systems and Structures. Volume 27. doi:10.1177/1045389X15606998
- Hunter, L., Kinnaird, B., Maclean, K. (2007) Life of Well Isolation Implemented in Major North Sea Development. Society of Petroleum Engineers. doi:10.2118/110804-MS
- Iglesias, G. R., Lopez-Lopez, M. T., Duran, J. D. G., Gonzalez-Caballero, F., Delgado, A. V. (2012) Dynamic Characterization of Extremely Bidisperse Magnetorheological Fluids. Journal of Colloid and Interface Science. Volume 377. doi:10.1016/j.jcis.2012.03.077
- Ismail, Z., Aziz, I. A. B., Umar, L., Nordin, N. A. B., Nesan, T. P., Rodriguez, F. R., Zapata, F. G., Garcia, G., Qaguih, A., Subroto, B., Dow, B. (2012) Automated Managed Pressure Drilling Allows Identification of New Reserves in a HPHT Exploration Well in SB Field, Offshore Malaysia. Society of Petroleum Engineers. doi:10.2118/151518-MS
- Jacobs, S., and Donnelly, J. (2011a) Crossing the Technology Chasm: Managed Pressure Drilling. Journal of Petroleum Technology. doi:10.2118/0211-0030-JPT
- Jacobs, S., and Donnelly, J. (2011b) Crossing the Technology Chasm: Permanent Downhole Monitoring. Journal of Petroleum Technology. doi:10.2118/0711-0026-JPT
- Janasi, S. R., Emura, M., Landgraf, F. J. G., Rodrigues, D. (2002) The Effects of Synthesis Variables on the Magnetic Properties of Coprecipitated Barium Ferrite Powders. Journal of Magnetism and Magnetic Materials. Volume 238. doi:10.1016/S0304-8853(01)00857-5

- Jayaraman, T. V., Srisukhumbowornchai, N., Guruswamy, S., Free, M. L. (2007) Corrosion Studies of Single Crystals Of Iron-Gallium Alloys In Aqueous Environments. *Corrosion Science*. Volume 49. doi:10.1016/j.corsci.2007.05.010
- Jellison, M. J., Prideco, G., Hall, D. R., Howard, D. C., Hall, H. T. Jr., Long, R. C., Chandler, R. B., Pixton, D. S. (2003) Telemetry Drill Pipe: Enabling Technology for the Downhole Internet. Society of Petroleum Engineers. doi:10.2118/79885-MS
- Jiang, W., Zhang, Y., Xuan, S., Guo, C., Gong, X. (2011) Dimorphic Magnetorheological Fluid with Improved Rheological Properties. *Journal of Magnetism and Magnetic Materials*. Volume 323. doi:10.1016/j.jmmm.2011.07.024
- Jiles, D. C., (1995) Theory of magnetomechanical effect. *Journal of Physics D: Applied Physics*. Volume 28. doi:10.1088/0022-3727/28/8/001
- Jun, J. B., Uhm, S. Y., Ryu, J. H., Suh, K. D. (2005) Synthesis and Characterization of Monodisperse Magnetic Composite Particles for Magnetorheological Fluid Materials. *Colloids and Surfaces A: Physicochemical and Engineering Aspects*. Volume 260. doi:10.1016/j.colsurfa.2005.03.020
- Kaneko, H. Homma, M., Nakamura, K., Miura, M. (1972) Fe-Cr-Co Permanent Magnet Alloys Containing Silicon. *Institute of Electrical and Electronics Engineers Transactions on Magnetics*. Volume 8. doi:10.1109/TMAG.1972.1067517
- Kellogg, R. A., (2003) Development and Modeling of Iron-Gallium Alloys. Doctoral Dissertation. Iowa State University.
- Kellogg, R. A., Flatau, A. B., Clark, A. E., Wun-Fogle, M., Lograsso, T. A., (2002) Temperature and Stress Dependencies of the Magnetic and Magnetostrictive properties of $\text{Fe}_{0.81}\text{Ga}_{0.19}$. *Journal of Applied Physics*. Volume 91. doi:10.1063/1.1452216
- Kellogg, R. A., Russell, A. M., Lograsso, T. A., Flatau, A. B., Clark, A. E., Wun-Fogle, M. (2004). Tensile Properties of Magnetostrictive Iron-Gallium alloys. *Acta Materialia*. Volume 52. Doi:10.1016/j.actamat.2004.07.007
- Lagorce, L. K., Allen, M. G. (1997) Magnetic and Mechanical Properties of Micromachined Strontium Ferrite/Polyimide Composites. *Journal of Microelectromechanical Systems*. Volume 6. doi:10.1109/84.650127
- Lehner, J. K., & Garcia, J. (2015, September 28). Aluminum Alloy Enhanced Drill String Saves Over \$500,000 by Increasing Small Rig Depth Capacity in Marcellus. Society of Petroleum Engineers. doi:10.2118/174913-MS

- Liu, Y. D., Choi, H. J., Choi, S. B. (2012) Controllable Fabrication of Silica Encapsulated Soft Magnetic Microspheres with Enhanced Oxidation-Resistance and their Rheology under Magnetic Field. *Colloids and Surfaces A: Physicochemical and Engineering Aspects*. Volume 403. Doi:10.1016/j.colsurfa.2012.04.002
- Liu, X., Wang, J., Gan, L. M., Ng, S. C. (1999) Improving the Magnetic Properties of Hydrothermally Synthesized Barium Ferrite. *Journal of Magnetism and Magnetic Materials*. Volume 195. doi:10.1016/S0304-8853(99)00123-7
- Lopez-Lopez, M. T., Zugaldia, A., Gonzalez-Caballero, F., Duran, J. D. G. (2006) Sedimentation and Redispersion Phenomena in Iron-Based Magnetorheological Fluids. *Journal of Rheology*. Volume 50. doi:10.1122/1.2206716
- Mallinson, J. C. (1973) One-Sided Fluxes—A Magnetic Curiosity? *Institute of Electrical and Electronics Engineers Transactions on Magnetism*. Volume MAG-9. doi:10.1109/TMAG.1973.1067714
- Mehrabi, M., Miska, S., & Merlo, A. (2014, March 4). Complex Wells: New Perspective on the Selection of Optimal Drillpipe. *Society of Petroleum Engineers*. doi:10.2118/167947-MS
- Miao, C., Shen, R., Wang, M., Shafrir, S. N., Yang, H., Jacobs, S. D. (2011) Rheology of Aqueous Magnetorheological Fluid using Dual Oxide-Coated Carbonyl Iron Particles. *Journal of the American Ceramic Society*. Volume 94. doi:10.1111/j.1551-2916.2011.04423.x
- Mildrum, H. F., Hartings, M. F., Wong, K. D., Strnat, K. J. (1974) An Investigation of the Aging of Thermally Prestabilized Sintered Samarium-Cobalt Magnets. *Institute of Electrical and Electronics Engineers Transactions on Magnetism*. Volume 10. doi:10.1109/TMAG.1974.1058383
- Morrish, A. H., Haneda, K. (1983) Surface Magnetic Properties of Fine Particles. *Journal of Magnetism and Magnetic Materials*. Volume 35. doi:10.1016/0304-8853(83)90468-7
- Mrlik, M., Ilcikova, M., Sedlacik, M., Mosnacek, J., Peer, P., Filip, P. (2014) Cholesteryl-Coated Carbonyl Iron Particles with Improved Anti-Corrosion Stability and their Viscoelastic Behavior Under Magnetic Field. *Colloid and Polymer Science*. Volume 292. doi:10.1007/s00396-014-3245-5
- Nelson, E. (1990) Well Cementing. *Developments in Petroleum Science*. Volume 28.
- Ngatu, G. T., and Wereley, N. M. (2007) Viscometric and Sedimentation Characterization of Bidisperse Magnetorheological Fluids. *Institute of Electrical and Electronics Engineers Transactions on Magnetism*. Volume 43. doi:10.1109/TMAG.2007.893867
- Ngatu, G. T., Wereley, N. M., Karli, J. O., Bell, R. C. (2008) Dimorphic Magnetorheological Fluids: Exploiting Partial Substitution of Microspheres by Nanowires. *Smart Materials and Structures*. Volume 17. doi:10.1088/0964-1726/17/4/045022

- Nordin, N. A. B., Umar, L., Aziz, I. A. B., Nas, S., Woo, W. K. (2012) Dynamic Modeling of Wellbore Pressures Allows Successful Drilling of a Narrow Margin HPHT Exploration Well in Malaysia. Society of Petroleum Engineers. doi:10.2118/155580-MS
- Nygaard, R. (2010) Well Design and Well Integrity-Wabamun Area CO₂ Sequestration Project (WASP). Energy and Environmental Systems Group at Institute for Sustainable Energy, Environment and Economy.
- Nygaard, R., and Lavoie, C. R. (2010) Well Integrity and Workover Candidates for Existing Wells in the Wabamun Area CO₂ Sequestration Project (WASP). Society of Petroleum Engineers. doi:10.2118/137007-MS
- Olberg, T. S., Laastad, H., Lesso, B., Newton, A. (2008) The Utilization of the Massive Amount of Real-Time Data Acquired in Wired Drillpipe Operations. Society of Petroleum Engineers. doi:10.2118/112702-MS
- O'Reilly, W. (1984) Rock and Mineral Magnetism. Springer. ISBN: 978-1-4684-8468-7
- Phule, P. P., Mihalcin, M. P., Genc, S. (1999) The Role of the Dispersed-Phase Remnant Magnetization on the Redispersibility of Magnetorheological Fluids. Journal of Materials Research. Volume 14. doi:10.1557/JMR.1999.0407
- Pillai, V., Kumar, P., Multani, M. S., Shah, D. O. (1993) Structure and Magnetic Properties of Nanoparticles of Barium Ferrite Synthesized Using Microemulsion Processing. Colloids and Surfaces A: Physicochemical and Engineering Aspects. Volume 80. doi:10.1016/0927-7757(93)80225-4
- Quey, R., Dawson, P. R., Barbe, F. (2011) Large-scale 3D random polycrystals for the finite elements method: Generation, meshing and remeshing. Computer Methods in Applied Mechanics and Engineering. Volume 200. Doi:10.1016/j.cma.2011.01.002
- Rabinow, J. (1948) The Magnetic Fluid Clutch. Electric Engineering. Volume 67. doi:10.1109/EE.1948.6444497
- Randhol, P., and Carlsen, I. M. (2008) Assessment of Sustained Well Integrity on the Norwegian Continental Shelf. SINTEF Petroleum Research.
- Ratnam, D. V., Wells, M. G. H. (1974) Properties of Mischmetal-Cobalt Magnets. Journal of Applied Physics. Volume 18. doi:10.1063/1.2947227
- Ravi, K., Vargo, R., Lasley, B. (2008) Successful Cementing Case Study in Tuscaloosa HPHT Wells. Society of Petroleum Engineers. doi:10.2118/115643-MS

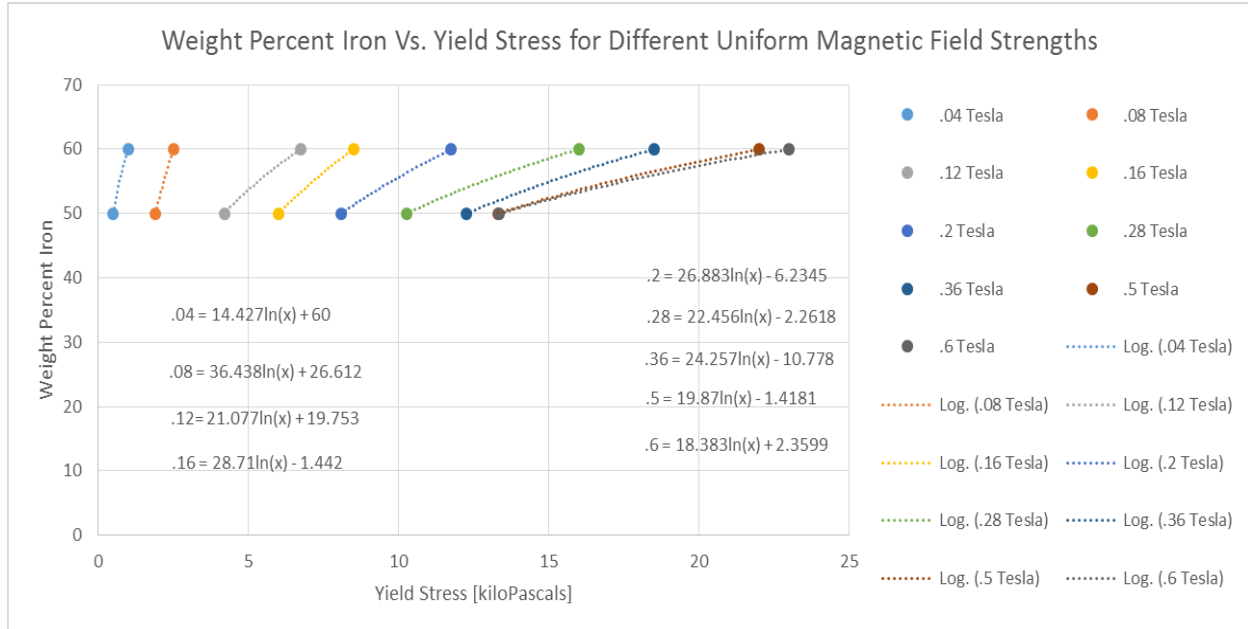
- Ryu, Jungho, Priya, Shashank, Carazo, Alfredo Vazquez, Uchino, Kenji, Kim, Hyoun-Ee (2001) Effect of Magnetostrictive Layer on Magnetoelectric Properties in Lead Zirconate Titanate/Terfenol-D Laminate Composites. Journal of the American Ceramic Society. Volume 84, Issue 12. doi:10.1111/j.1151-2916.2001.tb01113.x
- Sagawa, M., Fujimura, S., Togawa, N., Yamamoto, H., Matsuura, Y. (1984) New Material for Permanent Magnets on a Base of Nd and Fe. Journal of Applied Physics. Volume 55. doi:10.1063/1.333572
- Shadravan, A., and Amani, M. (2012) HPHT 101- What Every Engineer or Geoscientist Should Know About High Pressure High Temperature Wells. Society of Petroleum Engineers. doi:10.2118/163376-MS
- Spaggiari, A., and Dragoni, E. (2012) Effect of Pressure on the Flow Properties of Magnetorheological Fluids. Journal of Fluids Engineering. Volume 134. doi:10.1115/1.4007257
- Stacey, F. D. and Banerjee, S. K. (1974) The Physical Principles of Rock Magnetism. Elsevier Scientific Publishing Company. ISBN: 978-0-4445-6973-8
- Stiles, D. (2006) Effects of Long-Term Exposure to Ultrahigh Temperatures on Mechanical Parameters of Cement. Society of Petroleum Engineers. doi:10.2118/98896-MS
- Szymura, S., Sojka, L. (1986) Microstructure and Magnetic Properties of Fe-Cr-Co-(Si) Permanent Magnet Alloys. Materials Chemistry and Physics. Volume 15. doi:10.1016/0254-0584(86)90027-1
- Szewczyk, R., Bieñkowski, A., (2003) Magnetoelastic Villari Effect in High-Permeability Mn-Zn Ferrites and Modeling of this Effect. Journal of Magnetism and Magnetic Materials. Volumes 254-255. doi:10.1016/S0304-8853(02)00784-9
- Tan, L., Pu, H., Jin, M., Chang, Z., Wan, D., Yin, J. (2010) Iron Nanoparticles Encapsulated in Poly(AAm-co-MAA) Microgels for Magnetorheological Fluids. Colloids and Surfaces A: Physicochemical and Engineering Aspects. Volume 360. doi:10.1016/j.colsurfa.2010.02.022
- Tellefsen, K., Ding, S., Saasen, A., Amundsen, P. A., Fjogstad, A., & Torkildsen, T. (2012, January 1). The Effect of Drilling Fluid Content on Magnetic Shielding of Downhole Compasses in MWDs. Society of Petroleum Engineers. doi:10.2118/150548-MS
- Torkildsen, T., Edvardsen, I., Fjogstad, A., Saasen, A., Amundsen, P. A., & Omland, T. H. (2004, January 1). Drilling Fluid affects MWD Magnetic Azimuth and Wellbore Position. Society of Petroleum Engineers. doi:10.2118/87169-MS

- Tovar, J., Rodriguez, Z., Quiroga, F., Greaves, R., Melendez, H., Arocha, J., Bland, R., Hebert, M. (1999, January 1). ORIMATITA®. An Improved Hematite for Drilling Fluids. Society of Petroleum Engineers. doi:10.2118/53939-MS
- Ugwu, I. (2008) Cement Fatigue and HPHT Well Integrity with Application to Life of Well Prediction. Thesis. Texas Agriculture and Mechanical University.
- Waag, T. I., Torkildsen, T., Amundsen, P. A., Nyrnes, E., Saasen, A. (2012) The Design of BHA and the Placement of Magnetometer Sensors Influence How Magnetic Azimuth is Distorted by the Magnetic Properties of Drilling Fluids. Society of Petroleum Engineers. doi:10.2118/151039-MS
- Walker, C. O. (1983, December 1). Alternative Weighting Material. Society of Petroleum Engineers. doi:10.2118/11116-PA
- Wang, X., Gordaninejad, F. (2006) Study of Magnetorheological Fluids at High Shear Rates. *Rheologica Acta*. Volume 45. doi:10.1007/s00397-005-0058-y
- Webster, W. L. (1925). Magneto-striction in iron crystals. *Proceedings of the Royal Society of London. Series A, Containing Papers of a Mathematical and Physical Character*, 570-584.
- Weems, M., Moore, D, and Leach, C. (2016, April 12) Managed Pressure Drilling as Well Control in Deepwater GOM: Challenges to Current Modes of Thinking. Society of Petroleum Engineers. doi:10.2118/179179-MS
- Wereley, N. M., Chaudhuri, A., Yoo, J. H., John, S., Kotha, S., Suggs, A., Radhakrishnan, R., Love, B. J., Sudarshan, T. S. (2006) Bidisperse Magnetorheological Fluids Using Fe Particles at Nanometer and Micron Scale. *Journal of Material Systems and Structures*. Volume 17. doi:10.1177/1045389X06056953
- Wu, R. (2002) Origin of Large Magnetostriction in FeGa Alloys. *Journal of Applied Physics*. Volume 91. doi:10.1063/1.1450791
- Wu, W. P., Zhao, B. Y., Wu, Q., Chen, L. S., Hu, K. A. (2006) The Strengthening Effect of Guar Gum on the Yield Stress of Magnetorheological Fluid. *Smart Materials and Structures*. Volume 15. doi:10.1088/0964-1726/15/4/N04
- Wun-Fogle, M., Restoff, J. B., Cuseo, J. M., Garshelis, I. J., Bitar, S. (2009). Magnetostriction and Magnetization of Common High Strength Steels. *Institute of Electrical and Electronics Engineers Transactions on Magnetics*, Volume 45. doi:10.1109/TMAG.2009.2021531
- Wyslocki, J. J., Olszewski, J., Wyslocki, B., Szymura, S. (1990) Magnetic Hardening Mechanism In Low-Cobalt Fe-Cr-Co Alloys. *Institute of Electrical and Electronics Engineers Transactions on Magnets*. Volume 26. doi:10.1109/20.104832

Zhang, X. Z., Gong, X. L., Zhang, P. Q., Wang, Q. M. (2004) Study on the Mechanism of the Squeeze-Strengthen Effect in Magnetorheological Fluids. *Journal of Applied Physics*. Volume 96. doi:10.1063/1.1773379

Zhao, X., and D. G. Lord. "Application of the Villari effect to electric power harvesting." *Journal of applied physics* 99, no. 8 (2006). doi:10.1063/1.2165133

APPENDIX A: ADDITIONAL SIMULATIONS



Logarithmic Regression empirical formulas and data used to interpolate lower weight percent iron microspheres potential magnetorheological properties.

In order for the operator to stay within the pore pressure / fracture pressure window then it must be known how much the magnetic assembly tool would alter the fluid's rheological properties. The problem with this is that experiments involving magnetorheological fluids typically involve either a viscometer where the fluid is always under the influence of a uniform magnetic field, or very low flowrates. Even so, these experiments give initial values needed for rough estimates of potential rheological properties without having to model the complexities associated with the magnetic fields from multiple magnets affecting the fluid's yield stress. To account for the fact that the higher magnetic field strengths of 1 tesla seen at the magnet's surface will not be seen throughout the entire annulus, a lower magnetic field strength must be assumed such that if it is continuous and constant throughout the same length of annulus that it will have same pressure drop effect as the more realistic, highly complex magnetic field and rheological model having much higher magnetic field strengths at the drill pipe.

In order to make an initial estimation of the potential pressure drop due to the influences of the weight percent by iron of the magnetorheological fluid as well as the magnetic field strength from the magnets, data points from Ngatu et al. 2008 were used. The higher weight percent of iron particles were used to interpolate values for yield stress for a lower weight percent iron, specifically 30% by weight. As the resulting increase in yield stress for any constant weight percent of iron particles asymptotically approaches a maximum value that corresponds to a maximum magnetic field saturation, the lower weight percent interpolation would have to match this same trend. A natural logarithmic function was created using the 60% by weight and 50% by weight for each associated magnetic field strength given in Ngatu et al. 2008. These equations were then used to interpolate what the response to those magnetic field strengths would be for 30% iron by weight. It should be noted that these functions should not be used for the higher, above 0.4Tesla (4000Gauss) magnetic field strengths, due to the values obtained at these magnetic field strengths being lower than previous magnetic field strengths. This is because the 50% iron particles by weight has reached its maximum saturation while the 60% iron particles by weight has not. Therefore the 60% iron particles by weight continues to have an increase in yield stress with increases in magnetic field strength whereas the 50% iron particles by weight does not.

The logarithmic regression leads to a yield stress of 5.371364295 kPa at 0.36 Tesla (3600 Gauss) for a magnetorheological fluid that contains 30% iron particles by weight.

$$5.371364295 \text{ kiloPascal} * \frac{14.7 \text{ PSI}}{101325 \text{ Pa}} * \frac{144 \text{ in}^2}{1 \text{ ft}^2} * 100 \text{ ft}^2 = 11228 \frac{\text{pounds}}{100 \text{ ft}^2}$$

This value of 11228 pounds per 100 square feet, when input into the Bingham Plastic model with slot approximation gives a change in pressure per unit length of approximately 14 pounds per square inch per foot for a 14 3/4" section being drilled with 10 3/4" drill collars. In this scenario the tool is designed such that it would be flush with 10 3/4" drill collars.

For the scenario in which the drilling mud is 11.5 pounds per gallon equivalent (PPGE), the plastic viscosity was assumed to be 30 centipoise. Given the same drill collar and hole size this gives approximately 0.01717 PSI per foot frictional pressure losses. This leads to an equivalent circulating density of 11.83 PPGE. Though the drill collars are not present for the entire length of the well, it will be assumed that this equivalent circulating density is the same regardless of drill pipe, heavy drill pipe, or drill collars being used. The reason for this is that the difference in frictional pressure losses between the drill collars and drill pipe sections would be minimal, whereas the pressure drop across the magnets would be several orders of magnitude higher. Also, any desired change to the equivalent circulating density could theoretically be achieved by a combination of changes in the rheological properties and density of the drilling fluid being used to allow for the 11.83 PPGE circulating density.

For the scenario to be discussed later in which the drilling mud is 16 PPG, the frictional pressure losses outside of the magnetic field will be assumed to be the same as in the drilling mud actually used in the paper. This leads to an equivalent circulating density of 16.2 PPGE. This is done because of the lack of rheological data for a mixture with this fluid density.

RATCHET

The first embodiment of magnetic gradient drilling that will be discussed is ratcheted. This assumes that a ratchet system can be used to allow proper shielding between the magnets and the annular fluid when the magnetorheological affects are not desired. This also assumes the existence of multiple ratchets that can each be controlled individually from the surface. There will therefore be multiple magnetic assembly tools to create magnetic fields, and their associated pressure drops, at multiple points along the drilled interval. The first of these tools does not have to be ratcheted, as the operators could choose to not switch from standard drilling fluids to a magnetorheological

drilling fluid until the first tool reaches the first desired tool activation depth. This section will show the removal of the liner using 5 separate magnetic assembly tools, 4 of which would have to be ratchet operated.

A look at this mud window, starting from the surface, shows that there is a very long interval where the lowest fracture equivalent circulating density is approximately 13 pounds per gallon. This allows for the use of a mud density, with associated frictional pressure losses, that would remain below 13 PPGE until the 2017 meter (6617 feet) casing setting point. This is what was done on the Sepat Barat Deep well number 2. The problem is that at the liner bottom the pore pressure equivalent circulating density is 15.6 pounds per gallon. With magnetic gradient drilling it is possible to “step up” the equivalent circulating density to continue to, and even slightly past, this liner setting depth before setting the first casing.

The first magnetic assembly tool is set approximately 28 meters (92 feet) behind the drill bit. This would place the tool easily within the bottom hole assembly. If the operator switches from standard drilling fluid to magnetorheological fluid with the drill bit at 1796 meters (5892 feet) the tool will be from 1760 meters (5774 feet) to 1769 meters (5800 feet). It should be noted that this is 9 meters of tool (~30 feet); which is the length of standard drill pipe. It should be noted that all of the magnetic assembly tools will be the same length and assumed to have the same effect. The purpose of this tool is not to have significant effect immediately, but is required for sharp changes in the pore pressure deeper in the hole. Drilling with this single tool affecting the hole will continue until 1893 meters (6210 feet).

When the drill bit reaches 1893 meters (6210 feet) the ratchet mechanism shielding the second magnetic assembly tool will need to be activated by the operator. The second magnetic assembly tool should be located approximately 88 meters (289 feet) behind the first magnetic assembly tool.

This tool will also be activated when it occupies the space between 1760 and 1769 meters. Therefore when the second magnetic assembly tool is activated, the first magnetic assembly tool will be located from 1857 meters (6092 feet) to 1866 meters (6122 feet). This will allow safe drilling to continue until the next tool use at the original casing setting point of 2015 meters (6611 feet).

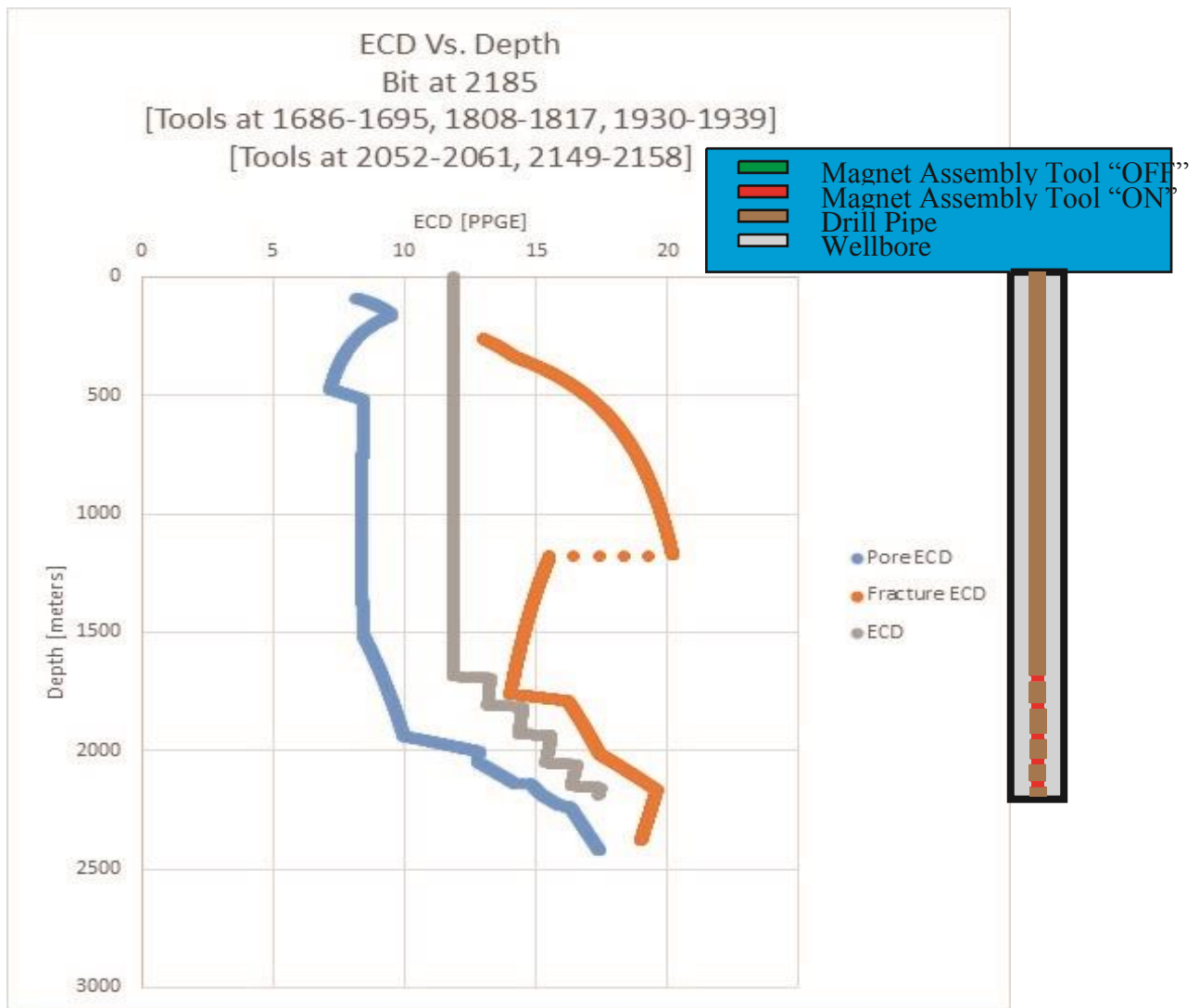
When the drill bit reaches 2015 meters (6611 feet) the ratchet mechanism shielding the third magnetic assembly tool will need to be activated by the operator. The third magnetic assembly tool is located approximately 113 meters (371 feet) behind the second magnetic assembly tool. This places the drill bit at 2015 meters, the first tool from 1979 to 1988 meters, the second tool from 1882 to 1891 meters, and the third tool from 1760 to 1774 meters. This also leaves a kick margin of 1111 PSI and a fracture margin of 1116 PSI. This setup will allow the operator to continue until the shielding from the fourth tool is ratcheted out of the way by the operator when the drill bit reaches 2137 meters (7011 feet).

At 2137 meters the operator will need to activate the ratchet on the fourth magnetic assembly tool. This will again happen when that tool is between 1760 and 1774 meters. This tool will be spaced similarly to the previous two tools, which is 113 meters behind where the previous tool ends. This will give place a drill bit at 2137 meters, the first tool from 2101-2110 meters, the second tool from 2004 to 2013 meters, the third tool from 1882 to 1891 meters and the fourth tool from 1760 to 1774 meters. This is also the point where the location of the first tool becomes significantly important due to the sharp increase in the pore pressure near the drill bit.

The last section, drilling to 2222 meters (7290 feet) was slightly more challenging to accomplish with the given inputs. It can be seen in the next images that simply continuing drilling with the current tool layout would almost help the operator reach the desired depth of 2213 meters. The

problem is that the pore pressure just above the lowest tool is slightly higher than the equivalent circulating density. This problem could be corrected with some slight back pressure being applied at the surface, but it would be preferential to continue using the tools as they are. It should also be noted that the actual target in order to remove the liner is 2215 meters. Therefore drilling will continue to 2185 meters before activation of the final magnetic assembly tool.

Now that the bit is at 2185 meters the operator will move the final ratchet to allow the fifth magnetic assembly tool to influence the magnetorheological fluid. This will allow for safe drilling to a depth of 2222 meters (7290 feet) without further incidence. This places the drill bit at 2222 meters; and tools at 1723-1732, 1845-1854, 1967-1976, 2089-2098, and 2186-2195 meters. This also means that the previous casing setting point of 2017 meters has been extended to beyond the 2213 meter liner setting depth; allowing for the removal the liner.



Bit at 2185 meters with 5 magnetic assembly applying magnetic fields

The most significant drawback associated with this method is the large number ratchets that have to be activated at different times.

If this analysis is started at the 2017 meter casing depth then it would be best to use the 16.5 PPGE leak off test results instead of the interpolated fracture pressure at this depth. It is also not known what the leak off pressure below this point is and whether there is an immediate formation change that would allow for a much higher leak off pressure. It is assumed that there is a formation change that would allow for the activation of a single tool slightly below this depth, though this is not the only possible solution as will be described in slightly more detail in this sections conclusion.

First it is assumed that the well is drillable to the liner setting depth of 2213 meters, 7260 feet, as was the case in the actual well, without the need for magnetic gradient drilling. Unlike the actual

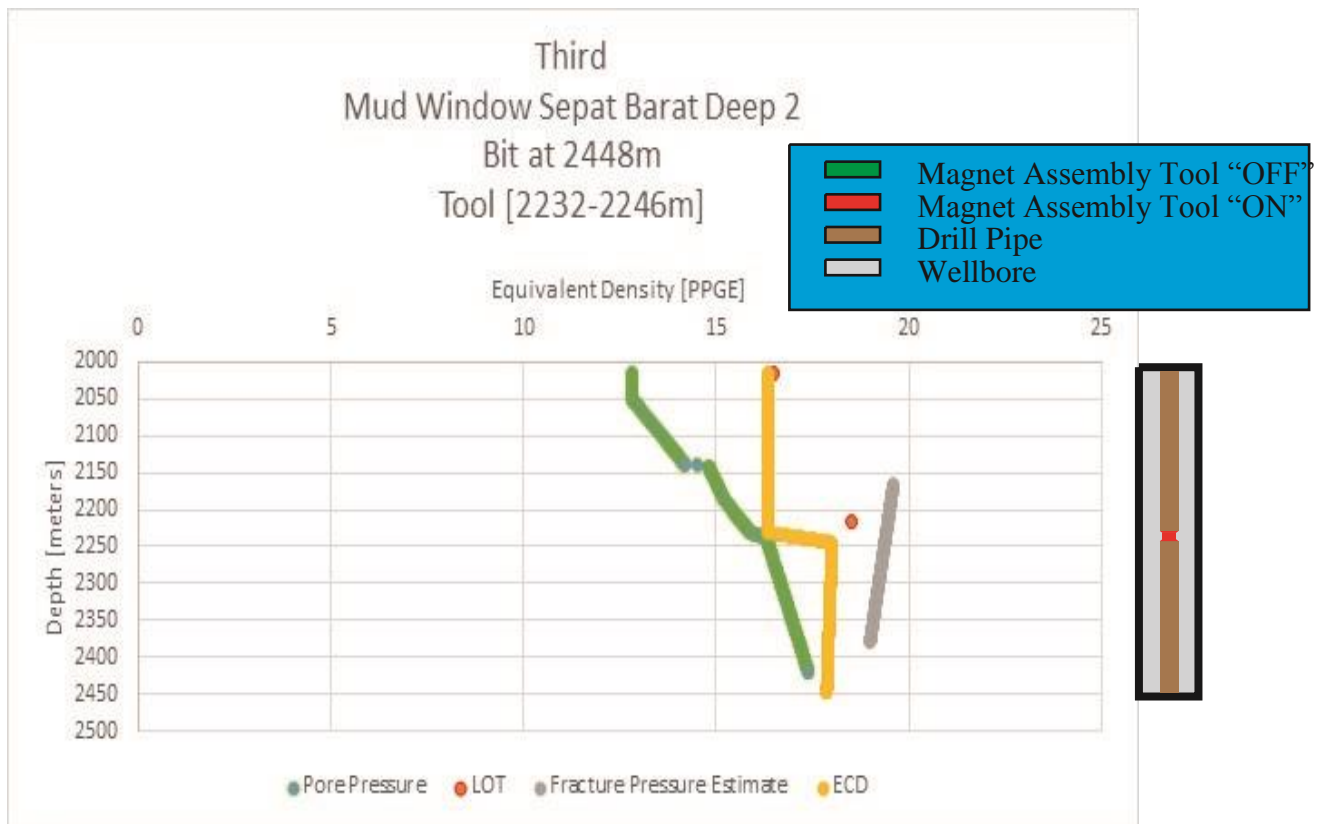
well though, it is undesirable to set the liner at this depth because the object is to remove it. Therefore the tool will be located approximately 203 meters, 666 feet, behind the drill bit. The drilling fluid used in the actual Sepat Barat Deep well 2 was 16 pounds per gallon static and had 16.2 PPGE circulating density due to frictional pressure losses (Ismail et al. 2012) (Nordin et al. 2012). An assumption that the change in weighting material will not significantly change the frictional pressure losses outside the influence of a magnetic field has been made for simplicity.

Final Mud Density Window for lower section of Sepat Barat Deep 2

Also, as mentioned in the previous subsection, any changes to the rheological properties that would affect the equivalent circulating density could be corrected by changes in the mud density, such that a combination of the mud density and frictional pressure losses equals the 16.2 PPGE circulating density seen in the field.

After reaching 2232 the drilling fluid is switched to a magnetorheological drilling fluid. The tool is already located between 2016 and 2030 meters depth. This gives a tool length of 14 meters (~46 feet). This would be the length of 1 and a half standard 30 foot sections of drill pipe. This could also be created as a single 46 foot section of tool. With this tool activated the well will be below the leak off test pressure at 2017 meters and far below the linearly interpolated formation fracture pressure seen in ratchet section.

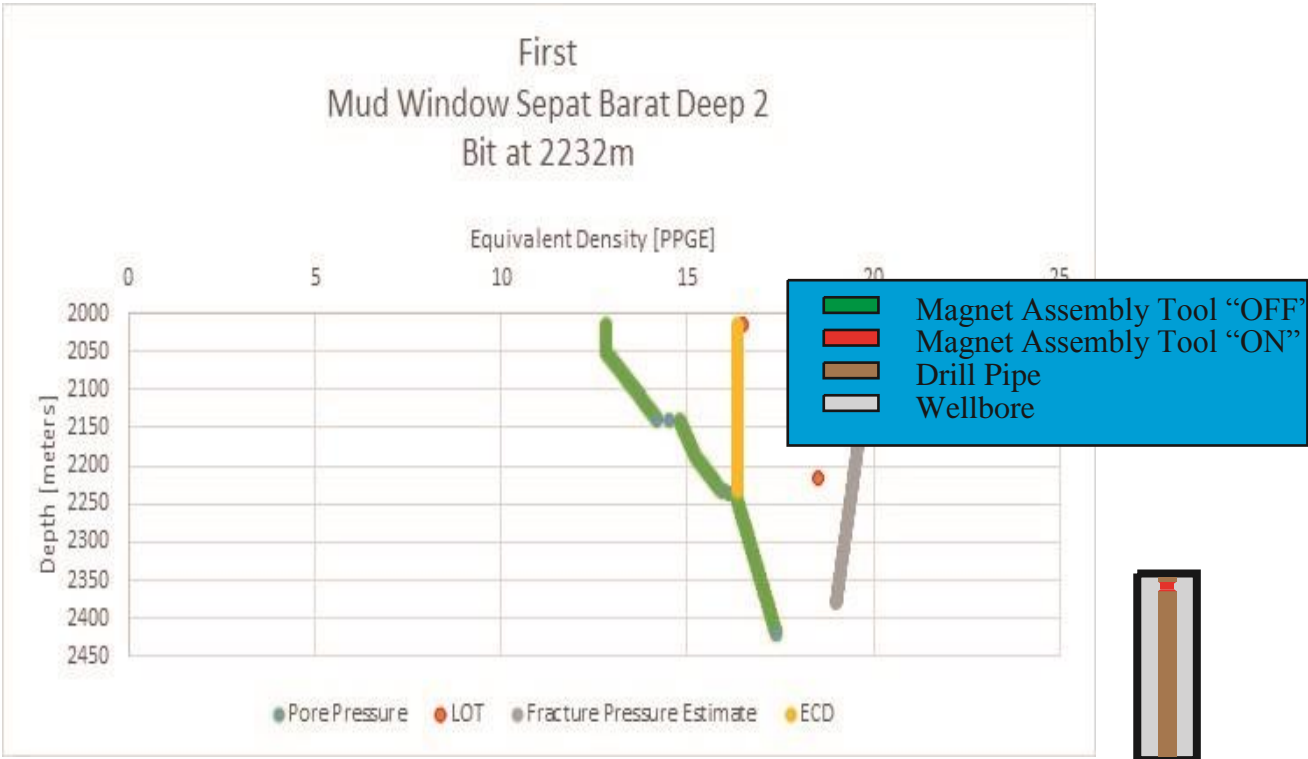
Now that the drilling fluid has been switched over it is safe to continue drilling until the next casing setting point 2426 meters (7959 feet). Not only is it safe to drill to the casing setting depth, but due to the location of the magnet assembly tool it is possible continue drilling until the drill bit reaches 2448 meters (8031 feet). As seen in the following image, the drill bit remains far below the calculated assembly fracture pressure as well as the leak of test pressure performed at 2215 meters, which yielded an equivalent circulating density of 18.5 PPG.



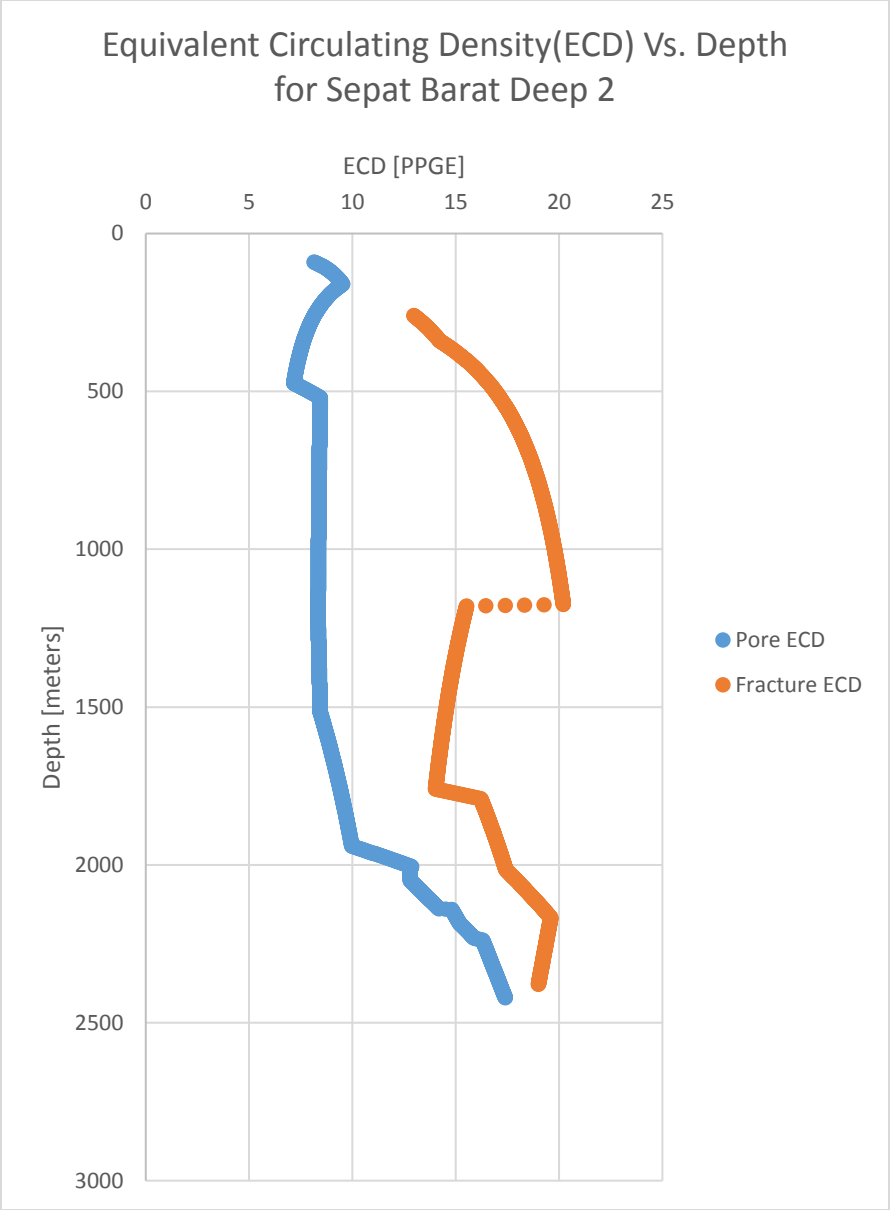
Bit at 2448 meters with a single magnet

Now that the drill bit is at 2448 meters it is time to set the next string of casing. To reiterate, through the use of a single magnet assembly tool in combination with magnetorheological fluid it was possible to combine the liner and the string of casing that would have been set after it into a single casing setting point.

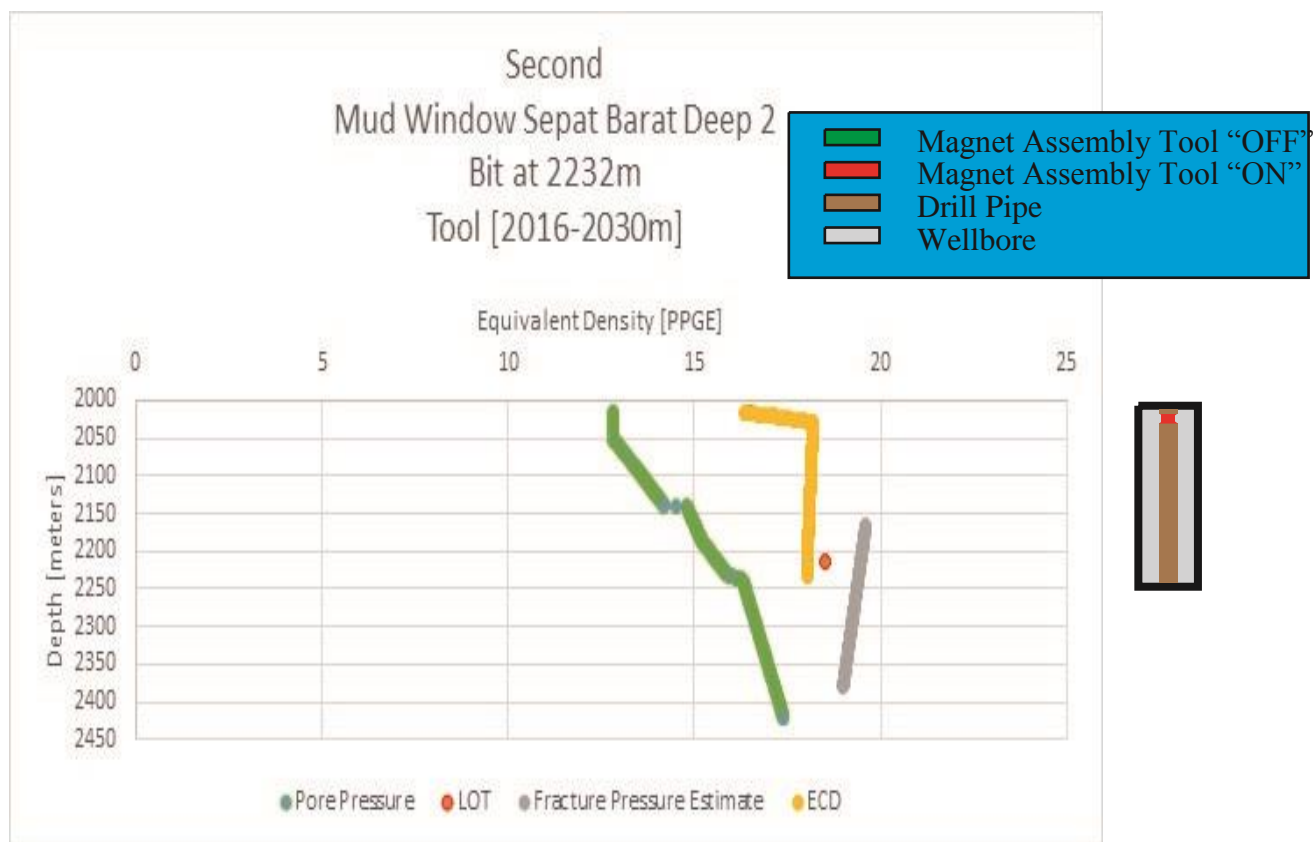
APPENDIX B: ADDITIONAL SIMULATION MUD WINDOW GRAPHS



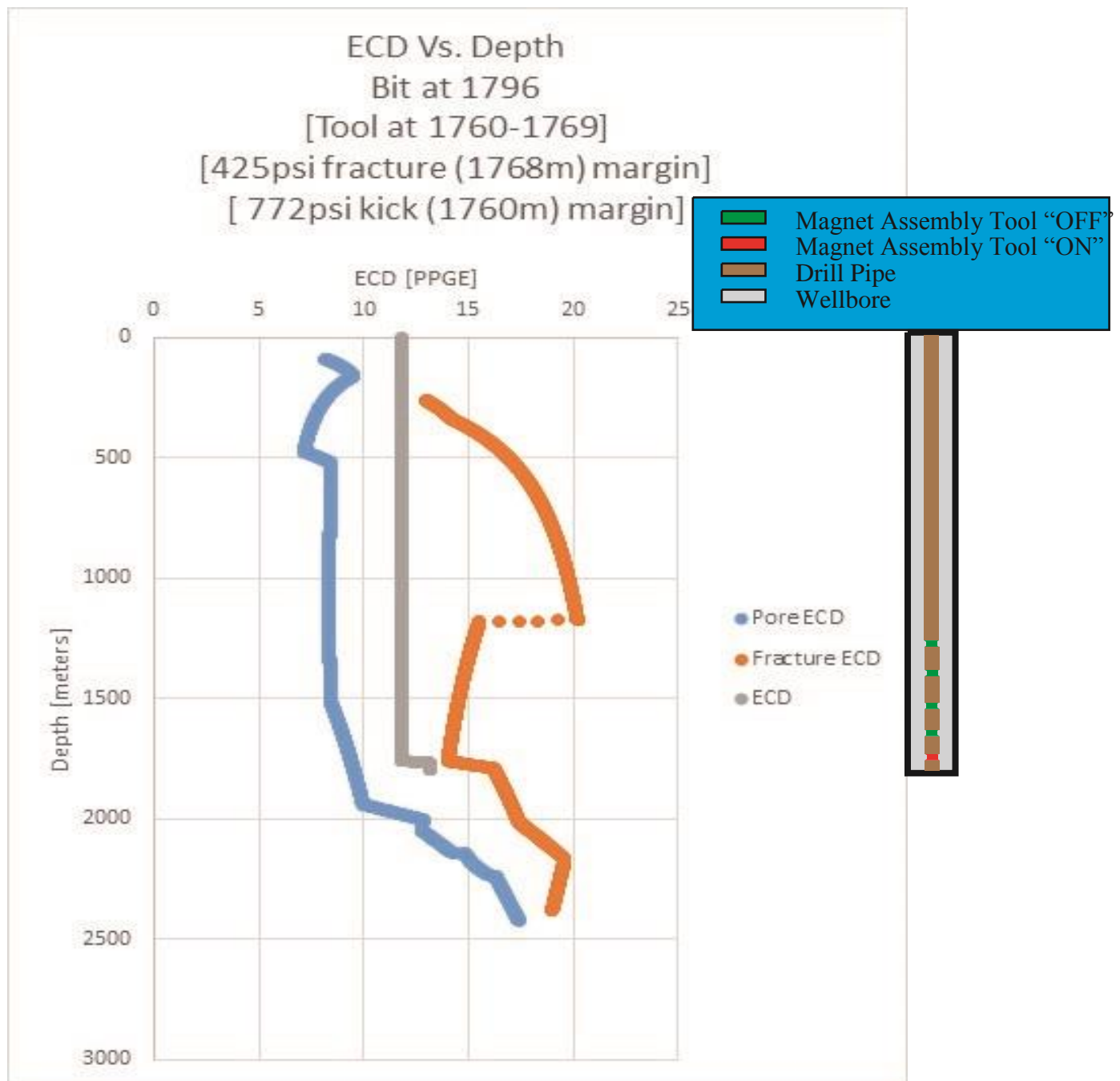
Drill bit at 2232 meters before switching to magnetorheological drilling fluid



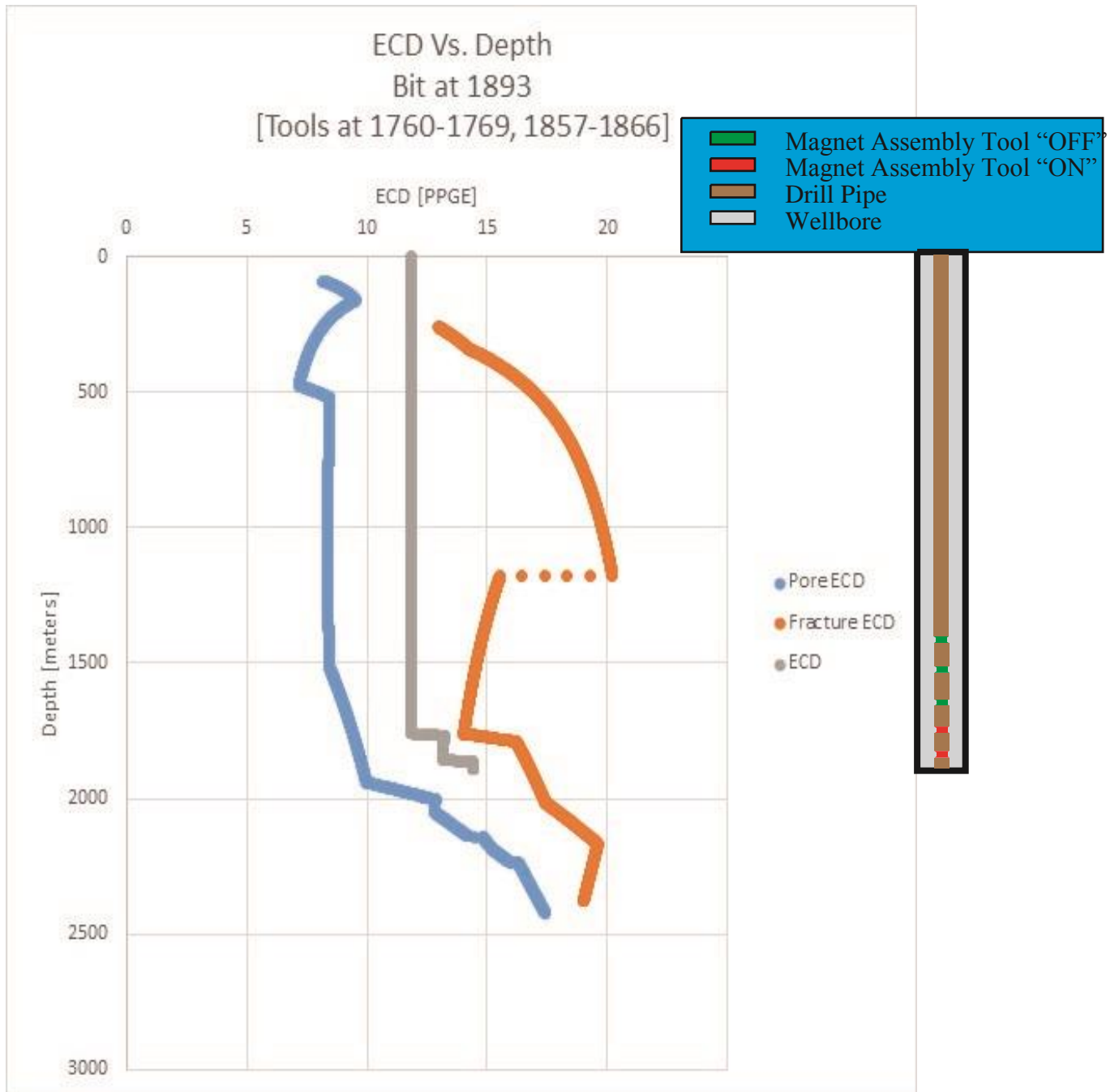
Equivalent Circulating Density for Sepat Barat Deep 2 well.



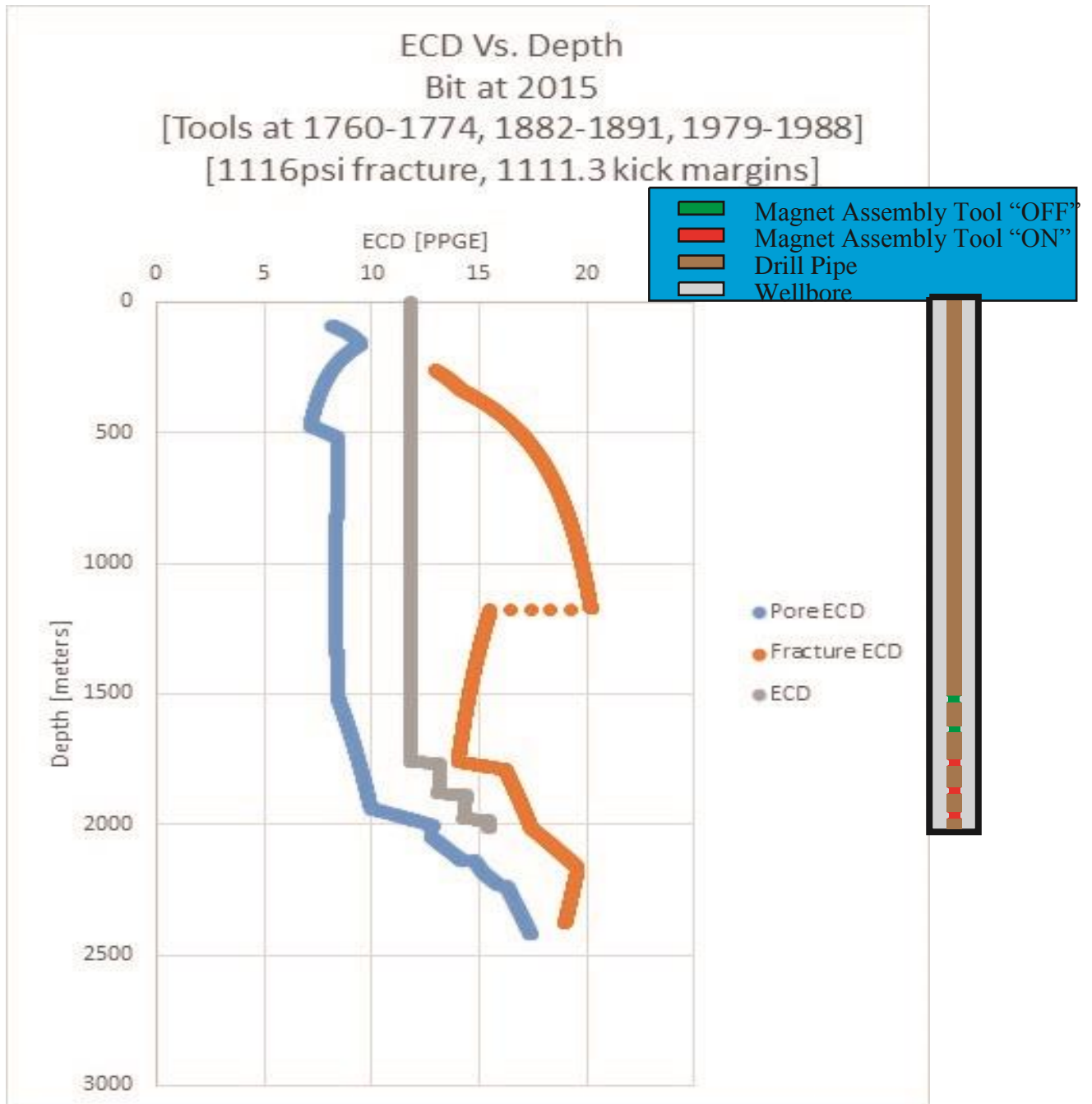
Drill bit at 2232 meters after switching to magnetorheological drilling fluid



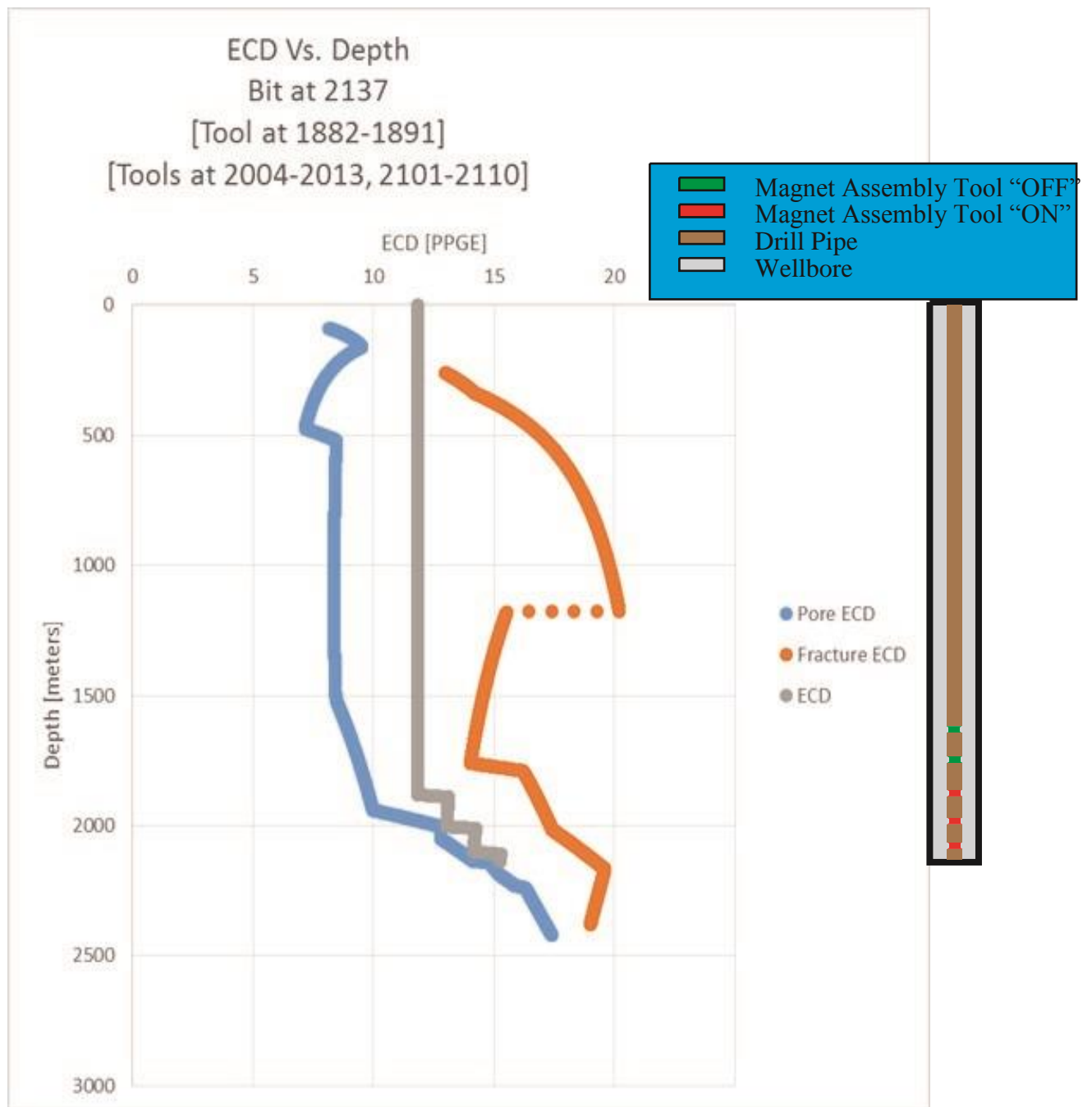
Equivalent circulating density for Sepat Barat Deep 2 well with the drill bit at 1796 meters and a magnet assembly tool applying a magnetic field from 1769-1760 meters.



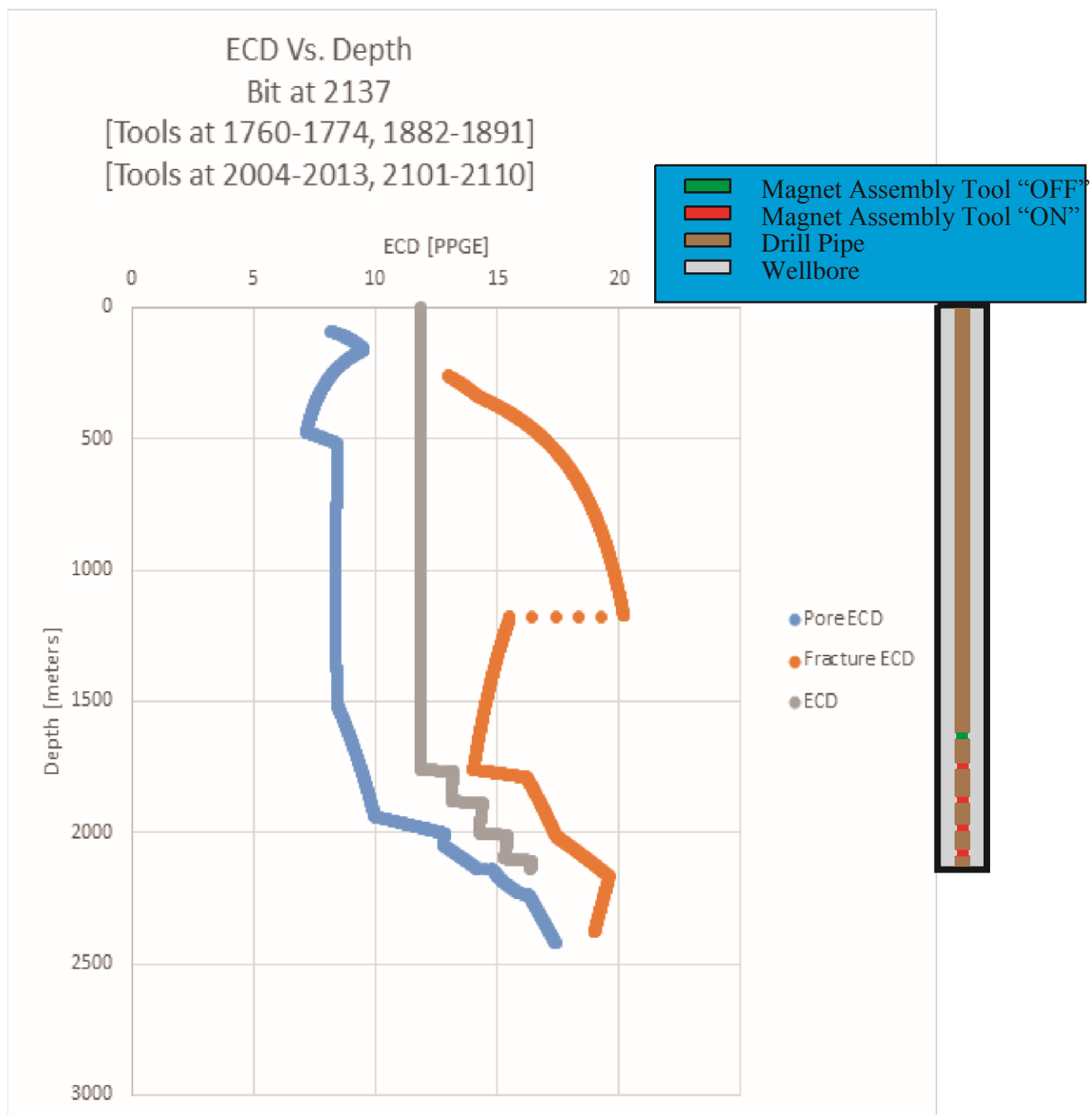
Equivalent circulating density for Sepat Barat Deep 2 well with the drill bit at 1893 meters, and magnet assembly tools apply a magnetic field from 1857-1866 meters as well as 1760-1769 meters.



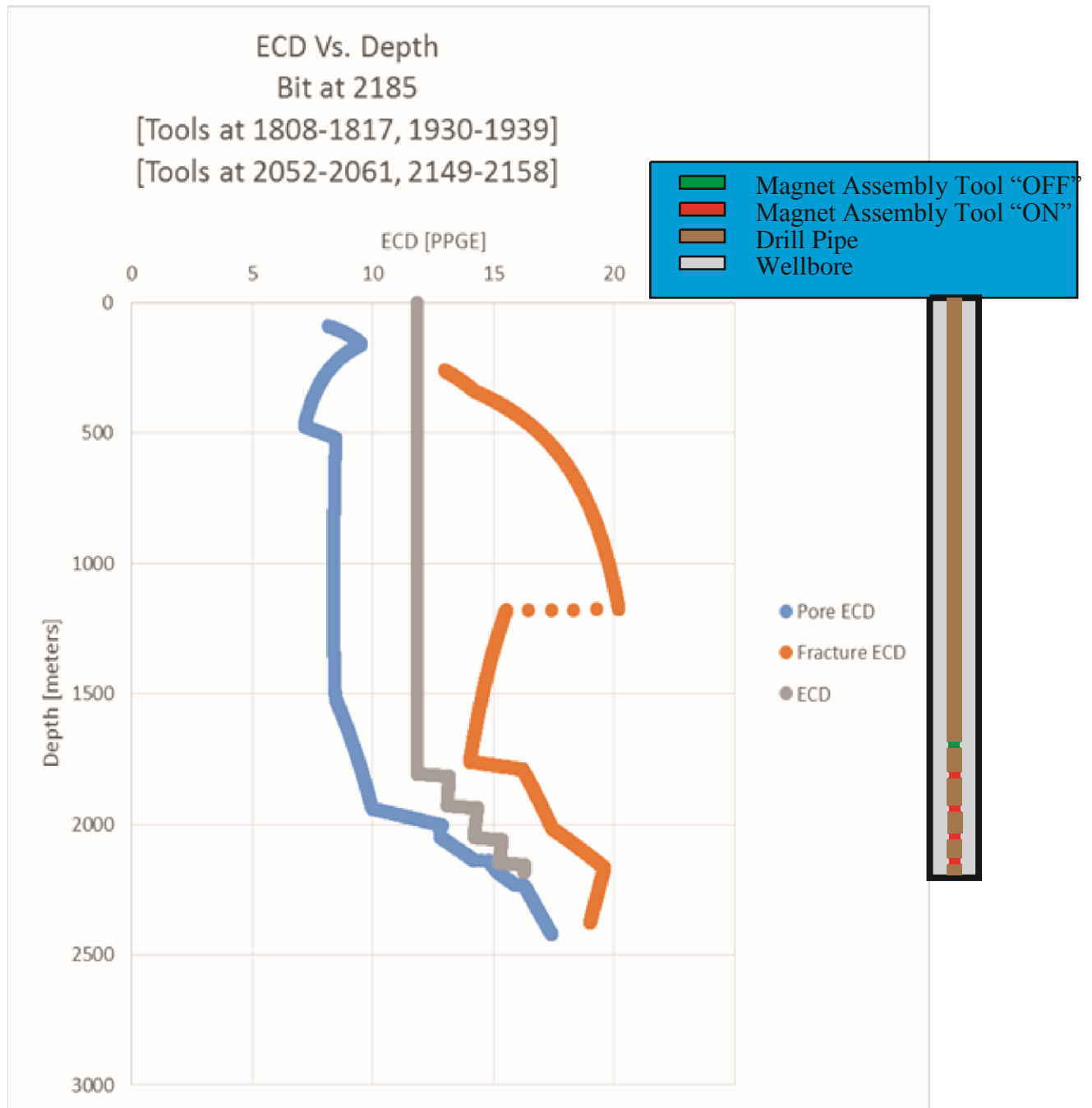
Equivalent circulating density for Sepat Barat Deep 2 well with the drill bit at 2015 meters, and magnet assembly tools apply a magnetic field from 1979-1988 meters as well as 1882-1891 meters and 1760-1774 meters.



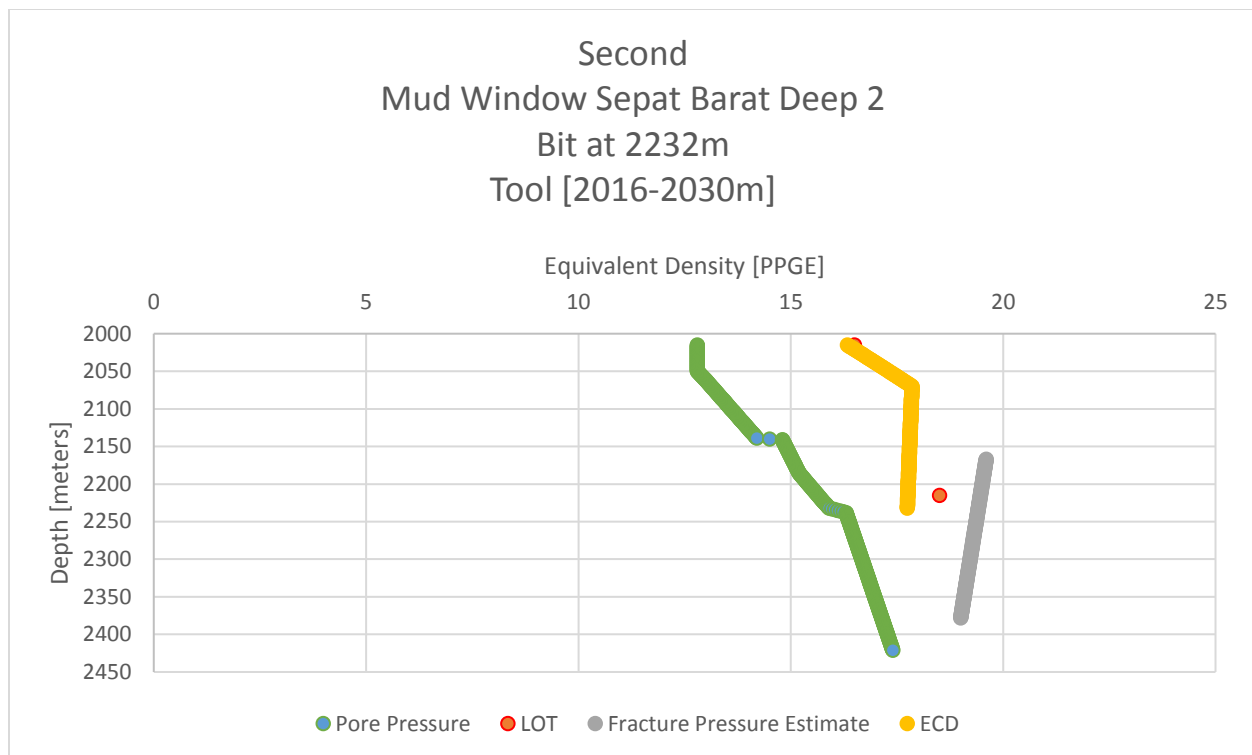
ECD with Pore pressure ECD and Fracture pressure ECD with bit at 2137 and fourth magnetic assembly tool not applying a magnetic field.



ECD with Pore pressure ECD and Fracture pressure ECD with bit at 2137 and fourth magnet assembly tool applying a magnetic field.

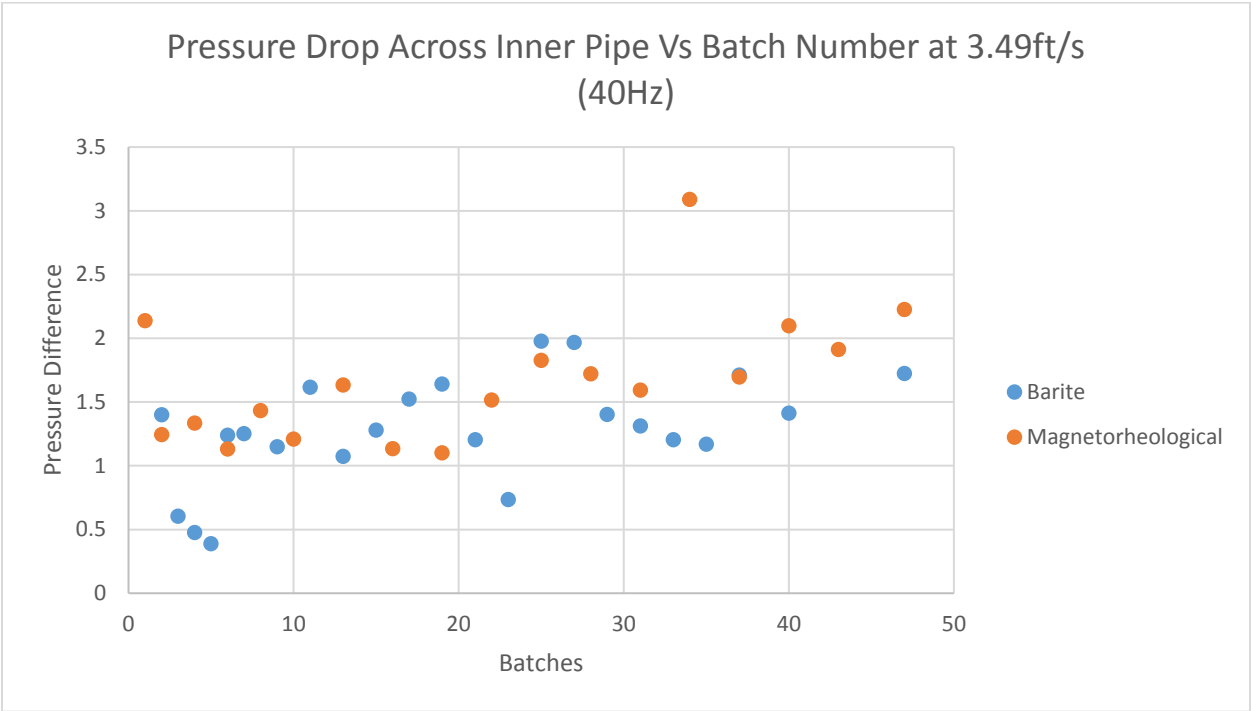


Bit at 2185 meters with 4 magnetic assembly tools applying a magnetic field and 1 magnetic assembly tool not applying a magnetic field.

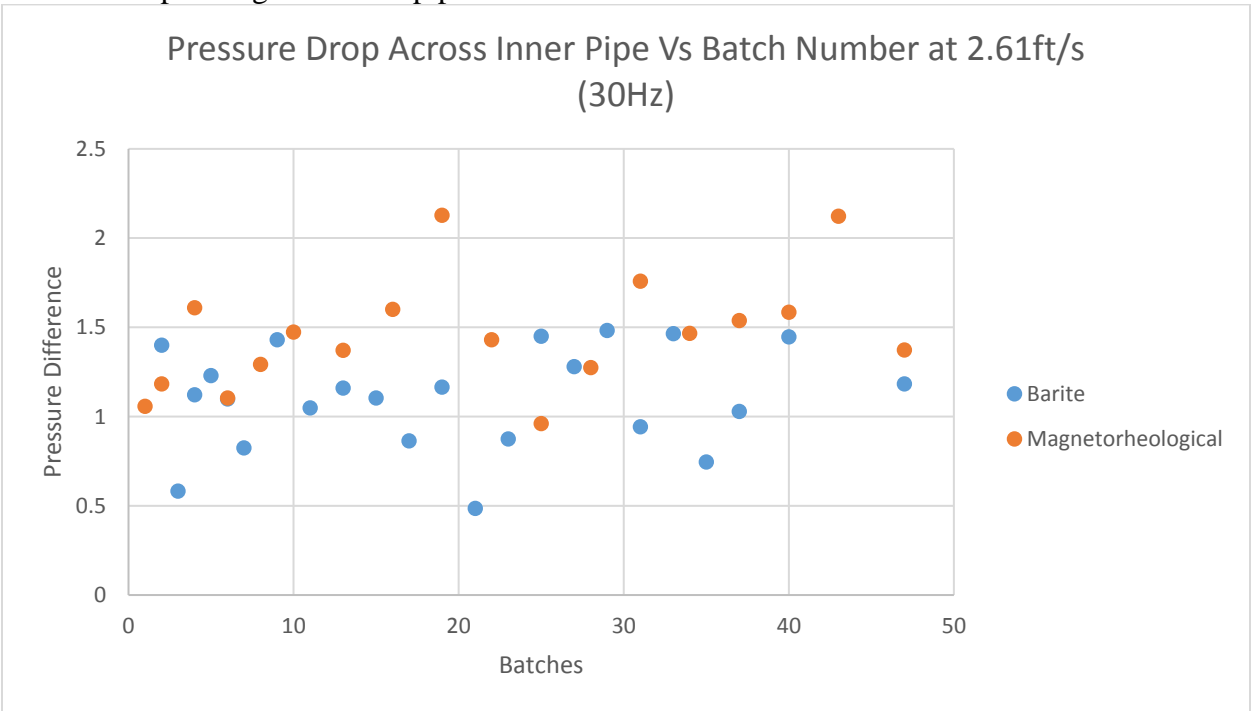


Bit at 2232 meters with tool applying magnetic field. This is using the pressure differentials obtained from the flow loop experiments.

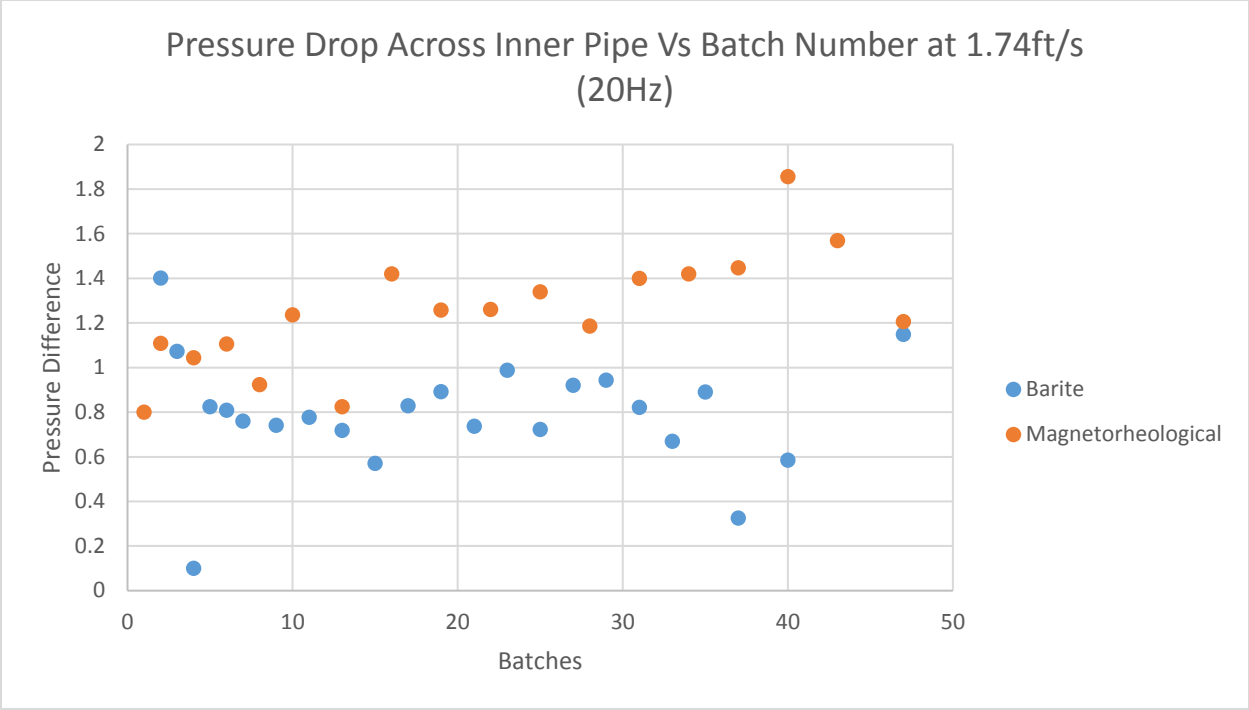
APPENDIX C: ADDITIONAL FLOW LOOP GRAPHS



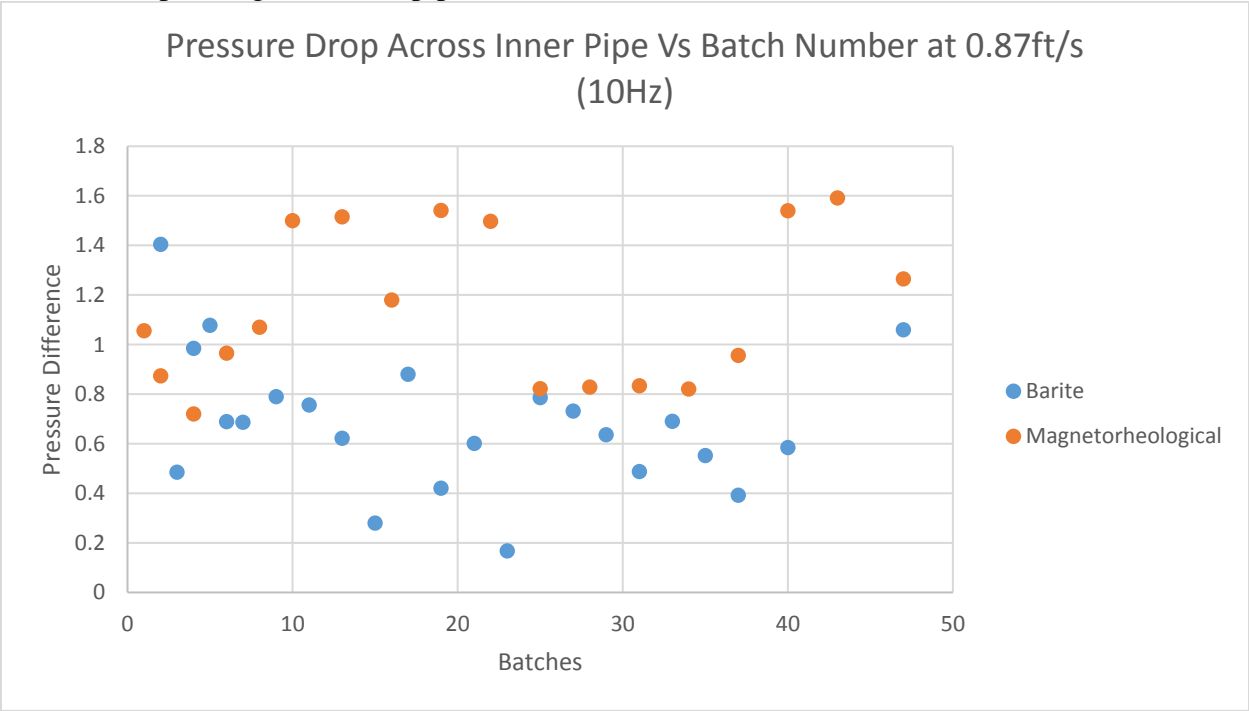
Pressure drop through the inner pipe at 40Hz.



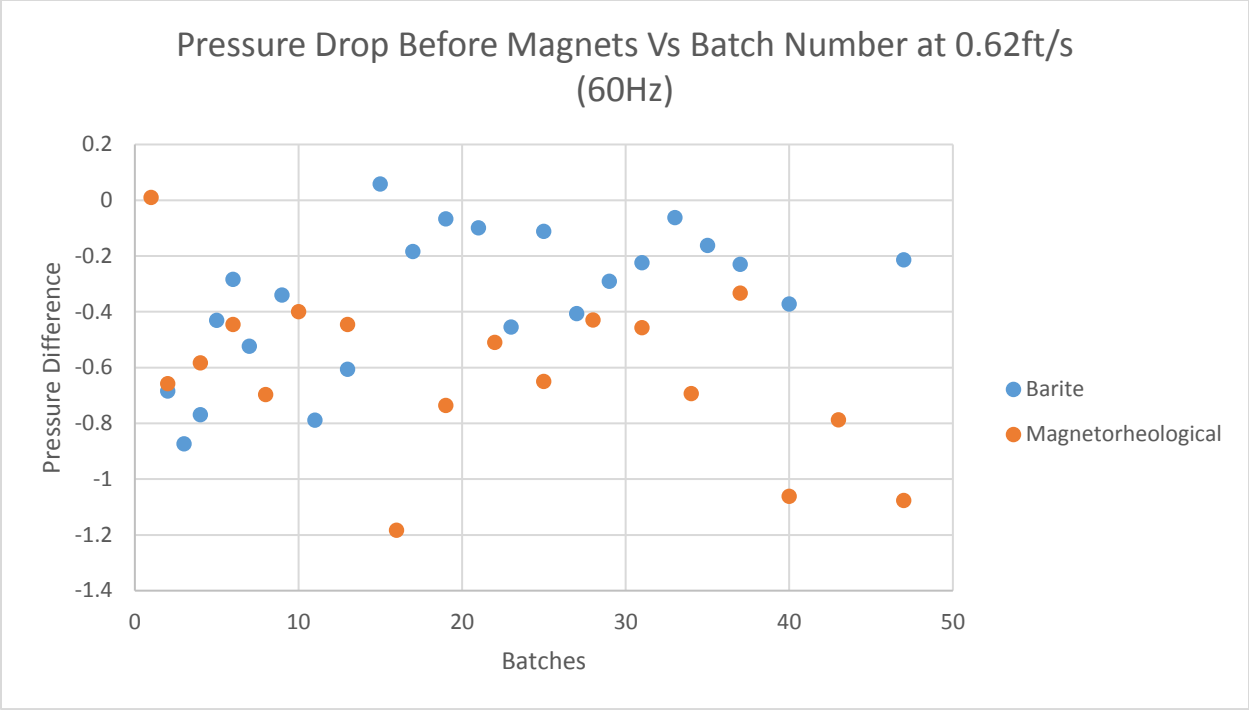
Pressure drop through the inner pipe at 30Hz.



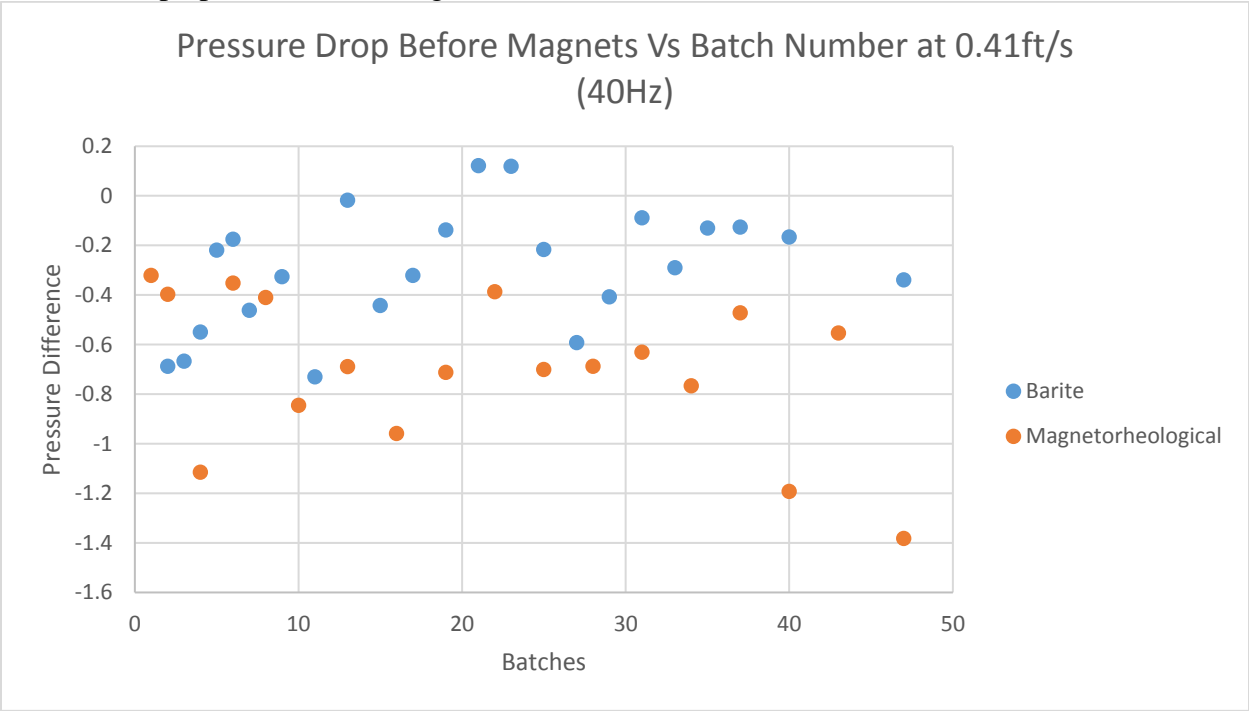
Pressure drop through the inner pipe at 20Hz.



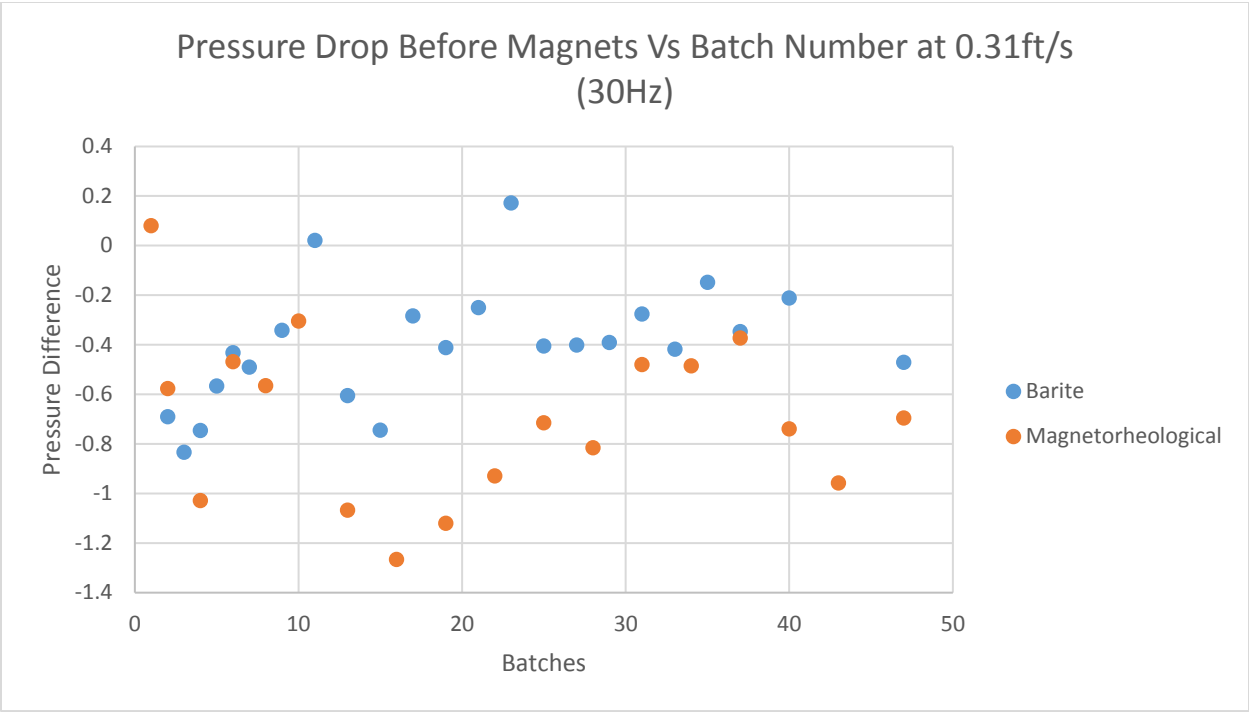
Pressure drop though the inner pipe at 10Hz.



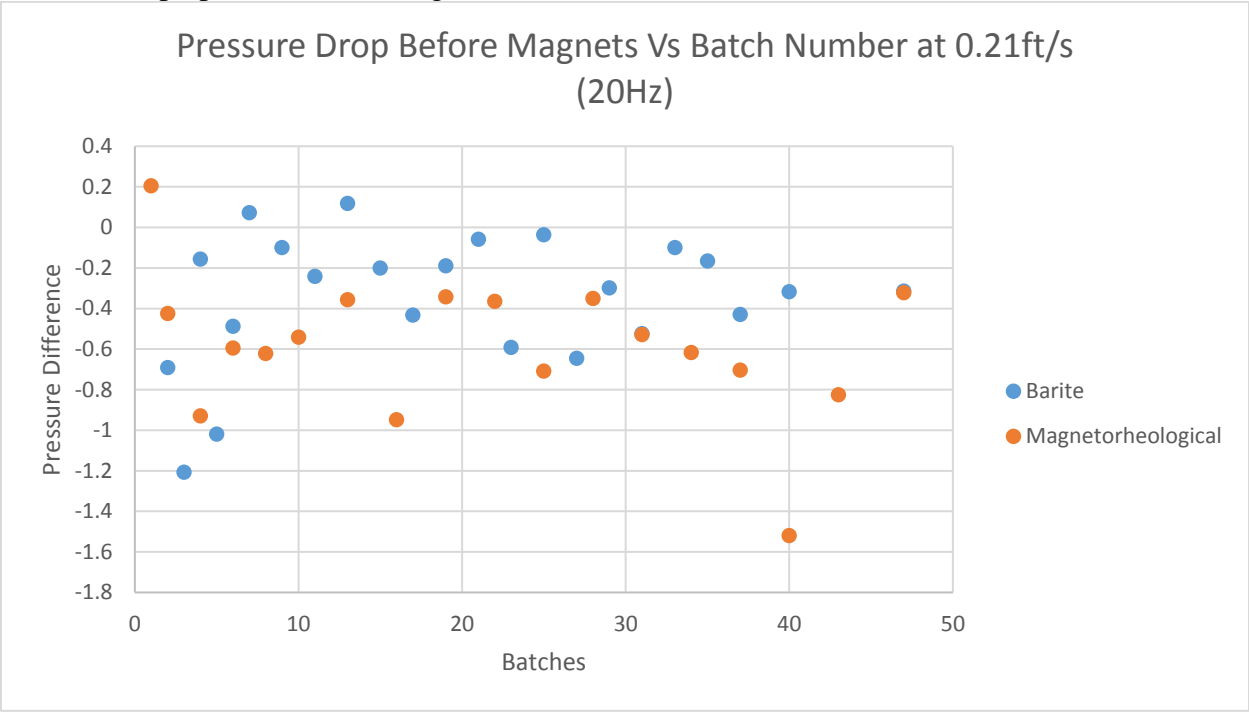
Pressure drop upstream of the magnets in the annulus at 60Hz.



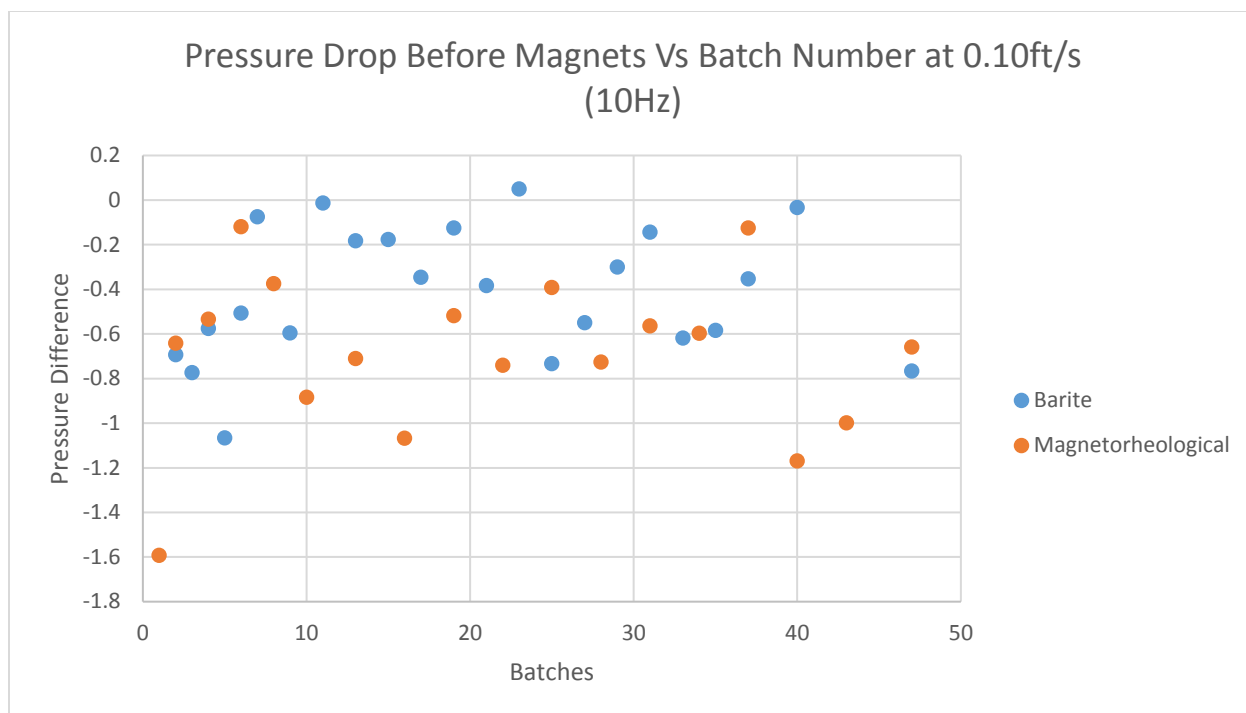
Pressure drop upstream of the magnets in the annulus at 40Hz.



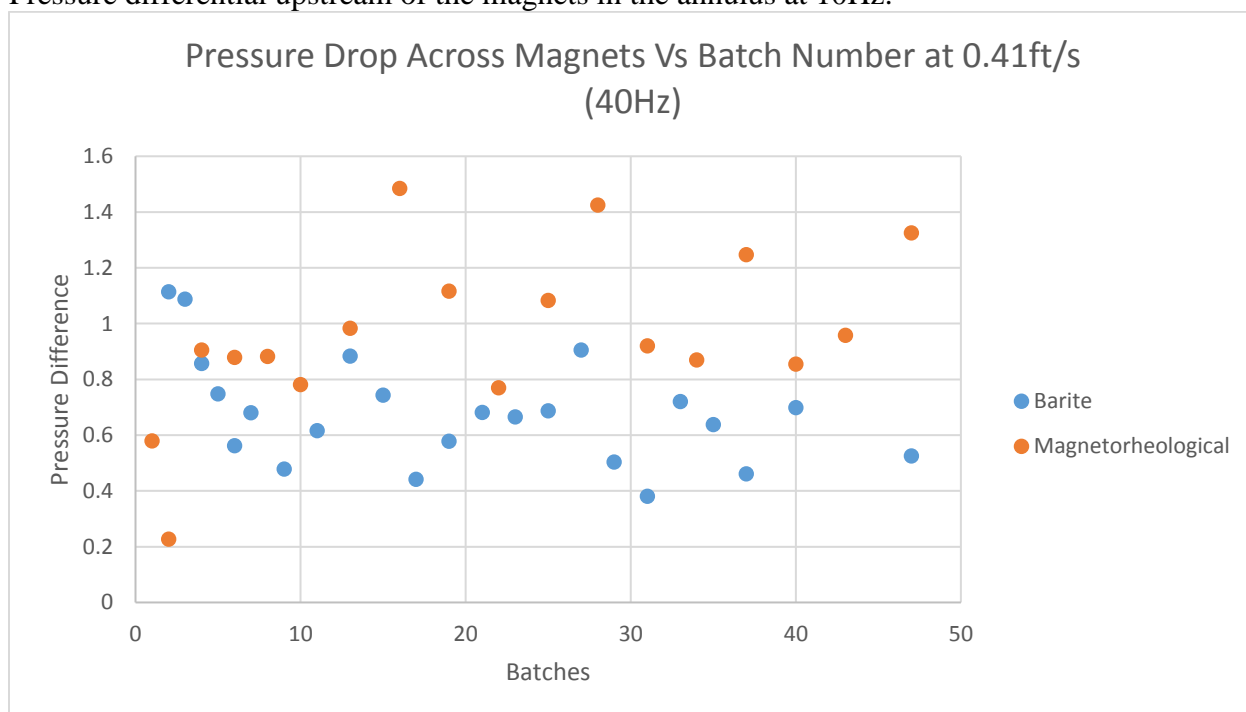
Pressure drop upstream of the magnets in the annulus at 30Hz.



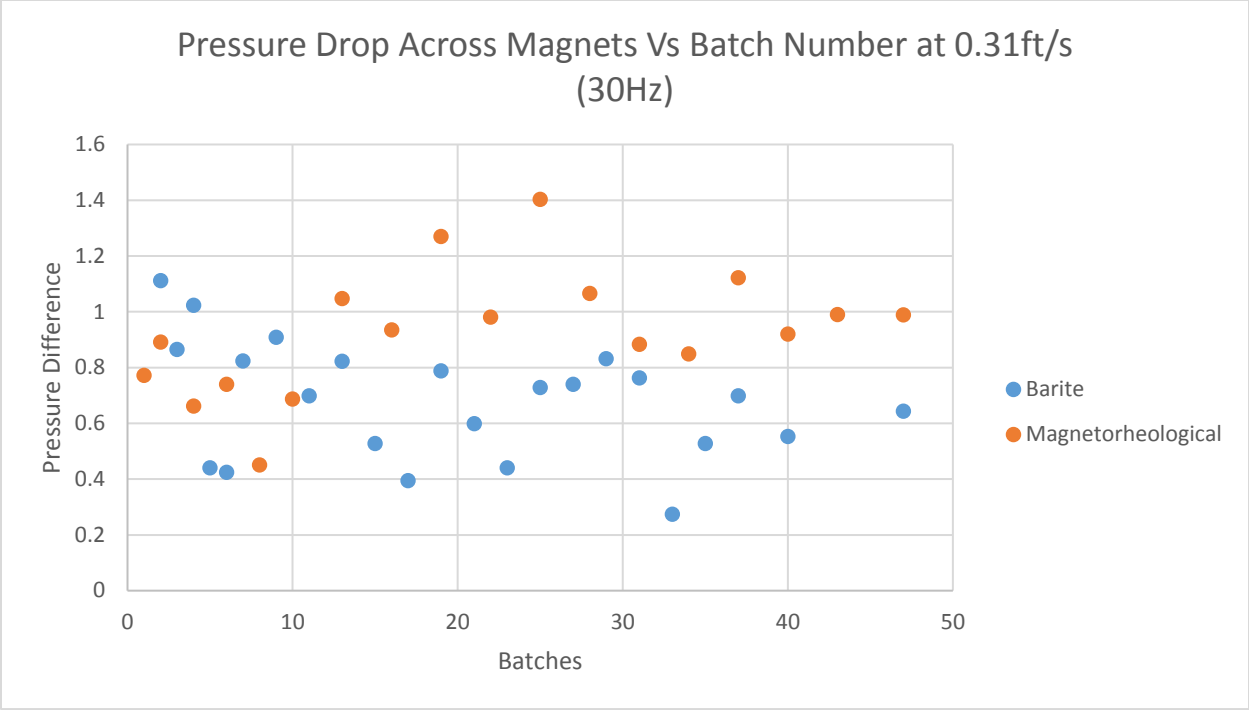
Pressure differential upstream of the magnets in the annulus at 20Hz.



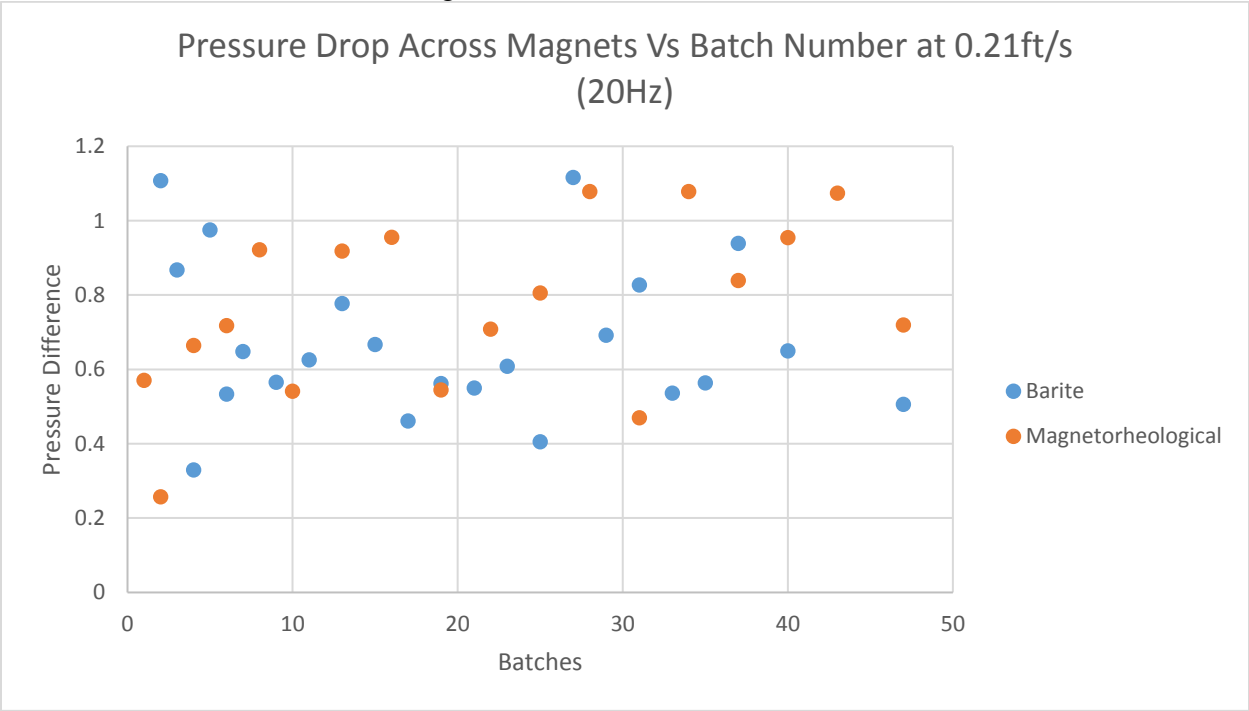
Pressure differential upstream of the magnets in the annulus at 10Hz.



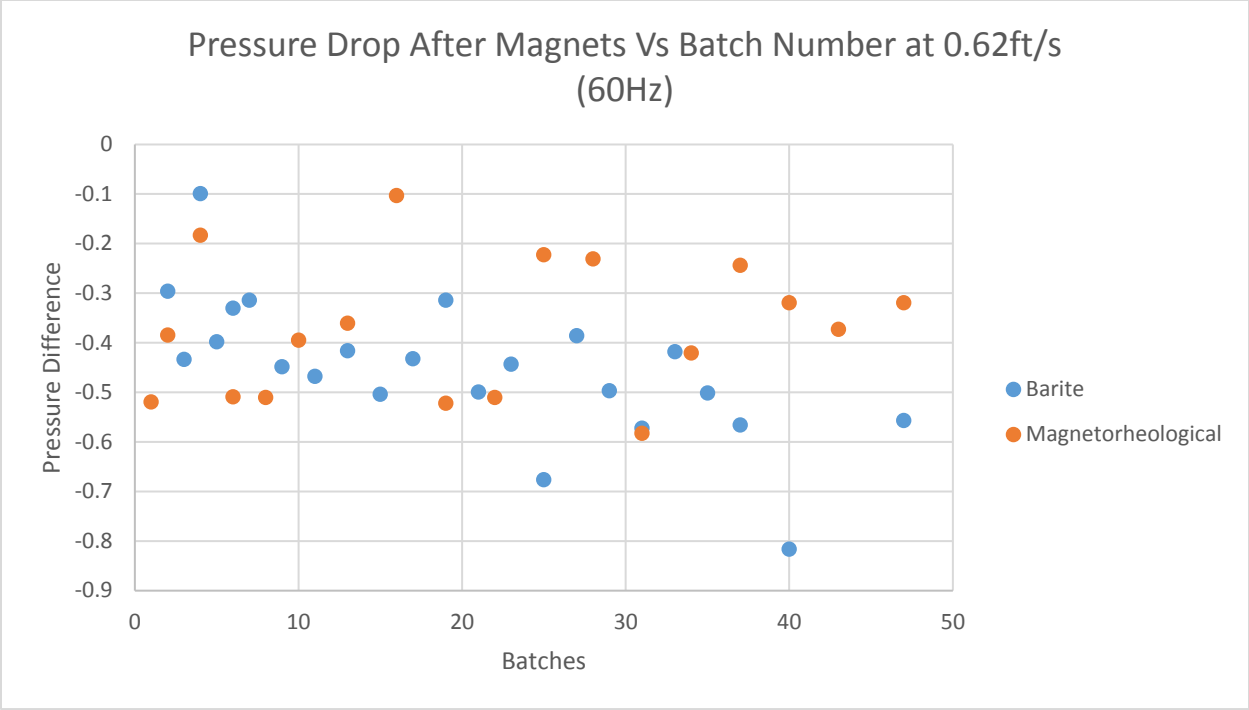
Pressure differential across the magnets in the annulus at 40Hz.



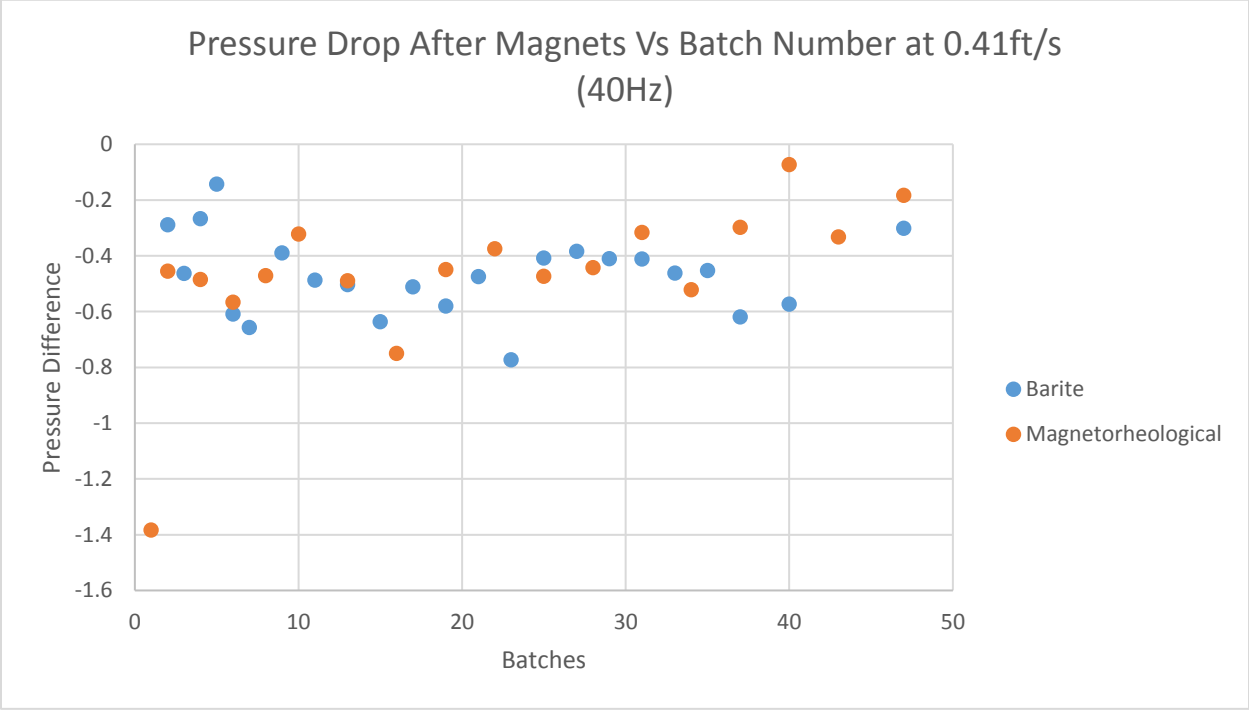
Pressure differential across the magnets in the annulus at 30Hz.



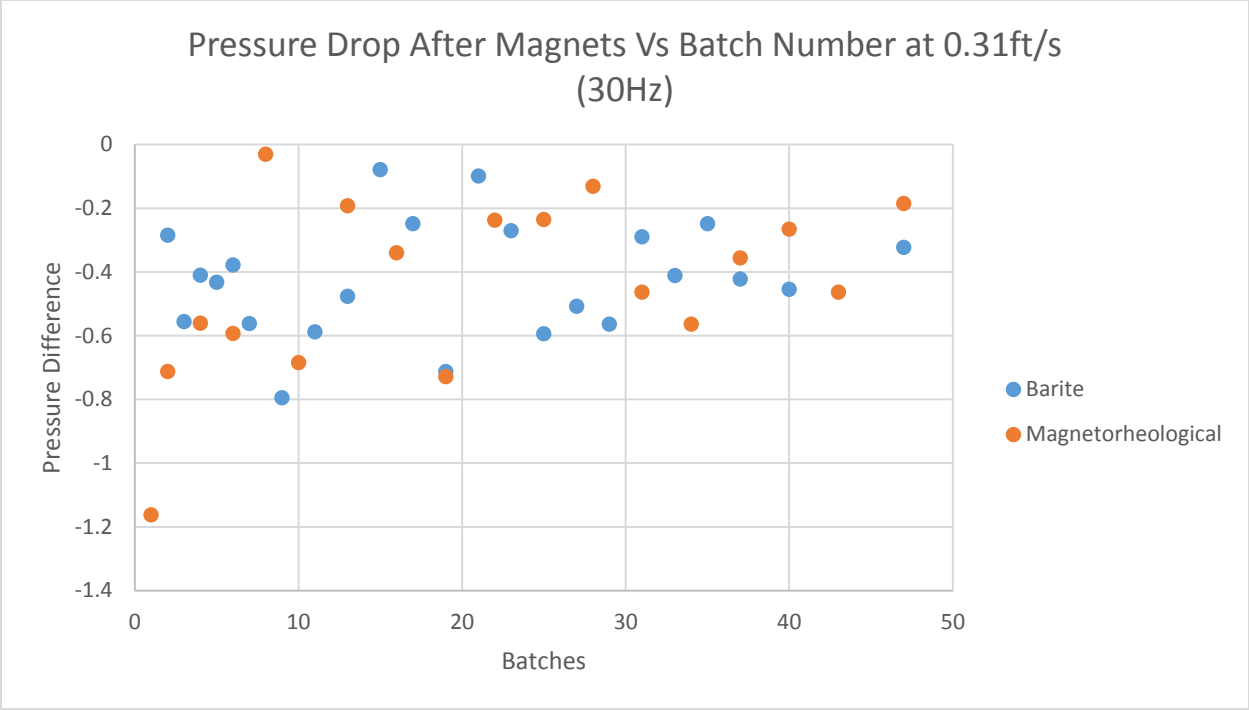
Pressure differential across the magnets in the annulus at 20Hz.



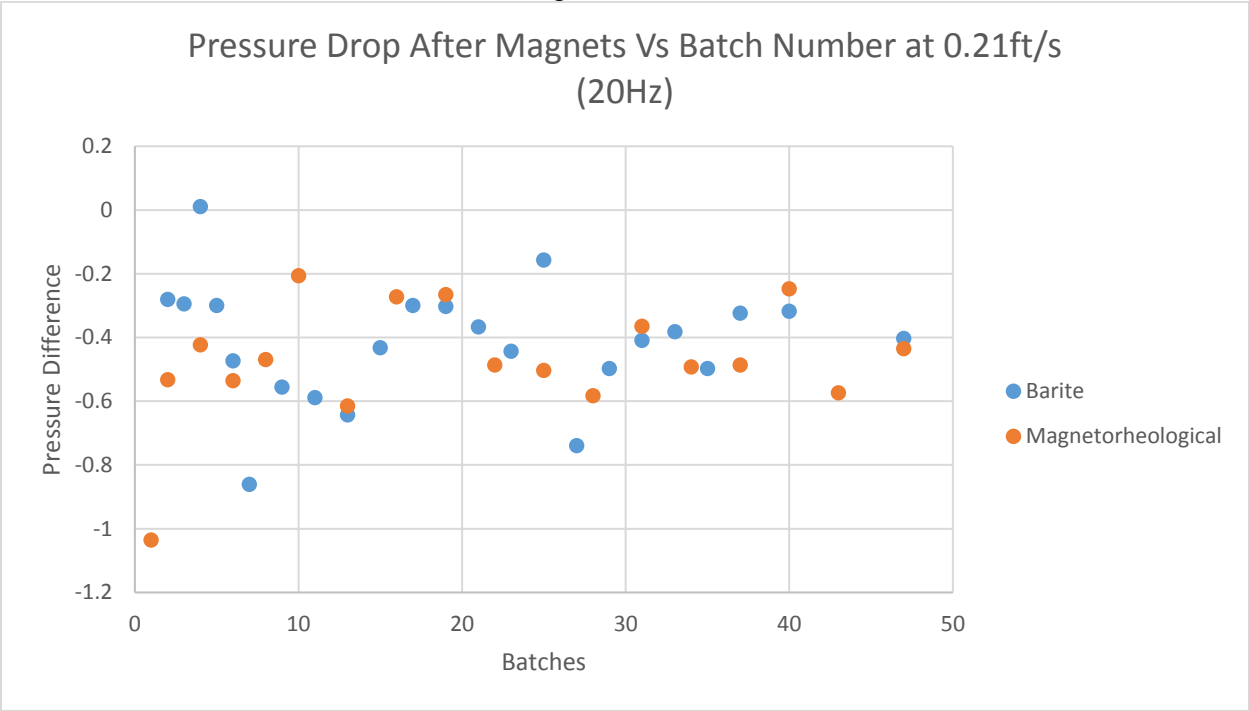
Pressure differential after the magnets in the annulus at 60Hz.



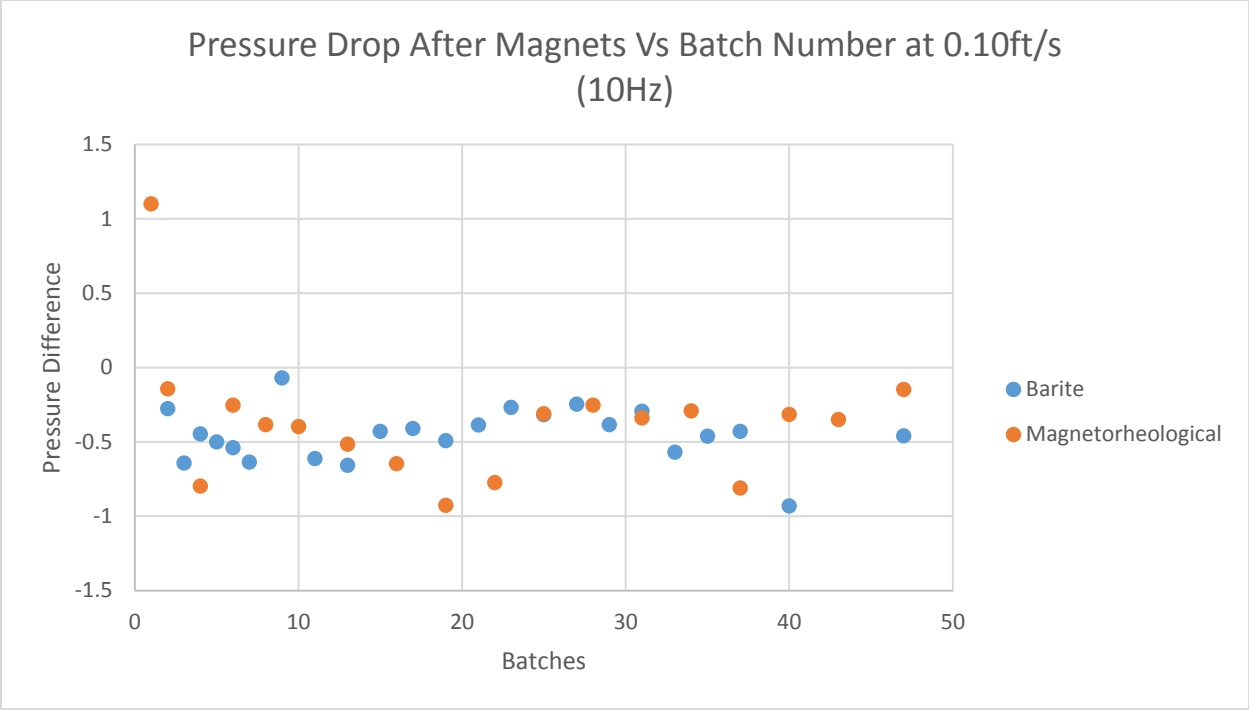
Pressure differential downstream of the magnets in the annulus at 40Hz.



Pressure differential downstream of the magnets in the annulus at 30Hz.



Pressure differential downstream of the magnets in the annulus at 20Hz.



Pressure differential downstream of the magnets in the annulus at 10Hz.

APPENDIX D: ADDITIONAL POST EXPERIMENT IMAGES



Image of gelled particles around magnets showing magnetic field lines



Image of gelled particles around magnets showing magnetic field lines



Image of gelled particles around magnets after a portion had been physically removed



Image of gelled particles around magnets after a large amount had been physically removed



Image showing gelled fluid aligned with magnetic field lines



Image showing magnetorheological fluid aligned with magnetic field lines of large magnet ring.

APPENDIX E: TABLE OF MAGNETIC FIELD STRENGTHS

Table showing magnetic field strength, in Gauss, at different circumferential phases and radial distance from magnets

Magnet Ring Number		1	2	3	4
Phase Degrees	Segment Size Vertical Distance [inches]	Large S facing out	Large N facing out	Small N facing out	Small S facing out
0	0	325 S	313 N	108 N	322 S
45	0	290 S	288 N	162 N	298 S
90	0	270 S	278 N	99 N	273 S
135	0	260 S	325 N	112 N	234 S
180	0	365 S	280 N	108 N	241 S
225	0	270 S	300 N	124 N	255 S
270	0	310 S	318 N	190 N	216 S
315	0	300 S	308 N	180 N	264 S
0	0.25	63 S	60 N	*	14 S
		40-45			
0	0.5	S	45 N	*	6 S
0	0.75	25 S	31 N	*	5 S
0	1	13 S	15 N	*	4 S
0	1.25	16 S	17 N	*	6 S
0	1.5	12 S	11 N	*	4 S
0	1.75	7 S	9 N	*	2 S
0	2	3 S	6 N	*	1 S

Table showing magnetic field strength of magnets based on location on magnet or between magnets within the same ring.

		1	4
Ring Size		Large N over S	Small S over N
Locations			
On magnet	downstream	186 N	206 S
	middle	306 N	247 S
	upstream	336 N	267 S
In-Between Magnet	downstream	61 N	
	middle	70 N	78 S
	upstream	57 N	

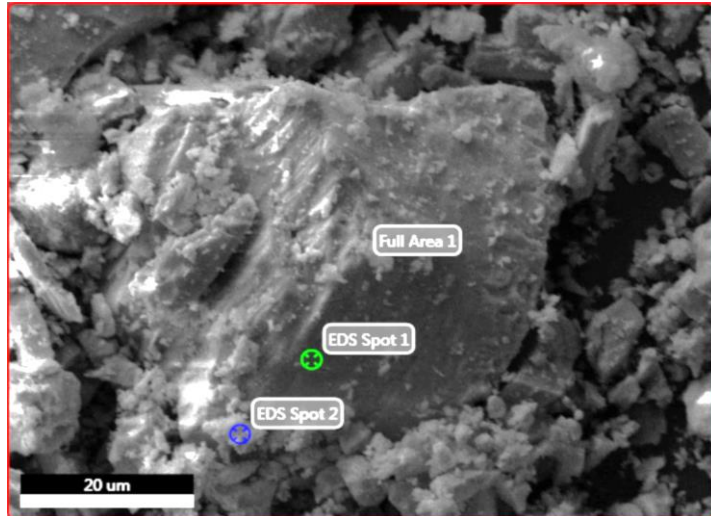
Table showing magnetic field strengths in Gauss at different distances between individual rings.

Readings Between	Distance	Location Degrees	Halfway between large 0	1/4 from large to small 0	1/2 from large to small 0	3/4 from large to small 0	Halfway between small 0
	0	0	20 S	72 S	37S	31 S	3 N
	0.25	0	6 S	4 N	8S	4 N	6 S
	0.5	0	6 N	11 N	0 N/S	4 N	2 S
	0.75	0	7 N	11N	4 N	2 N	0 N/S
	1	0	8 N	8N	3 N	1 N	0 N/S
	1.25	0	11 N	7 N	4 N	3 N	0 N/S
	1.5	0	12 N	6 N	5 N	3 N	0 N/S
	1.75	0	6 N	5 N	4 N	3 N	0 N/S
	2	0	5 N	4 N	3 N	3 N	0 N/S



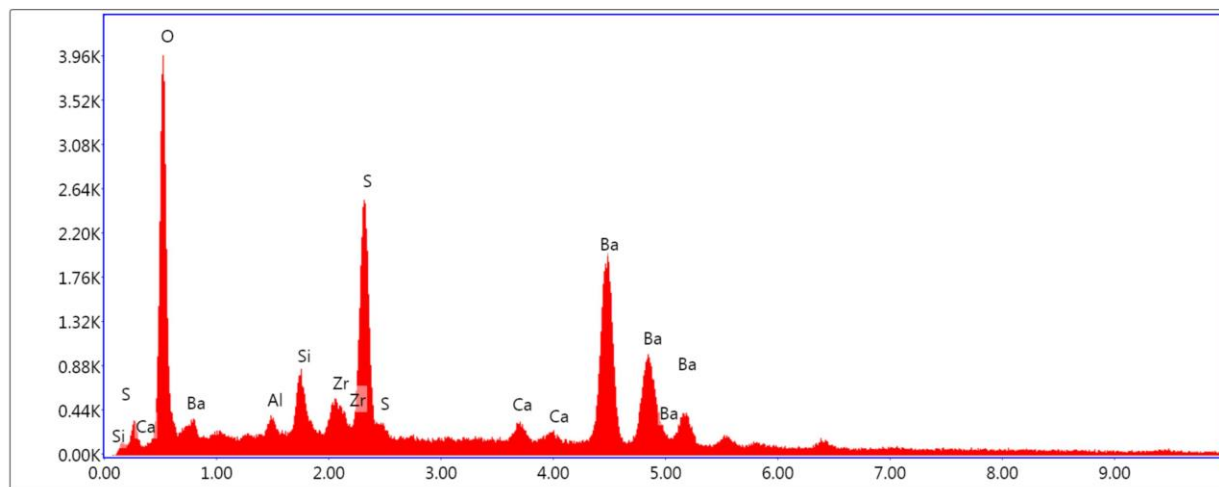
Image showing a 0 Gauss reading with the probe placed against the inside of the inner pipe next to the magnets.

APPENDIX F: ADDITIONAL SEM/EDS IMAGES, TABLES AND GRAPHS



SEM image showing EDS spots for API Barite particle.

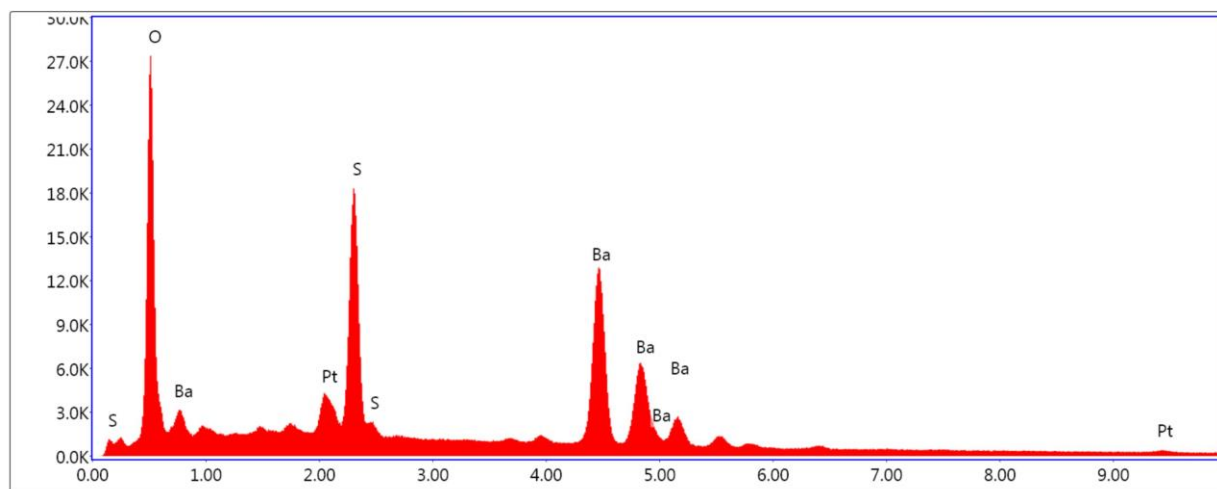
Barite EDS Full Area 1 Graph and Table.



Lsec: 100.0 0 Cnts 0.000 keV Det: Octane Plus Det

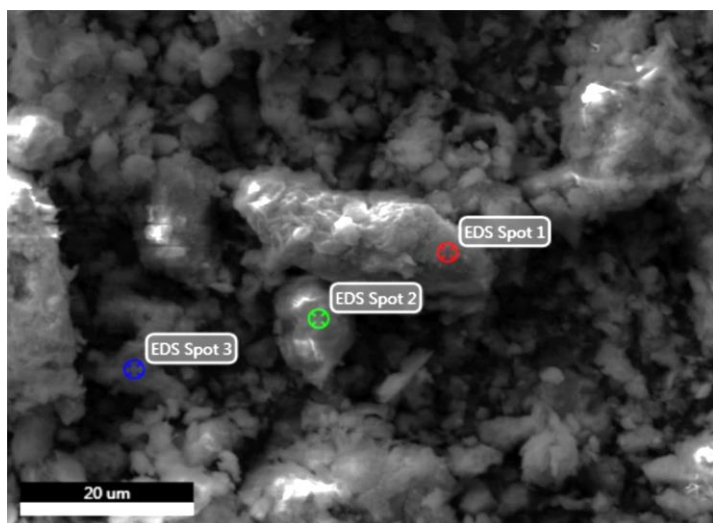
Element	Weight %	Atomic %	Net Int.	Error %	Kratio	Z	R	A	F
O K	25.31	62.72	276.39	7.45	0.1497	1.3143	0.8407	0.4501	1.0000
AlK	1.25	1.83	23.54	11.60	0.0071	1.1728	0.8913	0.4825	1.0065
SiK	2.61	3.68	58.38	8.54	0.0188	1.1995	0.9002	0.5935	1.0099
ZrL	3.06	1.33	33.18	10.03	0.0231	0.9067	1.0651	0.8098	1.0267
S K	10.49	12.97	224.40	4.90	0.0942	1.1766	0.9171	0.7512	1.0166
CaK	1.33	1.31	20.33	15.98	0.0149	1.1386	0.9477	0.9122	1.0801
BaL	55.96	16.15	232.97	3.73	0.4693	0.7977	1.1185	1.0221	1.0286

Barite EDS Spot 2 Graph with Table



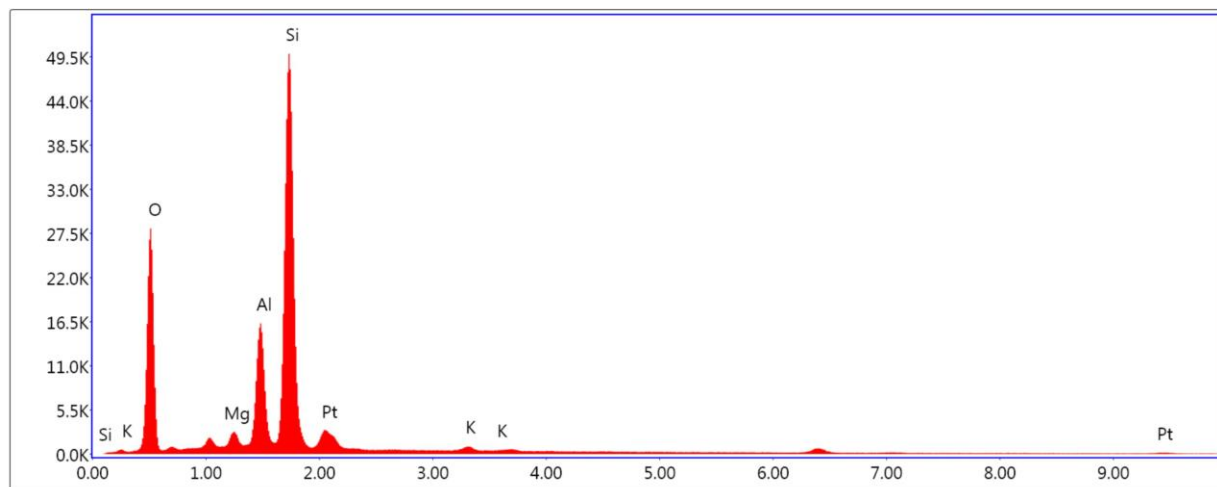
Lsec: 100.00 Cnts 0.000 keV Det: Octane Plus Det

Element	Weight %	Atomic %	Net Int.	Error %	Kratio	Z	R	A	F
O K	26.99	67.61	1943.72	6.56	0.1755	1.3271	0.8343	0.4901	1.0000
PtM	3.07	0.63	198.98	5.56	0.0310	0.7644	1.2239	1.0258	1.2904
S K	11.85	14.81	1543.08	4.15	0.1080	1.1887	0.9110	0.7604	1.0088
BaL	58.10	16.95	1458.01	2.69	0.4896	0.8066	1.1126	1.0219	1.0225



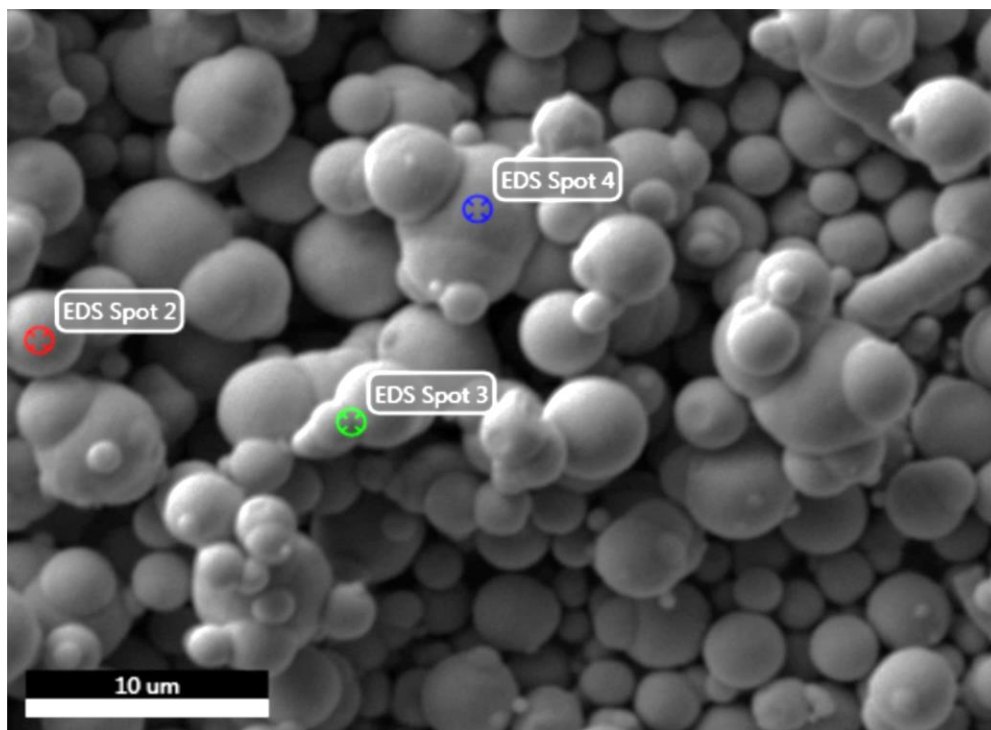
SEM image of Bentonite sample showing EDS locations.

Bentonite EDS Spot 1 Graph and Table



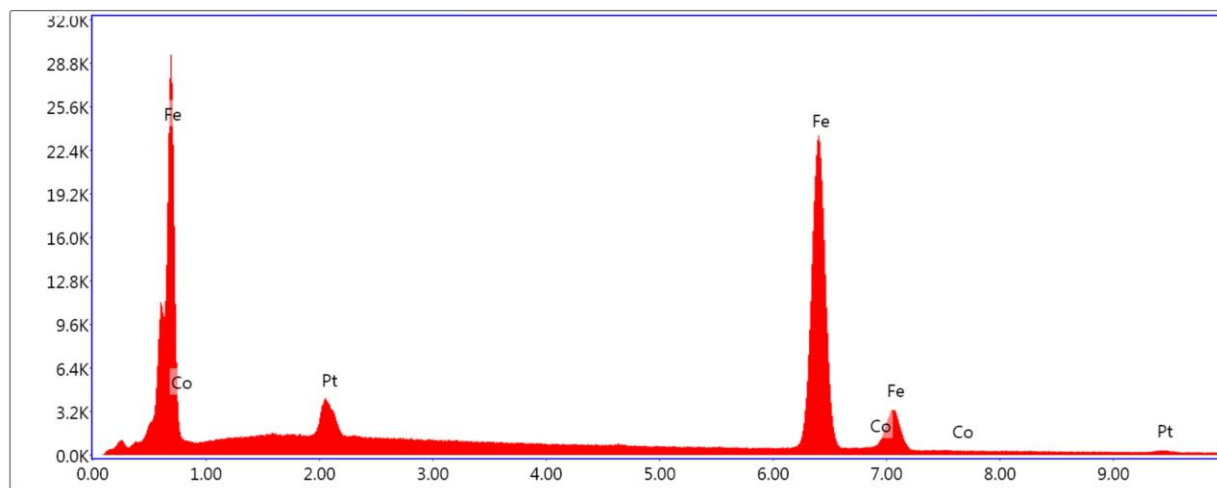
Lsec: 100.00 Cnts 0.000 keV Det: Octane Plus Det

Element	Weight %	Atomic %	Net Int.	Error %	Kratio	Z	R	A	F
O K	45.10	61.27	1866.34	7.13	0.2109	1.0807	0.9605	0.4327	1.0000
MgK	1.29	1.15	145.49	6.14	0.0090	0.9934	0.9947	0.7000	1.0069
AlK	10.42	8.40	1283.80	3.65	0.0808	0.9556	1.0019	0.8036	1.0097
SiK	36.21	28.02	4286.20	3.38	0.2872	0.9756	1.0086	0.8112	1.0024
PtM	6.13	0.68	207.92	4.10	0.0406	0.6138	1.3734	1.0307	1.0472
K K	0.85	0.47	56.77	6.40	0.0070	0.9003	1.0360	0.9062	1.0047



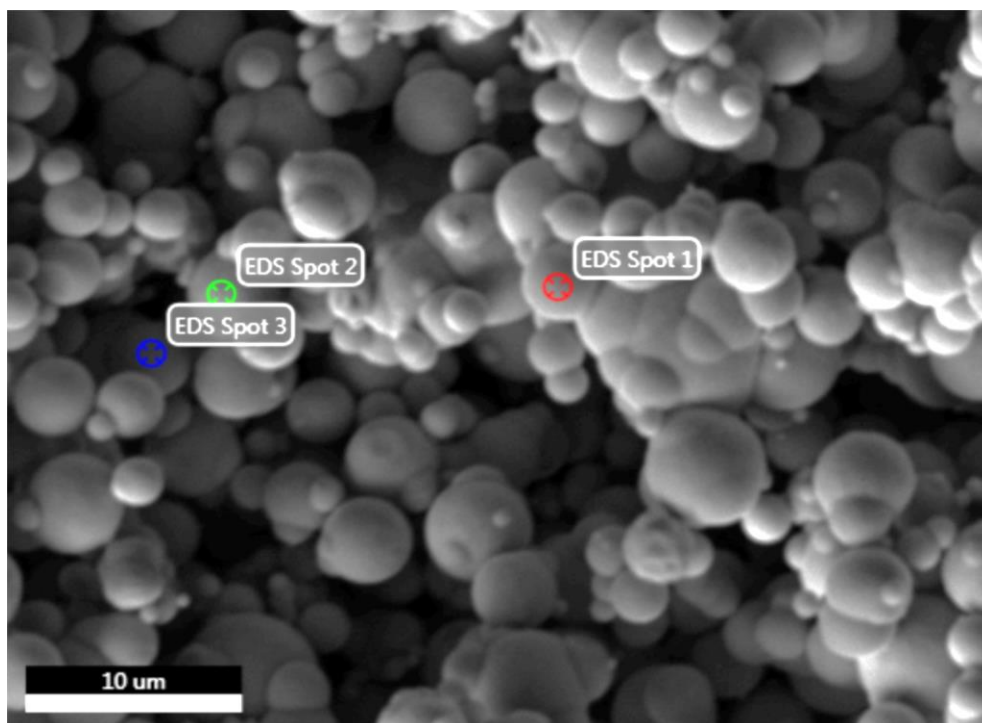
SEM image of iron microspheres showing EDS locations

Iron EDS Spot 4 Graph and Table



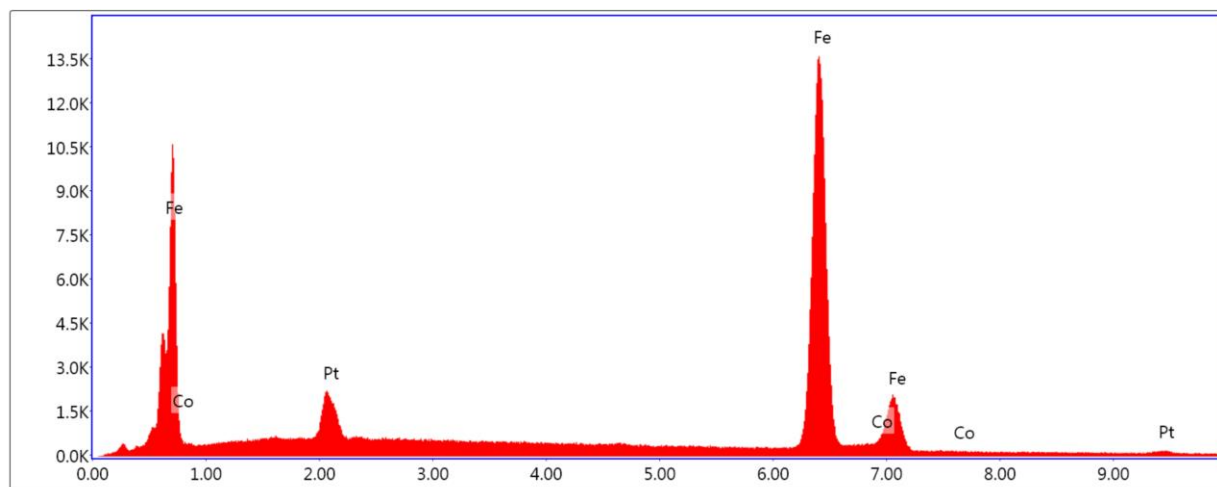
Lsec: 100.00 Cnts 0.000 keV Det: Octane Plus Det

Element	Weight %	Atomic %	Net Int.	Error %	Kratio	Z	R	A	F
PtM	3.26	0.96	218.98	6.72	0.0327	0.7520	1.2527	1.0502	1.2718
FeK	94.80	97.15	3306.27	2.52	0.9776	1.0106	0.9964	0.9976	1.0230
CoK	1.95	1.89	53.75	12.77	0.0196	0.9877	1.0005	0.9912	1.0288



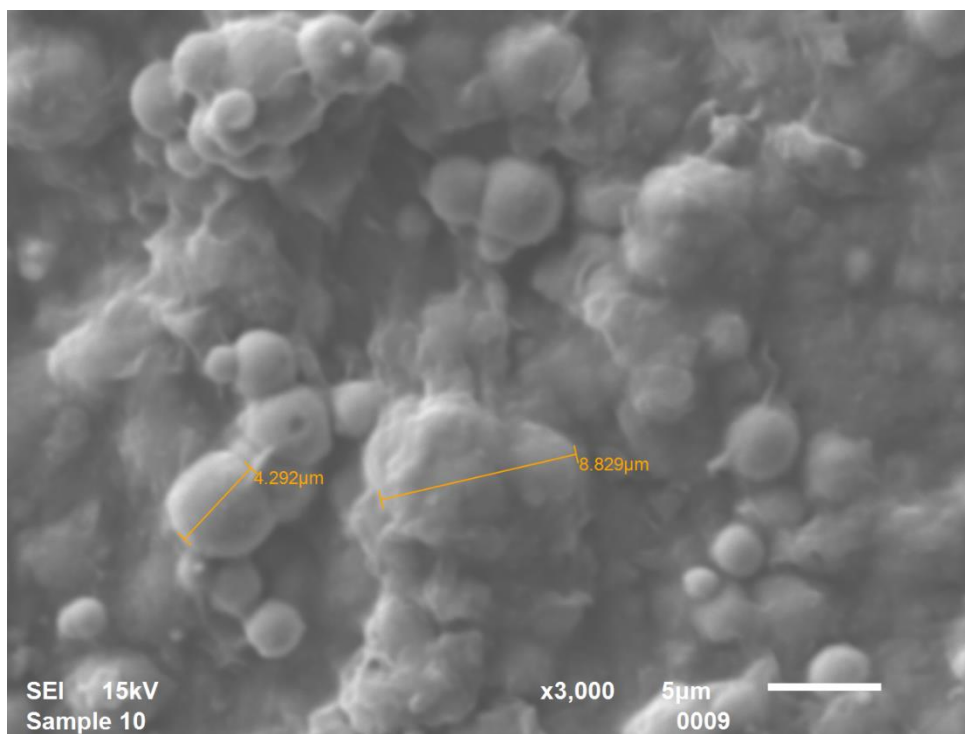
SEM image of iron microspheres at 107 days showing EDS locations.

Iron microspheres at 107 days EDS spot 3 graph and table

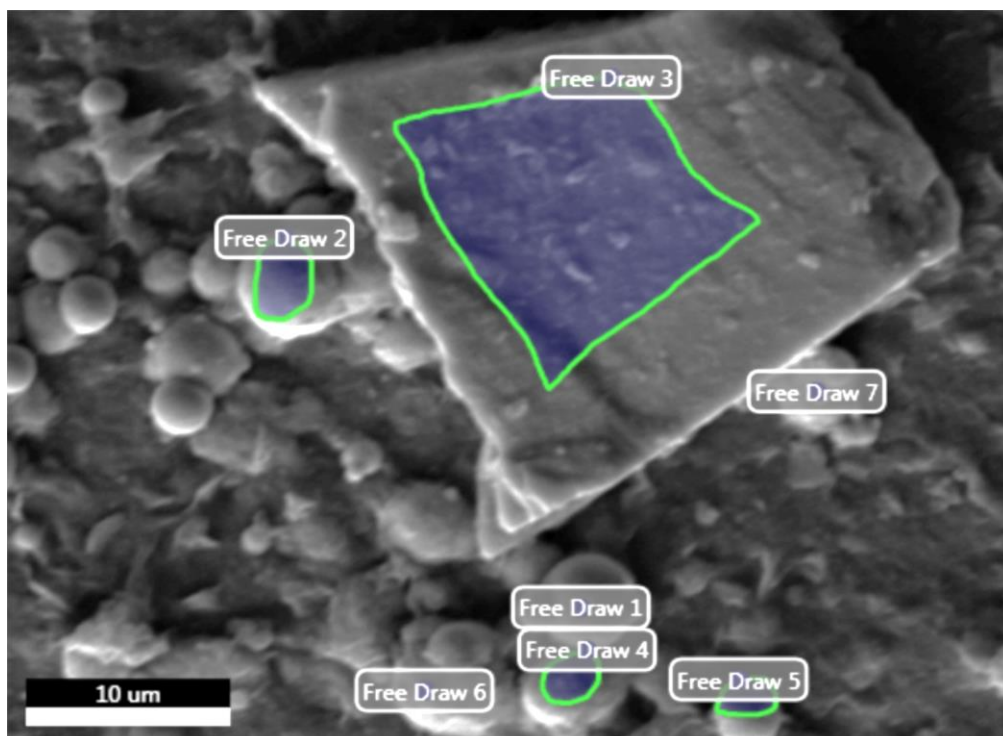


Lsec: 30.0 0 Cnts 0.000 keV Det: Octane Plus Det

Element	Weight %	Atomic %	Net Int.	Error %	Kratio	Z	R	A	F
PtM	2.81	0.82	372.88	4.72	0.0287	0.7515	1.2534	1.0507	1.2944
FeK	92.85	94.96	6359.02	2.58	0.9576	1.0097	0.9968	0.9978	1.0238
CoK	4.35	4.21	235.66	7.60	0.0438	0.9868	1.0009	0.9913	1.0290

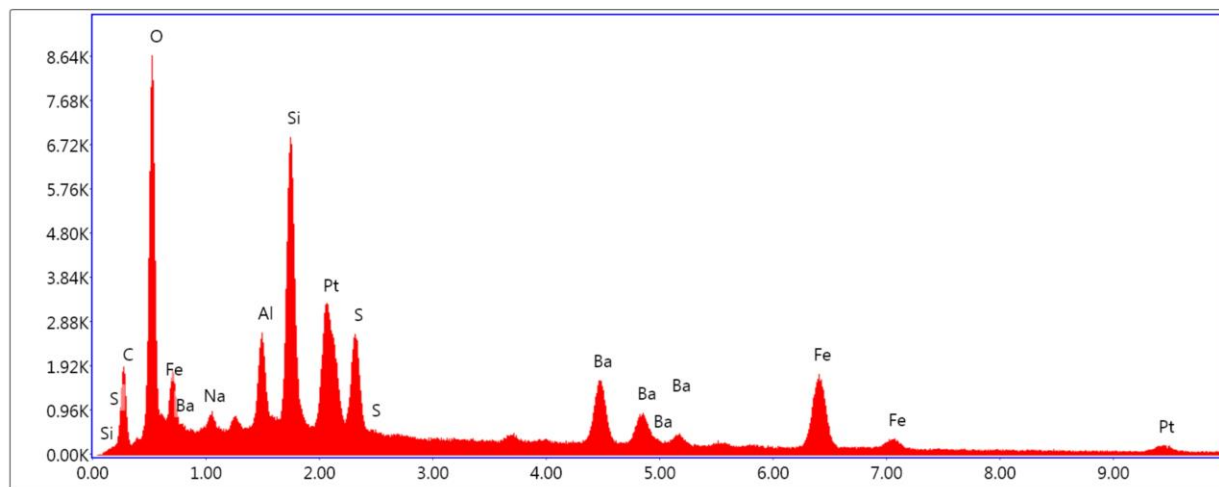


SEM image of sample 10 particles



SEM image of flow loop sample location 1 showing EDS locations.

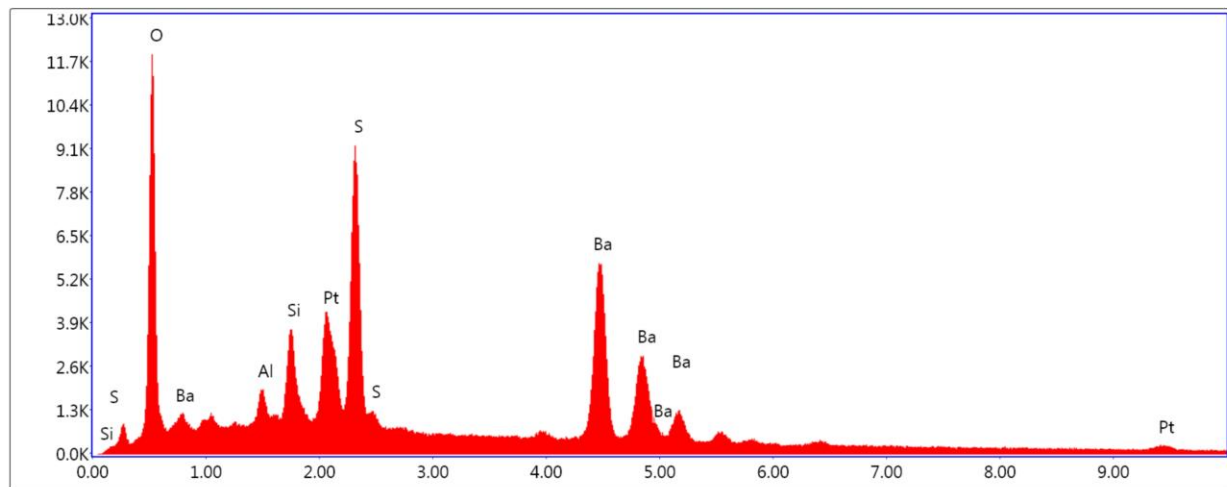
Flow Loop Sample Free Draw 1 graph and table



Lsec: 30.0 0 Cnts 0.000 keV Det: Octane Plus Det

Element	Weight %	Atomic %	Net Int.	Error %	Kratio	Z	R	A	F
C K	13.02	30.17	365.67	10.20	0.0378	1.2543	0.8690	0.2317	1.0000
O K	21.58	37.55	1791.61	8.00	0.0950	1.2004	0.8939	0.3665	1.0000
NaK	1.65	2.00	146.59	11.09	0.0063	1.0905	0.9244	0.3497	1.0013
AlK	3.29	3.39	565.54	6.68	0.0206	1.0684	0.9423	0.5829	1.0036
SiK	9.22	9.14	1787.43	5.07	0.0686	1.0921	0.9505	0.6790	1.0039
PtM	10.76	1.54	771.94	4.76	0.0864	0.6882	1.2983	1.0813	1.0784
S K	3.91	3.40	639.49	4.94	0.0320	1.0699	0.9658	0.7615	1.0026
BaL	18.29	3.71	565.80	5.19	0.1392	0.7208	1.1646	1.0358	1.0197
FeK	18.27	9.10	738.75	3.75	0.1673	0.9202	1.0191	0.9716	1.0246

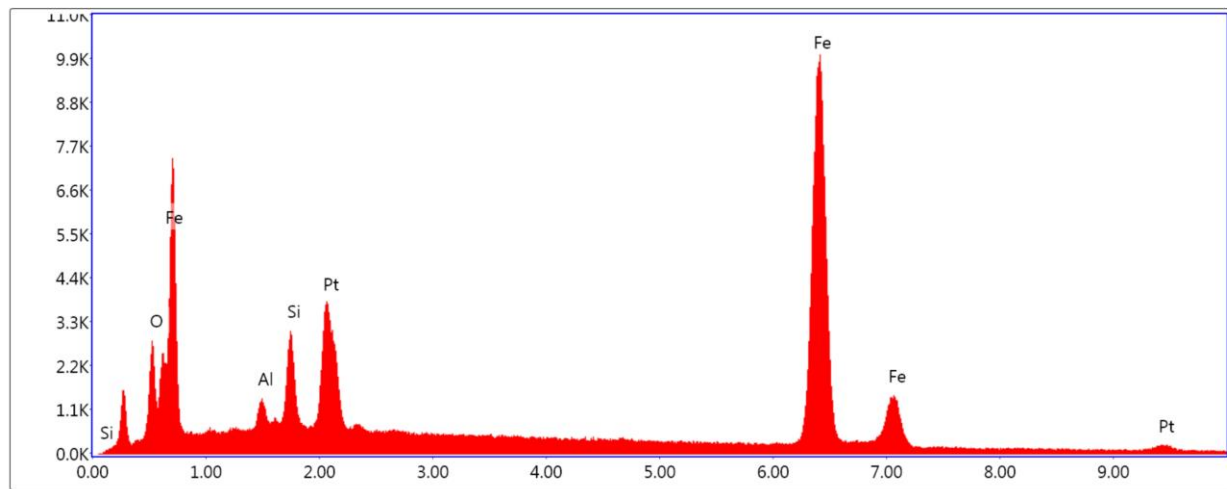
Flow Loop Sample location 1 Free Draw 3 graph and table



Lsec: 30.0 0 Cnts 0.000 keV Det: Octane Plus Det

Element	Weight %	Atomic %	Net Int.	Error %	Kratio	Z	R	A	F
O K	19.88	55.09	2457.63	7.47	0.1114	1.3527	0.8242	0.4142	1.0000
AlK	1.91	3.13	354.44	8.48	0.0110	1.2075	0.8749	0.4771	1.0038
SiK	3.80	6.00	839.62	6.55	0.0276	1.2351	0.8840	0.5839	1.0053
PtM	9.53	2.17	883.03	3.49	0.0845	0.7793	1.2108	1.0022	1.1345
S K	11.96	16.53	2449.28	4.69	0.1047	1.2119	0.9013	0.7193	1.0042
BaL	52.92	17.08	2123.75	2.90	0.4469	0.8233	1.1031	1.0090	1.0167

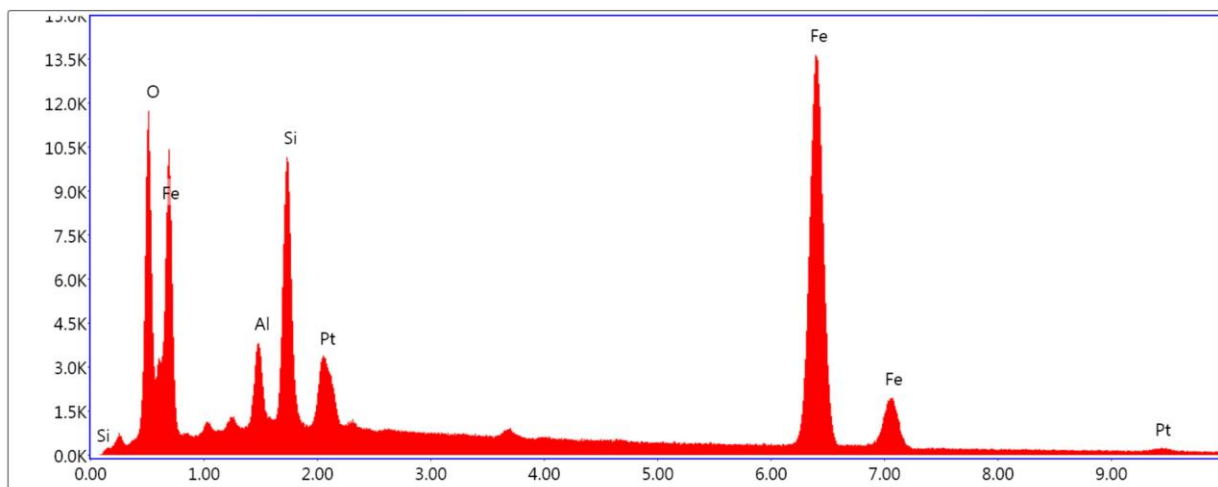
Flow Loop Sample location 1 Free Draw 4 graph and table



Lsec: 30.0 0 Cnts 0.000 keV Det: Octane Plus Det

Element	Weight %	Atomic %	Net Int.	Error %	Kratio	Z	R	A	F
O K	3.77	12.31	547.39	7.36	0.0237	1.3042	0.8574	0.4823	1.0000
AlK	0.84	1.63	155.93	10.61	0.0046	1.1617	0.9075	0.4724	1.0029
SiK	2.69	5.00	606.52	6.88	0.0190	1.1876	0.9163	0.5942	1.0041
PtM	8.47	2.27	824.03	4.39	0.0753	0.7487	1.2535	1.0484	1.1339
FeK	84.24	78.80	4645.60	2.66	0.8600	1.0063	0.9968	0.9938	1.0209

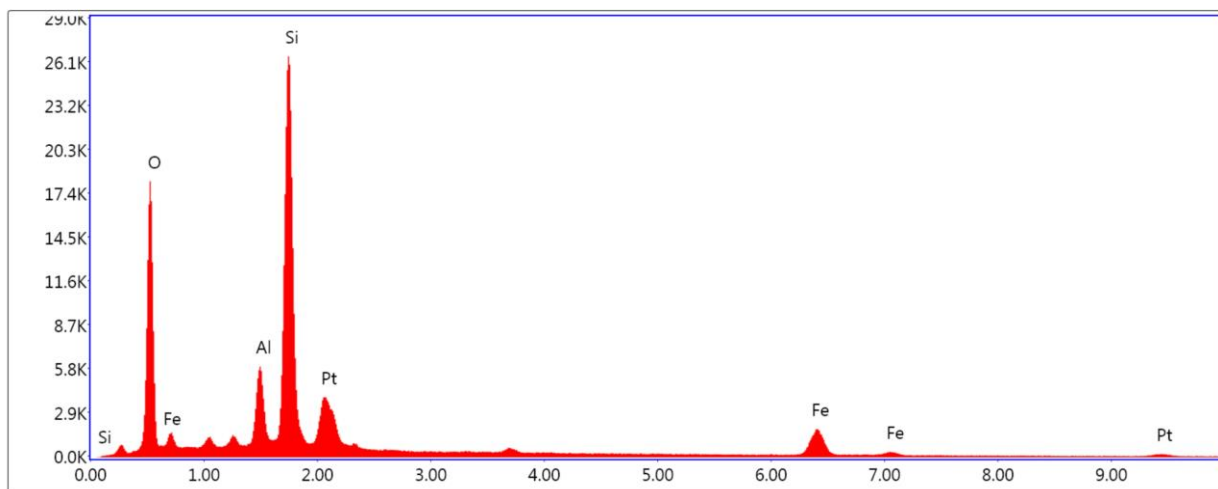
Sample 10 EDS 4 Spot graph and table



Lsec: 100.0 0 Cnts 0.000 keV Det: Octane Plus Det

Element	Weight %	Atomic %	Net Int.	Error %	Kratio	Z	R	A	F
O K	12.96	32.58	774.08	6.41	0.0843	1.2431	0.8842	0.5234	1.0000
AlK	2.27	3.39	216.06	7.55	0.0131	1.1059	0.9332	0.5191	1.0039
SiK	7.03	10.08	783.52	5.55	0.0505	1.1303	0.9416	0.6328	1.0046
PtM	3.99	0.82	192.22	5.76	0.0361	0.7122	1.2866	1.0560	1.2023
FeK	73.75	53.13	1924.99	2.57	0.7173	0.9519	1.0135	0.9982	1.0236

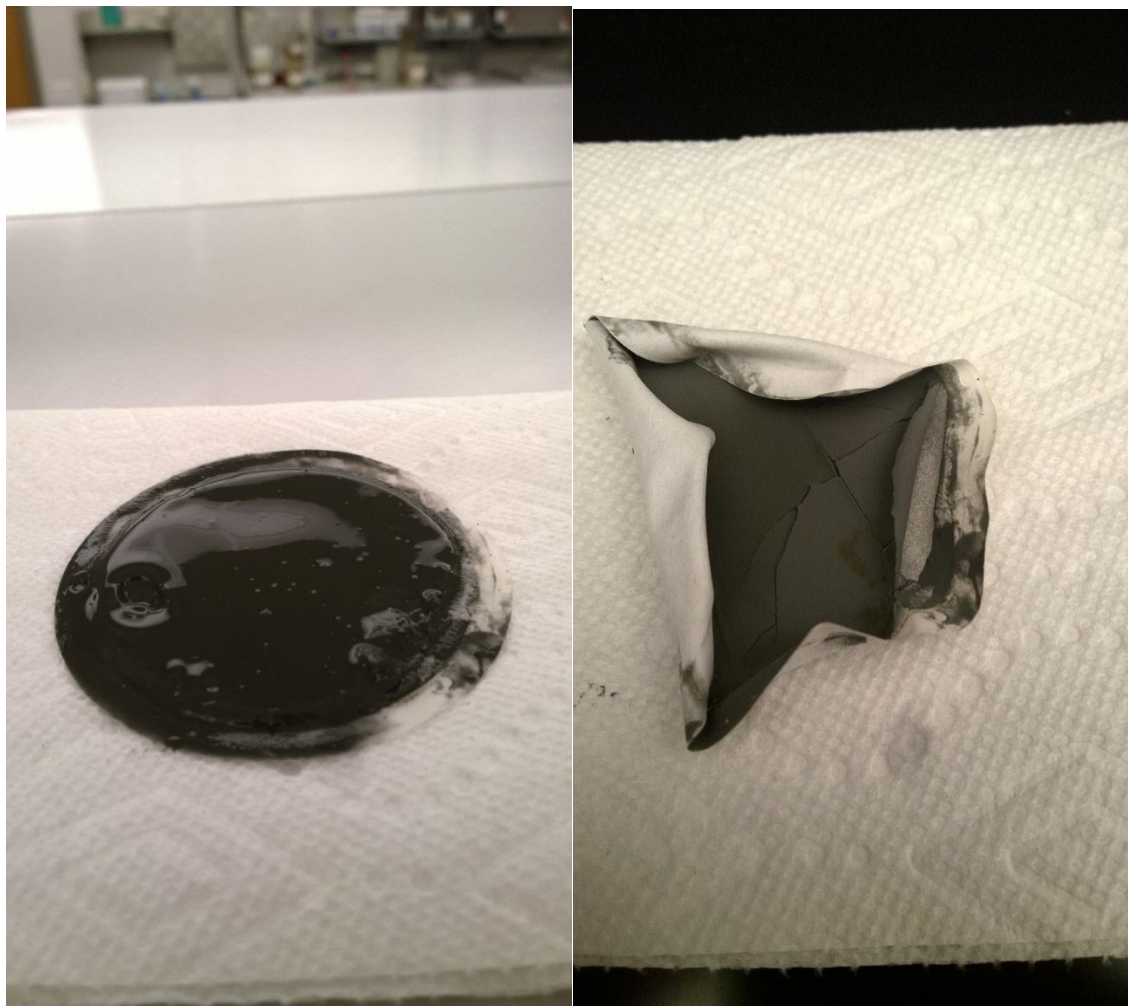
Flow Loop Sample location 2 Free Draw 5 graph and table



Lsec: 30.0 0 Cnts 0.000 keV Det: Octane Plus Det

Element	Weight %	Atomic %	Net Int.	Error %	Kratio	Z	R	A	F
O K	34.64	57.10	3707.55	7.34	0.1662	1.1485	0.9239	0.4176	1.0000
AlK	5.79	5.66	1354.13	5.06	0.0416	1.0194	0.9697	0.7011	1.0055
SiK	29.17	27.39	7163.96	3.91	0.2326	1.0415	0.9774	0.7637	1.0026
PtM	13.36	1.81	996.98	2.99	0.0943	0.6558	1.3332	1.0319	1.0434
FeK	17.03	8.04	784.59	3.53	0.1503	0.8704	1.0356	0.9920	1.0219

APPENDIX G: ADDITIONAL LAB OBSERVATION IMAGES AND NOTES



Images of Sample 2 filter paper immediately (left) and 24 hours (right) after API filter press test.



Images of Sample 2 filter paper at 5 days (left) and 7 days (right) after filter press test.

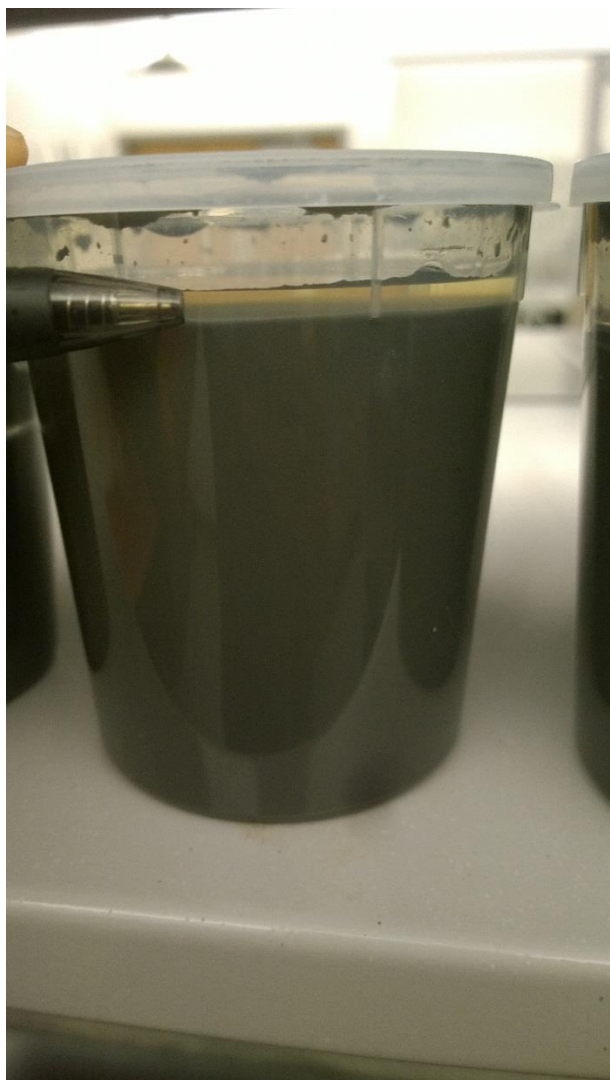


Image of Sample 3 taken 19 days after mixing showing the liquid water separating out of solution.

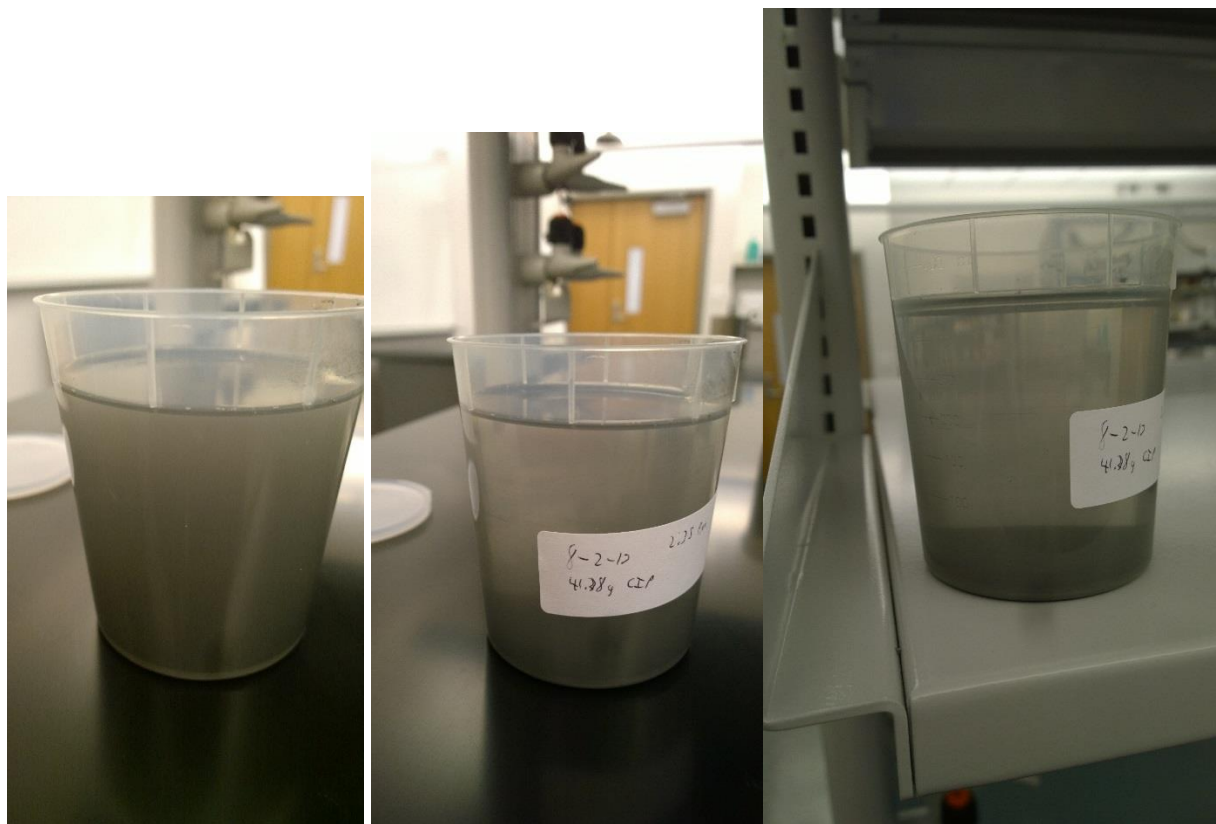


Image of Sample 5 taken at (from left to right) 4 minutes, 12 minutes and 17 minutes after mixing



Image of Sample 5 at approximately 98 hours after mixing. Notice that particles on the edge of the container do not have the same discoloration seen at the bottom of the container.

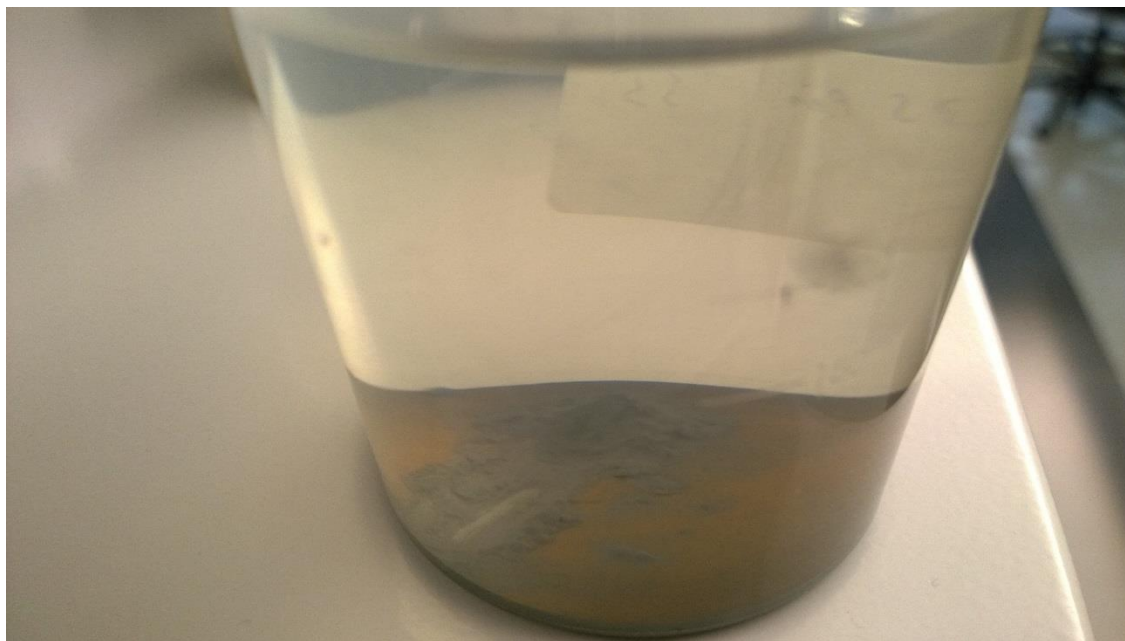


Image of Sample 5 at 8 days after mixing. Bottom has been scraped to reveal that the rust is only on the surface.



Sample 6 approximately 10 days (left) and 11 days (right) after mixing.

The above image shows particles that have caked onto the container wall as the fluid level has decreased from approximately 350mL to approximately 225mL.

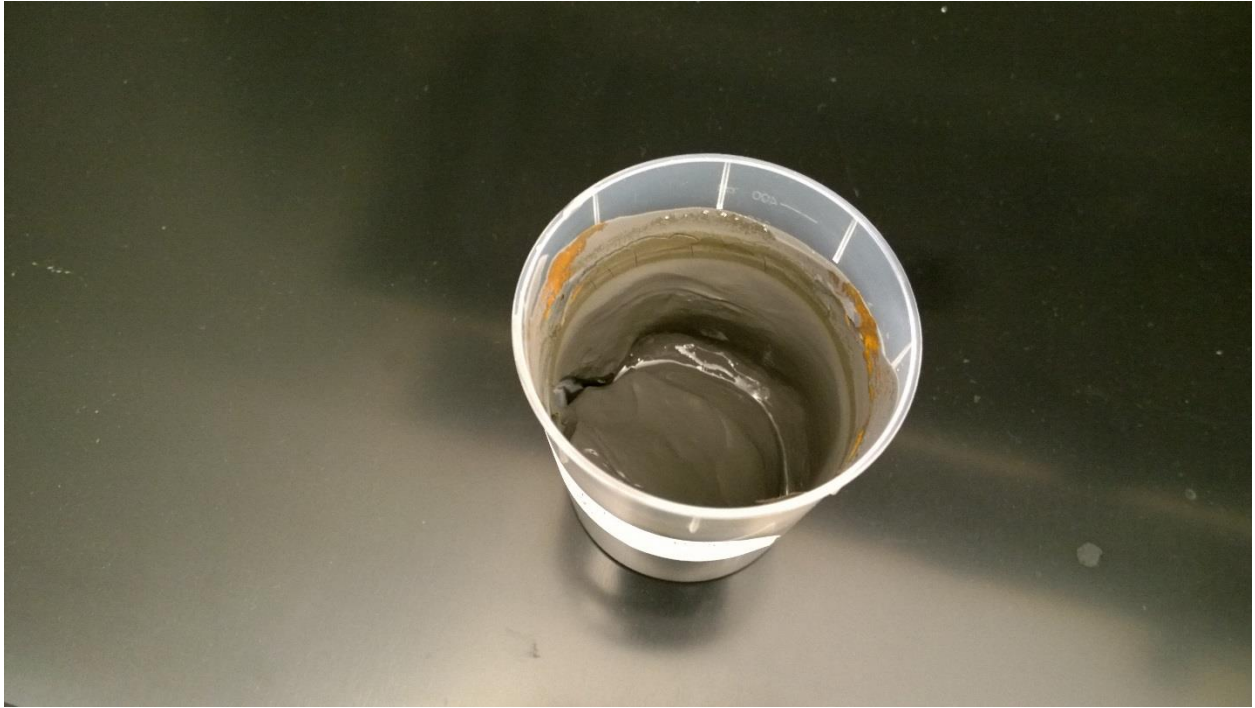
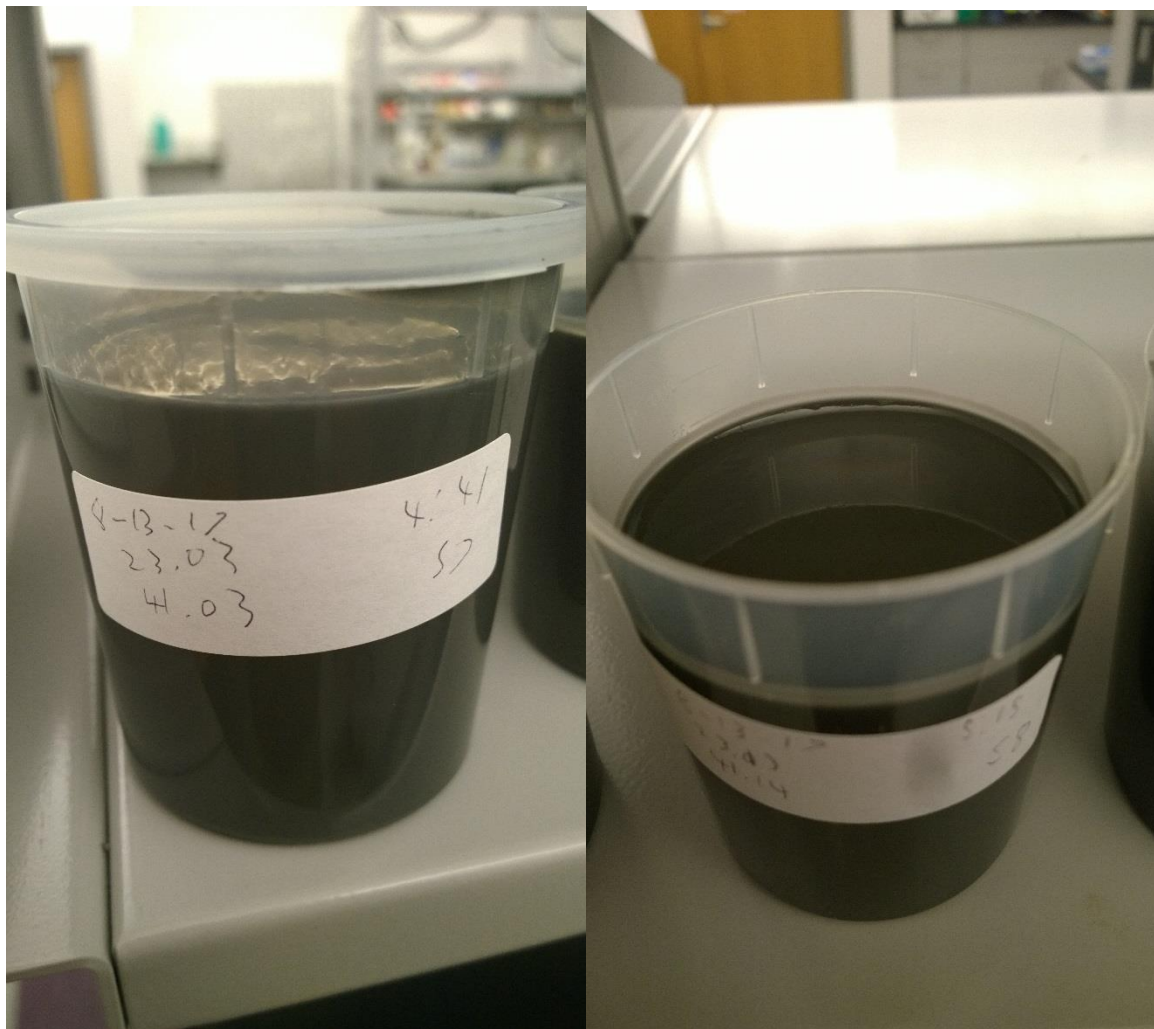


Image of Sample 6 at 25 days after mixing.



Sample 6 at 40 days after mixing.



Sample 7 (left) and Sample 8 (right) 23 ½ hours after mixing.

At 4 days after mixing the bottom of the containers were physically checked, similar to what had previously been done, to confirm that there were not settled particles in Sample 7 (closed top) or Sample 9 (open top).

VITA

Garrett Nielsen was born in Houston, Texas in 1991. He grew up in Bellaire, Texas, where he graduated from Bellaire High School in 2010. He completed his undergraduate in Petroleum Engineering at Louisiana State University in May, 2015. He plans to graduate with a master's degree in May 2018 and then head off to gain experience in the field.